

**DIRECT-FIRED HEAT PUMP FOR MULTI-PASS WATER HEATING
USING MICROCHANNEL HEAT AND MASS EXCHANGERS**

A Dissertation
Presented to
The Academic Faculty

by

Christopher Mahlo Keinath

In Partial Fulfillment
of the Requirements for the Degree
Doctor of Philosophy in Mechanical Engineering

Georgia Institute of Technology

December 2015

Copyright © Christopher M Keinath 2015

DIRECT-FIRED HEAT PUMP FOR MULTI-PASS WATER HEATING USING MICROCHANNEL HEAT AND MASS EXCHANGERS

Approved by:

Dr. Srinivas Garimella, Advisor
George W. Woodruff School of
Mechanical Engineering
Georgia Institute of Technology

Dr. Caroline Genzale
George W. Woodruff School of
Mechanical Engineering
Georgia Institute of Technology

Dr. William Wepfer
George W. Woodruff School of
Mechanical Engineering
Georgia Institute of Technology

Dr. Laurence Jacobs
School of Civil and Environmental
Engineering
Georgia Institute of Technology

Dr. Sheldon Jeter
George W. Woodruff School of
Mechanical Engineering
Georgia Institute of Technology

Date Approved: July 24th, 2015

ACKNOWLEDGEMENTS

I would like to express my deepest gratitude to my advisor, Dr. Srinivas Garimella, for his support and guidance throughout my graduate education. I would not be where I am today without his trust in my technical abilities. His mentorship has helped me to grow as an engineer and individual. I hope and know that this is the beginning of a long association. I would also like to thank the other members of my Ph.D. committee: Dr. William Wepfer, Dr. Sheldon Jeter, Dr. Caroline Genzale, and Dr. Laurence Jacobs for their guidance and expertise.

I would like to thank all of the current and past members of the Sustainable Thermal System Laboratory for their support, feedback and friendship. I would specifically like to thank Dr. Ananda Nagavarapu and Dr. Brendon Keinath for their help and guidance during my initial development as a researcher. I would also like to specifically thank Dr. Brian Fronk, Dr. Jeffrey Milkie, Dr. Alex Rattner, Dhruv Hoysall, Malcolm Macdonald and Marcel Staedter for their friendship and feedback along the way. In addition, I would like to thank Michael Garrabrant and Stone Mountain Technologies Incorporated for their assistance during my graduate studies.

Finally, I would like to thank my family. The person I am today is the result of many people, the most impactful of which have been my parents, grandparents, brothers and soon to be wife. Thank you for your unwavering support.

TABLE OF CONTENTS

	Page
ACKNOWLEDGEMENTS	III
LIST OF TABLES	IX
LIST OF FIGURES	XI
NOMENCLATURE	XIV
SUMMARY	XVI
CHAPTER 1. INTRODUCTION	1
1.1 Water Heaters	2
1.2 Absorption Heat Pump	4
1.3 Heat Exchanger Miniaturization	8
1.4 Present Investigation	11
1.5 Research Objectives	11
1.6 Structure of this Dissertation	12
CHAPTER 2. MODELING OF THE AMMONIA-WATER HEAT PUMP WATER HEATER AND STORAGE TANK FOR RESIDENTIAL APPLICATIONS.....	14
2.1 Introduction	14
2.1.1 Background	14
2.1.2 Prior Work	16
2.2 System Description.....	20
2.2.1 Main Loop	20
2.2.2 Auxiliary Loops.....	22

2.3	Modeling Approach.....	22
2.4	Baseline System Results.....	24
2.5	Parametric Analyses.....	26
2.6	Tank Coupled Modeling.....	31
2.6.1	Heat Pump Performance Equations.....	31
2.6.2	Cold Start.....	33
2.6.3	Response to a 76 Liter Draw	37
2.6.3	Stand-by Losses.....	39
2.7	Conclusions	40
CHAPTER 3.	BREADBOARD EVALUATION OF COMPACT HEAT AND MASS EXCHANGERS FOR THE ABSORPTION HEAT PUMP WATER HEATER	43
3.1	Introduction	43
3.1.1	Background	43
3.1.2	Prior Work.....	44
3.2	System and Component Description	50
3.2.1	System Description.....	50
3.2.2	Heat and Mass Exchangers.....	52
3.3	Experimental Approach.....	55
3.3.1	Instrumentation and Data Acquisition.....	56
3.4	Data Analysis	58
3.4.1	System-level State Points	59
3.4.2	Component Level Analysis	59

3.5	Results and Discussion.....	61
3.5.1	Absorber	61
3.5.2	Condenser.....	64
3.5.3	Desorber	66
3.5.4	Evaporator	67
3.5.5	Rectifier	70
3.5.6	Refrigerant Heat Exchanger	71
3.5.7	Solution Heat Exchanger.....	72
3.5.8	Overall System	73
3.5.9	Heat and Mass Exchanger Refinement	75
3.6	Conclusions	76
CHAPTER 4.	INTEGRATED PACKAGED HEAT PUMP WATER HEATER PROTOTYPE USING COMPACT HEAT AND MASS EXCHANGERS	78
4.1	Introduction	78
4.1.1	Overview	78
4.1.2	Prior Work.....	79
4.2	System and Component Description	83
4.2.1	Packaged system components	84
4.3	Experiments.....	87
4.3.1	Instrumentation and Data Acquisition.....	87
4.4	Data Analysis	90
4.5	Results and Discussion.....	92

4.5.1	Operation at baseline design conditions	92
4.5.2	Water and Ambient Temperature Sweeps	94
4.6	Model and Experiment Comparison.....	107
4.7	Conclusions	110
CHAPTER 5.	ENERGY AND COST COMPARISON OF RESIDENTIAL WATER HEATING TECHNOLOGIES	111
5.1	Introduction	111
5.1.1	Background	111
5.1.2	Prior Work	112
5.2	Rating Systems	115
5.3	Water Heater Designs.....	116
5.3.1	Gas Storage.....	116
5.3.2	Gas Tankless.....	118
5.3.3	Gas Heat Pump.....	119
5.3.4	Heating Oil-fired Units.....	119
5.3.5	Electric Storage	120
5.3.6	Electric Tankless	121
5.3.7	Electric Heat Pump.....	121
5.4	Energy and Cost Analysis	122
5.5	Results and Discussion.....	125
5.5.1	Base Case of 243 Liters per Day	126
5.5.2	Large Daily Total Draws	129

5.6	Conclusions	131
CHAPTER 6.	CONCLUSIONS AND RECOMMENDATIONS.....	133
6.1	Overview	133
6.2	Recommendations	136
APPENDIX A: BREADBOARD EXPERIMENTAL DETAILS		140
APPENDIX B: PACKAGED UNIT EXPERIMENTAL DETAILS		151
APPENDIX C: HEAT EXCHANGER FABRICATION DETAILS		161
REFERENCES	166

LIST OF TABLES

	Page
Table 1.1: Residential water heater efficiency comparison	3
Table 2.1: Cycle model design specifications.....	24
Table 2.2: Constants for <i>COP</i> and heat duty regression analysis	32
Table 3.1: Breadboard component sizing	54
Table 3.2: Resized microchannel components.....	75
Table 4.1: Theoretical model and experimental comparison at baseline conditions	93
Table 4.2: Experimental test matrix.....	94
Table 5.1: Water heater fuel pricing	123
Table 5.2: Water heating systems investigated.....	125
Table A.1.1: Absorber details	141
Table A.1.2: Condenser details.....	141
Table A.1.3: Desorber details	142
Table A.1.4: Evaporator details	142
Table A.1.5: Rectifier details	142
Table A.1.6: Refrigerant heat exchanger details.....	143
Table A.1.7: Solution heat exchanger details	143
Table A.2.1: Summary of instrumentation on the breadboard test facility.....	145
Table A.3.1: Example breadboard system data analysis and uncertainty calculation	148
Table B.1.1: Absorber details	152
Table B.1.2: Desorber details.....	152
Table B.1.3: Rectifier details	152
Table B.1.4: Monolith heat exchanger details	153

Table B.1.5: Solution pump and motor	153
Table B.1.6: Coupling-fluid pump details	154
Table B.1.7: Ambient heat exchanger	154
Table B.1.8: Ambient heat exchange fan.....	154
Table B.2.1: Summary of instrumentation on the packaged unit test facility	156
Table B.3.1: Example packaged unit data analysis and uncertainty calculation	158

LIST OF FIGURES

	Page
Figure 1.1: Schematic of the single-effect absorption heat pump	5
Figure 1.2: Operating conditions for cooling, heating and multi-pass water heating.....	8
Figure 1.3: Schematic of an alternating shim assembly	9
Figure 1.4: Schematic of the direct gas-fired desorber	10
Figure 2.1: Schematic of the gas-fired single-effect absorption heat pump water heater.	21
Figure 2.2: System <i>COP</i> and heating duty as a function of water inlet temperature.....	27
Figure 2.3: Change in high to low pressure difference.....	28
Figure 2.4: Concentration changes with water and ambient temperatures	29
Figure 2.5: Absorption system mass flow rates	30
Figure 2.6: Temperature of tank during cold start	34
Figure 2.7: <i>COP</i> and heating duty as a function of pass number	35
Figure 2.8: Water temperature as a function of pass number for 32°C ambient	37
Figure 2.9: Drawing of stratified tank after 76 liter draw.....	38
Figure 2.10: Multipass heating response to 76 liter draw	39
Figure 2.11: Multipass heating response to stand-by losses	41
Figure 3.1: Schematic of absorption heat pump	51
Figure 3.2: Discrete microchannel heat exchanger assembly.....	53
Figure 3.3: Test facility schematic.....	57
Figure 3.4: Test facility; breadboard (left), combustion room (right)	58
Figure 3.5: Absorber <i>UA</i> and heat duty	63
Figure 3.6: Absorber solution outlet approach temperature difference	64
Figure 3.7: Condenser <i>UA</i> and heat duty	65

Figure 3.8: High side pressure of breadboard system.....	66
Figure 3.9: Desorber heat duty and dilute solution outlet temperature.....	67
Figure 3.10: Evaporator UA and heat duty	68
Figure 3.11: Evaporator glide and coupling fluid inlet temperature.....	69
Figure 3.12: Rectifier UA and heat duty	71
Figure 3.13: Refrigerant heat exchanger effectiveness and heat duty	72
Figure 3.14: Solution heat exchanger UA and heat duty	73
Figure 3.15: System heating duty and COP	74
Figure 4.1: Schematic of an absorption heat pump.....	84
Figure 4.2: Images of packaged unit heat and mass exchangers	85
Figure 4.3: Packaged prototype heat pump.....	86
Figure 4.4: Schematic of packaged unit and auxiliary components	88
Figure 4.5: Photographs of the packaged unit and supporting facilities.....	89
Figure 4.6: Heating COP as a function of water and ambient temperatures	95
Figure 4.7: Heating duty as a function of water and ambient temperatures	96
Figure 4.8: High to low side pressure difference	98
Figure 4.9: Solution and refrigerant concentrations	99
Figure 4.10: Absorber temperature profiles.....	101
Figure 4.11: Condenser temperatures profiles	102
Figure 4.12: Desorber temperature profiles	103
Figure 4.13: Evaporator temperature profiles.....	104
Figure 4.14: Rectifier temperature profiles.....	105
Figure 4.15: Refrigerant heat exchanger temperature profiles	106
Figure 4.16: Solution heat exchanger temperature profiles	107
Figure 4.17: COP and heat duty, refined model and experiment comparison.....	109

Figure 5.1: Schematics of gas water heaters	117
Figure 5.2: Schematic of electric water heaters	120
Figure 5.3: Energy Factors for systems under investigation.....	123
Figure 5.4: Annual energy usage of water heaters investigated	126
Figure 5.5: Annual operating cost of water heaters investigated.....	127
Figure 5.6: Estimated payback period for water heaters investigated	128
Figure 5.7: Total lifetime cost for water heaters investigated	129
Figure 5.8: Annual energy usage for three daily draw amounts	130
Figure C.1: Photo-chemical etching process	162
Figure C.2: Fixtures used in vacuum brazing process	164

NOMENCLATURE

CAT	closest approach temperature (K)
CF	coupling fluid
COP	coefficient of performance $Q_{\text{heating}}/Q_{\text{input}}$
c_p	specific heat at constant pressure ($\text{kJ kg}^{-1} \text{K}^{-1}$)
D	diameter (m)
E	electrical input (W)
EF	energy factor
FHR	first-hour-rating for water heaters
GAX	generator-absorber heat exchange component or system
H	height (m)
h	convection heat transfer coefficient ($\text{W m}^{-2} \text{K}^{-1}$) or enthalpy (kJ kg^{-1})
HX	heat exchanger
k	thermal conductivity ($\text{W m}^{-1} \text{K}^{-1}$)
L	length (m)
LMTD	log-mean temperature difference (K)
LPM	liters-per-minute rating for water heaters
m	mass (kg)
\dot{m}	mass flow rate (kg s^{-1})
Nu	Nusselt number hD/k
p	pressure (Pa)
Q	heat transfer rate (W)
q	quality
t	time (s)
T	temperature ($^{\circ}\text{C}$)
UA	overall heat transfer conductance (W K^{-1})
v	specific volume ($\text{m}^3 \text{kg}^{-1}$)
x	concentration

Greek characters

Δ	finite difference, or mesh cell dimension (m)
ε	heat exchanger effectiveness
η	combustion efficiency
μ	dynamic viscosity ($\text{kg m}^{-1} \text{s}^{-1}$)
ρ	mass density (kg m^{-3})

Subscripts

abs	absorber
air	ambient air value
amb	ambient value
aux	auxiliary heat exchanger

avg	average value
CF	coupling fluid
cond	condenser
CS	concentrated solution (high in refrigerant)
des	desorber
dm	daily measured value
evap	evaporator
high- side	high pressure side of system
gas	natural gas
in	inlet value
low- side	low pressure side of system
NH ₃	pure ammonia value
NH ₃ - H ₂ O	ammonia-water mixture
out	outlet value, or outer fin value
rect	rectifier
ref	refrigerant flow value
RHX	refrigerant heat exchanger or precooler
sat	saturation conditions
SHX	solution heat exchanger

SUMMARY

Absorption heat pump water heaters offer improved performance compared to conventional direct-fired water heaters, with the potential for coefficients of performance well in excess of 1. A primary energy usage comparison with electric heat pumps shows that absorption systems can be competitive with current technology. However, the implementation of these systems in the residential and light commercial market has not been practical for several reasons, including a limited knowledgebase on absorption systems for this application and the lack of compact and economically viable heat and mass exchangers. An improved understanding of the coupled heat and mass transfer processes in thermally driven absorption systems to be used as heat pump water heaters was obtained over the course of this study. In addition, microchannel heat and mass exchangers that enable such compact gas-fired heat pump water heaters were developed and tested. Performance at design and off-design conditions over a range of water and ambient temperatures was simulated in detail with a system-level model developed for this purpose. The system-level model was coupled with a water-tank model to investigate several water heating scenarios including a cold start, response to a medium sized draw and response to stand-by losses. Heat and mass exchangers were designed using component-level heat and mass transfer models. The heat and mass exchangers were first installed and evaluated on a breadboard test facility. Insights from these experiments were then used to design and fabricate a monolithic unit integrating several of the microchannel heat and mass exchangers, coupled with a gas-fired desorber heat exchanger to yield a stand-alone water heater prototype. The performance of the prototype was investigated over a range of water and ambient temperatures. A

comparison of results was performed to investigate the deviation between model predictions and experimental values. A refined model was developed that more accurately predicted experimental results. Energy-use and cost analyses were performed and showed the potentially significant energy savings of thermally driven heat pump water heaters.

CHAPTER 1. INTRODUCTION

Water heating is the second largest source of residential energy consumption, accounting for 14-18% of household energy costs (DOE 2014). For this reason water heating has received increased attention, and technologies to reduce energy demand are under development. The majority of water heaters sold in the United States are direct-heated gas or electric systems with coefficients of performance (*COPs*) well below 1. Direct-heated units dominate the market because they are inexpensive and reliable. In 2009, eight million water heaters were sold in the U.S., only one million of which were Energy StarTM rated (Ryan *et al.* 2010). For a product to earn an Energy StarTM rating, the Environmental Protection Agency must certify that the unit meets a specific energy efficient requirement. Energy StarTM requirements are set forth for all types of water heaters, including direct-heated units. This means that many of the Energy StarTM appliances constituting the one million units are likely to have *COPs* less than 1. For these direct-fired units, incremental improvements have become the norm as their ratings approach the theoretical limit of 1. Alternative high performance water heaters with increased *COPs* continue to be pursued, but face a number of challenges for widespread adoption before making a significant impact on residential energy consumption.

These alternative water heater designs include solar thermal and heat pump water heaters. The success of solar thermal units is location dependent, and heat pump water heaters are a better solution in most locations. Heat pump water heaters reduce energy consumption by extracting heat from the surroundings in addition to the driving electrical or thermal input. As a result, electrically and thermally driven heat pump systems offer *COPs* above 1. Electrically driven vapor-compression systems are commercially available but rely on an already strained electrical grid while using synthetic refrigerants with high global warming potential. The absorption system is a thermally driven heat pump that uses heat as the primary energy input and uses natural refrigerants. These

systems are currently not commercially available due to a series of challenges, including the lack of a practically feasible and economically viable design.

The present study focuses on a thermally driven heat pump water heater using microchannel heat and mass exchangers. The discussion in this chapter and the following chapters focuses on the state of the art for each contributing topic: water heaters, absorption systems, and compact heat and mass exchangers. The research presented in this investigation addresses each of these topics to enable the development of a novel gas-fired heat pump water heater.

1.1 Water Heaters

A range of commercially available residential water heaters using gas, electricity, oil and solar thermal sources is available. Gas storage (non-condensing and condensing), electric storage (direct heated and heat pump), tankless (non-condensing, condensing and electric) and heating oil water heaters are considered in the present study. The direct heated systems are limited to $COPs < 1$, while heat pumps can achieve $COPs > 1$. Direct gas-fired systems use the high temperature flue gas to heat water via an in-tank exchanger, and standard electric systems use resistance elements to heat the water. Electric heat pumps use coiled tube condensers to heat the stored water. Detailed descriptions of these water heating systems are provided in Section 5.3. In 2012, of the roughly 8 million water heaters that sold in the U.S., 52 percent were gas-fired units (AHRI 2014). The energy source split for residential water heaters shows that there is a significant market potential for gas-fired heat pump systems in the United States. Commercially available electrically driven heat pump water heaters have seen limited market share and growth even though they offer the potential for significant savings. This could be attributed to the higher capital cost. Although the capital cost is higher than that of a standard unit, the ACEEE determined that an electrically driven heat pump water heater would have the lowest total cost over a 13 year period when compared with other commercially available units (ACEEE 2012). The market share of higher efficiency water

heaters is expected to grow as energy costs and demand continue to increase. Thermally driven heat pumps offer improved primary energy efficiencies compared to electric heat pumps but were not considered in the ACEEE comparison because they are not commercially available yet.

An efficiency comparison for water heater technologies, including thermally driven heat pumps, reinforces the fact that typical water heater efficiencies are limited and alternative technologies should be pursued to reduce energy demand and consumption. Table 1.1 presents a range of water heater types and their associated efficiencies and primary energy efficiencies. The primary energy efficiency accounts for electrical energy production and transmission losses. The table shows that a gas-fired heat pump water heater provides the highest energy efficiency based on primary energy. This highlights the fact that it may have the most potential; however, a significant amount research and development is needed to produce a commercially viable unit. Reducing thermally driven system size, refrigerant charge, and cost are all challenges that must be addressed to increase the opportunity for implementation and reduce residential energy consumption

Table 1.1: Residential Water Heater Efficiency Comparison(Garrabrant *et al.* 2013a)

Water Heater Type	System EF	Primary Energy EF
Conventional Gas Storage	0.60	0.60
Condensing Gas Storage	0.86	0.86
Non-Condensing Gas Tankless	0.82	0.82
Condensing Gas Tankless	0.92	0.92
High Efficiency Electric Storage*	0.95	0.33
Electric Heat Pump*	2.2	0.77
Gas-Fired Heat Pump	1.50	1.50

*Assuming a representative electric generation and transmission efficiency of 35%

and carbon footprint.

1.2 Absorption Heat Pump

Figure 1.1 is a schematic of a single-effect ammonia-water absorption heat pump. The five major components of the system are the absorber, desorber, rectifier, condenser and evaporator. Two additional recuperative heat exchangers are the solution heat exchanger and the refrigerant pre-cooler. Increasing recuperative heat exchange within the system improves the cycle coefficient of performance but increases complexity. The working fluid of the system is a binary mixture, where the more volatile component acts as the refrigerant and the other component as the absorbent. Water-Lithium Bromide and Ammonia-Water are the two working fluid pairs that are typically used due to their favorable properties. The advantages of using ammonia-water are its stability over a large range of temperatures and pressures, the high latent heat of vaporization for Ammonia, excellent thermophysical properties, and saturation pressure-temperature characteristics suitable for heat and cooling mode operation (Srikhirin *et al.* 2001). Other fluid pairs have been investigated, but these two remain the most prominent. In water-lithium bromide systems, water is the refrigerant and aqueous Lithium Bromide is the absorbent. Use of these systems is limited to applications above evaporator temperatures of 0°C because of the freezing point of water. The high specific volume of water vapor also limits its potential for use in miniaturized applications where reduced flow area would result in unacceptable pressure loss. The potential for crystallization at high concentrations of Lithium Bromide also makes it less desirable for many applications. For ammonia-water systems, ammonia is the refrigerant and water is the absorbent. These systems are used in applications including refrigeration, space conditioning, and water

heating. Ammonia has a much lower vapor-phase specific volume than water, making it more advantageous for use in miniaturized applications. For example, the specific volume of ammonia and water vapor assuming saturation at a temperature of 5°C are $0.243 \text{ m}^3 \text{ kg}^{-1}$ and $147 \text{ m}^3 \text{ kg}^{-1}$, respectively. Because in the ammonia-water fluid pair, the water is a volatile absorbent, systems that use this working fluid pair require a rectifier to purify the refrigerant by selectively condensing water from the desorbed vapor to minimize the impact of the rise in temperature (temperature glide) of the refrigerant-absorbent mixture as evaporation proceeds. The toxicity of ammonia is also an important factor, and minimizing system charge is a way of mitigating the risk associated with this

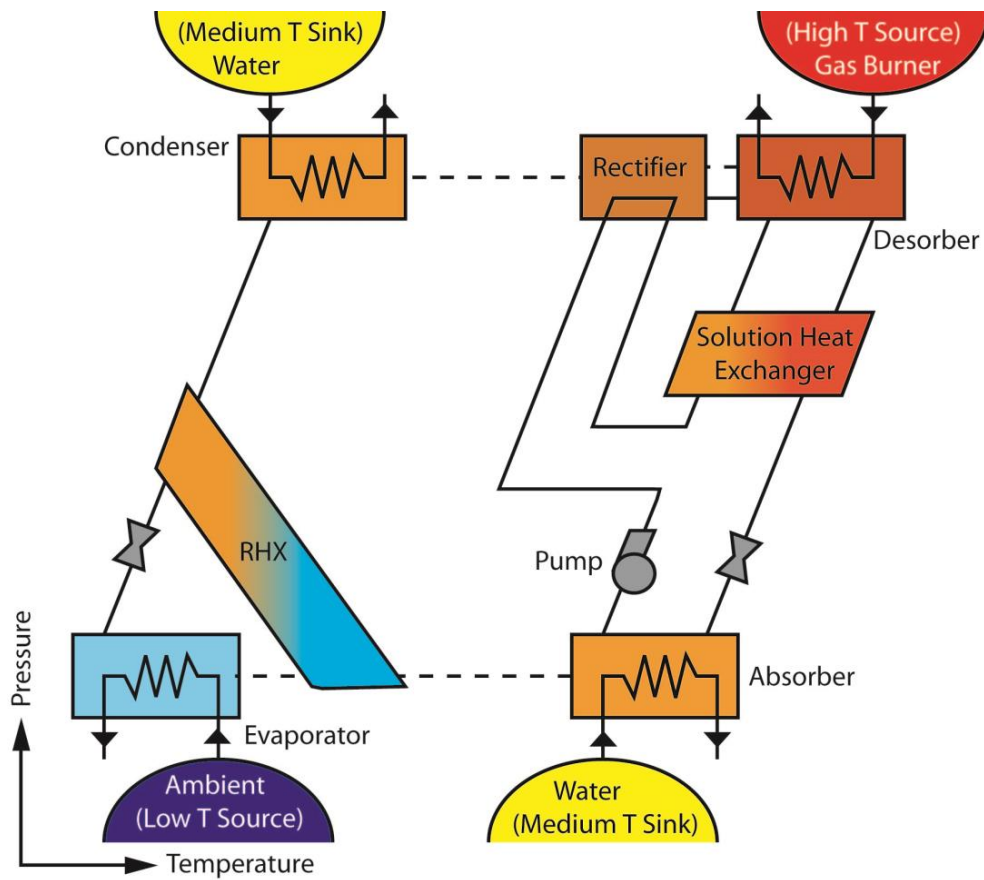


Figure 1.1: Schematic of the single-effect absorption heat pump

refrigerant.

The single-effect ammonia-water absorption heat pump is a two-pressure system in which the desorber, rectifier, condenser and solution heat exchanger operate on the high pressure side, and the absorber and evaporator operate on the low-pressure side. The system can be operated in heating and cooling modes. In heating mode operation (shown schematically in Fig. 1.1,) the desired heating is achieved at the absorber and condenser, and the evaporator provides low-temperature heat from the ambient.

High pressure refrigerant is generated in the desorber and flows to the rectifier where water is selectively condensed, improving refrigerant purity. The vapor then exits the rectifier and flows to the condenser where it leaves as liquid refrigerant. The heat of condensation is rejected to the medium temperature sink. The liquid refrigerant is further subcooled in the refrigerant precooler before flowing through an expansion device to the low-pressure side of the system. The refrigerant then flows through the evaporator where it receives low-temperature heat before exchanging heat with the condensed refrigerant flowing through the high-pressure side of the refrigerant precooler. The refrigerant then enters the absorber, where it is absorbed by the dilute solution. Dilute solution refers to solution that has a low concentration of ammonia or is weak in ammonia content. Concentrated solution exits the absorber and flow through a pump that takes the solution from the low system pressure to the high system pressure. Concentrated solution refers to solution that has a high concentration of ammonia or is strong in ammonia content. The solution recuperates heat in the solution heat exchanger before flowing to the desorber. In the desorber, refrigerant is generated from the concentrated solution, reducing its

ammonia content. It exits the desorber as dilute solution and flows to the solution heat exchanger where it exchanges heat with the concentrated solution. The dilute solution then flows across an expansion device to the low pressure side of the system before absorbing refrigerant vapor in the absorber. The heat of absorption is rejected to the medium temperature sink.

Adoption of these systems in the residential sector has been limited, while absorption systems have found more acceptance in larger capacity industrial settings. Heating and cooling mode applications typically require delivery of chilled or heated water at a specific temperature. As a result, these systems operate very differently than a multi-pass water heater, in which the water delivery temperature changes significantly over time. Figure 1.2 presents the operating conditions of interest for heating, cooling and multi-pass water heating (present study). The graph shows that heating-mode studies are performed with a specified hot water (absorber and condenser) coupling fluid temperature and the ambient (evaporator) conditions are varied. For cooling-mode operation, a specified chilled water (evaporator) coupling fluid temperature is specified and the ambient (absorber and condenser) conditions are varied. For the present study, operation over a more significant hot water (absorber and condenser) coupling fluid temperature and ambient (evaporator) temperature range is required.

1.3 Heat Exchanger Miniaturization

The use of mini and microchannel heat and mass exchangers has the potential to significantly reduce component size, cost and required fluid inventory. The use of smaller diameter passages allows for significant gains in heat transfer coefficients but comes at the cost of increased pressure drop. To mitigate this pressure loss, the strategy of increasing the number of channels in parallel is often pursued. Commercial fabrication of small capacity heat and mass exchangers compatible with the ammonia-water working fluid is limited and there are no cost-effective off-the-shelf (OTS) components available. The present investigation includes the development and fabrication of components where the use of mass production techniques could reduce component and overall unit cost.

Two compact heat and mass exchanger configurations are investigated as part of this study. They include modular microscale, and compact shell-and-tube heat exchanger

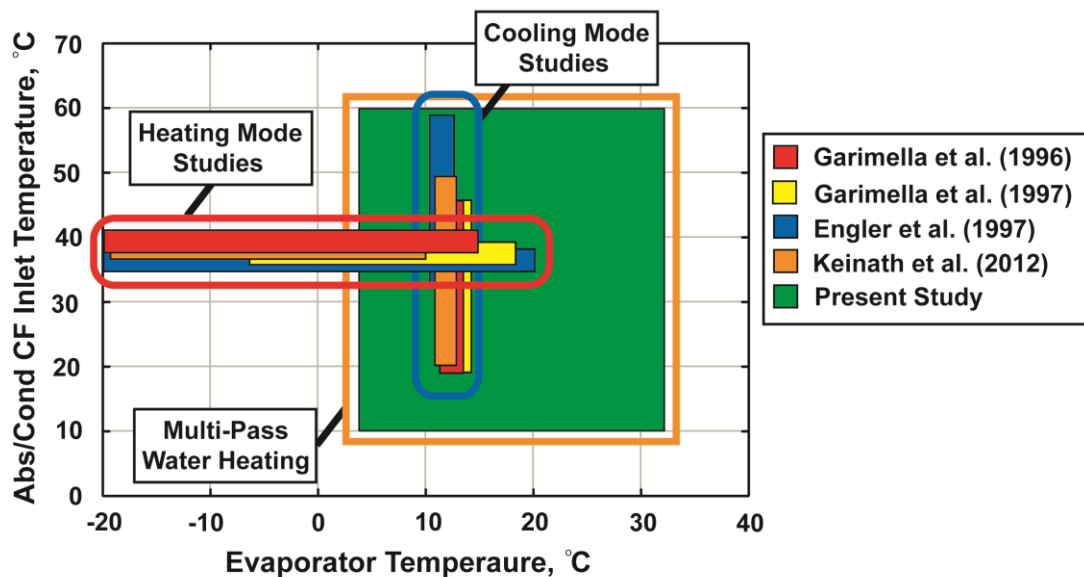


Figure 1.2: Operating conditions for cooling, heating and multi-pass water heating

designs. Microscale heat and mass exchangers are modular, scalable, and robust. They are fabricated in a multistep process that involves photochemical etching, electrostatic plating, and vacuum brazing. This design allows for integration of multiple components and even an entire system as shown by Determan and Garimella (2012). The compact shell-and-tube heat exchangers are bonded in a similar manner that requires brazing in a vacuum furnace.

Figure 1.3 is a schematic of a set of thin sheets of metal (shims) and an example of stacked shims with alternating microscale flow passages. Shim A allows for flow of the ammonia-water solution, while the passages in Shim B carry the coupling fluid. The versatility of the design allows for application to all of the absorption system components. The capacity of the heat exchanger can be changed by varying the number of channels, channel length and number of shims. High convective heat transfer coefficients are achieved in this design due to the low hydraulic diameter of approximately 0.442 mm. Pressure drop in these heat exchangers is mitigated by

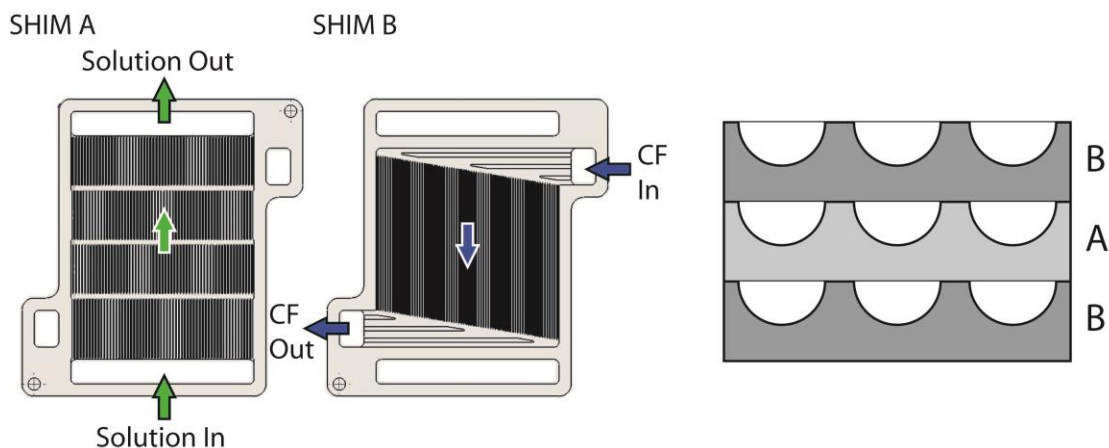


Figure 1.3: Schematic of an alternating shim assembly

increasing the number of shims or the number of channels in parallel. The alternating shim assembly allows for heat to be transferred between adjacent shims above and below. Figure 1.4 is a general schematic of a direct-fired desorber. Flue gases from combustion flow through a bundle of small flue tubes while solution flows counter current on the shell side of the heat and mass exchangers. Tubes with larger diameters are used in this design to reduce the pressure drop experienced by the flue gas across the heat exchanger. Unlike a typical shell-and-tube heat exchanger, there are two ports located near the top of the component: one for concentrated solution flow into the unit and another for refrigerant vapor flow out. Dilute solution flows out the bottom of the component. This design allows for a compact geometry while meeting flue gas side pressure drop requirements.

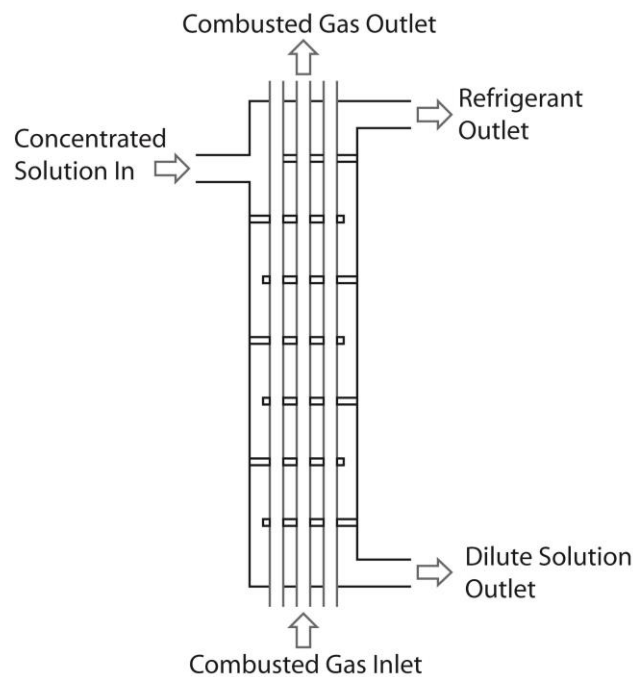


Figure 1.4: Schematic of the direct gas-fired desorber

1.4 Present Investigation

The present study seeks to make contributions to three topics: water heating, absorption heat pumps, and compact heat and mass exchangers, leading to the development of a novel, compact, gas-fired absorption heat pump water heater. Current water heater technology is approaching a fundamental *COP* limit of 1, and alternative technologies should be pursued to achieve further improvement. Energy and cost comparisons show that heat pumps have the potential address this need. While thermally driven heat pumps could serve as drop-in replacements for approximately 50 percent of the current market, there is no commercially available unit. Research specific to this application is needed to develop thermally driven systems as water heaters. The use of compact heat and mass exchangers could improve the potential for commercialization by reducing size and cost. Results from this study will further the base knowledge and development of thermally driven heat pumps as an option for high efficiency water heating.

1.5 Research Objectives

The specific objectives of the present study are as follows:

- Design and optimize an absorption heat pump system for residential water heating, and simulate its performance over a range of conditions.
- Design, fabricate, and experimentally investigate microchannel heat and mass exchangers for water heating.
- Design and fabricate a packaged direct-fired water heater prototype using monolithic assembly of several heat and mass exchangers.

- Evaluate the heating performance of the prototype over the range of expected water temperatures.

1.6 Structure of this Dissertation

The structure of this dissertation is as follows:

- **Chapter 2: Modeling of the ammonia-water heat pump water heater and storage tank for residential applications** – A detailed model of the gas-fired heat pump for multipass water heater is developed. The heat pump is optimized for baseline water inlet and ambient temperatures of 32°C and 20°C, respectively. Performance is investigated for a range of water inlet (14-60°C) and ambient (4-32°C) temperatures. System performance with a 227 liter storage tank is predicted for three scenarios: a cold start, response to a 76 liter draw, and response to stand-by losses.
- **Chapter 3: Breadboard evaluation of compact heat and mass exchangers for the absorption heat pump water heater** – Microchannel heat and mass exchangers are designed and fabricated using the state points from the cycle model presented in Chapter 2. The components are installed on a breadboard test facility where they are evaluated as part of a complete direct gas-fired absorption heat pump. Component and system level performance is evaluated by comparing results with those predicted by the system and component level models. Needed refinements to the heat and mass exchanges are determined based on the experimental study.
- **Chapter 4: Integrated packaged heat pump water heater prototype using compact heat and mass exchangers** – Refined heat and mass exchanger designed and presented in Chapter 3 are used in the development of a monolithic microchannel unit. The monolithic unit is integrated into a complete packaged prototype unit.

Performance of the prototype is optimized at the baseline conditions established in Chapter 2. Performance is investigated over water inlet (10-60°C) and ambient (10-32°C) temperature ranges. A model prediction-to-measured values comparison for the range of conditions investigated is performed.

- **Chapter 5: Energy and cost comparison of residential water heating technologies**
 - An annual energy use and operating cost comparison is performed between commercially available technologies and the gas-fired heat pump water heating system under development. Simple payback periods are calculated with respect to direct heated systems (electric resistance and non-condensing gas storage), as well as total lifetime cost and the impact of different daily draw volumes.
- **Chapter 6: Conclusions and Recommendations** – Important conclusions from the results and findings of this investigations are presented. Recommendations for future work are made.

CHAPTER 2. MODELING OF THE AMMONIA-WATER HEAT PUMP WATER HEATER AND STORAGE TANK FOR RESIDENTIAL APPLICATIONS

2.1 Introduction

2.1.1 Background

In 2009, manufacturers shipped eight million water heaters in the United States, one million of which were rated as Energy-Star[®] appliances. Water heating is the second largest energy consumer in households, accounting for 17% of total energy usage (Ryan 2010), making it a an ideal opportunity for the development of energy efficient systems. The ability to heat water more efficiently would allow for a significant reduction in household energy demand, and has led to increased interest in efficient water heaters at residential and light-commercial capacities. Investigations are being performed to improve upon gas-fired, electric-resistance, and electrically driven heat pump water heaters, as well as to evaluate thermally driven heat pump water heaters.

As there are a multitude of water heater designs, each system is evaluated with a standardized test to specify an Energy Factor (*EF*) rating. The Energy Factor is the overall efficiency of a water heater based on the energy used to produce and maintain hot water during a typical day. The Energy Factor is calculated based on the results of the 24-hour test. Testing procedures, installation, instrumentation and evaluation of results are specified by the US Department of Energy. System design and controls are targeted to maximize EF values. The Energy Factor is calculated using Equation 2.1 (DoE 2015a).

$$EF = \sum_{i=1}^6 \frac{m_i \cdot c_{pi} \cdot (57.2^{\circ}C - 14.4^{\circ}C)}{Q_{dm}} \quad (2.1)$$

Where Q_{dm} is the modified daily water heating energy consumed.

Most of the current water heating technologies have Energy Factors less than one. These technologies include electric resistance, high efficiency gas storage, whole-home gas tankless, and gas condensing water heaters. Solar thermal and heat pump water heaters are alternatives to these more common water heating technologies. Heat pumps outperform conventional water heater designs as they have Energy Factors greater than one. It should be noted that electrically driven vapor-compression heat pump water heaters are commercially available, while thermally driven heat pumps are under development for the residential market. Both heat pump designs offer a substantial improvement in efficiency when compared to conventional water heating methods because they augment the supplied heat with heat extracted from the ambient, allowing them to achieve efficiencies greater than one. The present modeling study focuses on thermally driven heat pumps. The corresponding Energy Factor is not estimated for the system under investigation because its value depends to some extent on the system controls, implementation and in situ performance of an actual heat pump water heater system. However, performance indicators are used to gauge system performance compared to other water heating systems. The Coefficient of Performance (*COP*) is used to characterize system performance. The heating *COP* is a measure of the desired heat provided over the driving input energy required.

The heating coefficient of performance (*COP*) of a thermally driven heat pump is typically lower than that of an electrically driven heat pump. However, electrically driven heat pumps use electricity as the primary energy input. After correcting for the thermal-to-electrical conversion associated with the use of electrical energy, the thermally driven

heat pump has a better overall efficiency. As an example, consider electrically and thermally driven heat pumps with nominal *COPs* of 3 and 1.5, respectively. Accounting for the thermal-to-electric conversion with a factor of 0.318 (DoE 2013) results in primary energy *COPs* of 0.96 and 1.5 for the electrically and thermally driven heat pumps, respectively.

The present study investigates the performance of a thermally driven heat pump water heater for several expected water heating scenarios. While *EF* ratings are not estimated, the efficiency of the water heater, which is a major factor in this rating, is highlighted. The absorption heat pump that is the primary driver for the water heater under consideration, is explored in detail here.

2.1.2 Prior Work

2.1.2.1 *Water Heating Technologies*

Investigations on the various water heater technologies mentioned above are available in the literature. Schoenbauer *et al.* (2011) investigated the use of gas-fired storage water heaters, instantaneous water heaters, and condensing instantaneous water heaters for residential applications by performing field tests in ten households. The 15-month study allowed for the evaluation of each water heater unit and showed that instantaneous water heaters yielded a reduction in operational costs when compared to the standard gas-fired storage unit. However, the high installation cost and a lengthy payback period make the instantaneous units economically undesirable. The study also highlights discrepancies between the *in situ* and rated Energy Factors. In this study, all of the water heaters performed below their *EF* ratings, in part because draw patterns for each household were found to be different than that used in the *EF* rating test. They noted solar-thermal and

heat pump water heaters as potential alternatives to the systems investigated in their study. Minimum water heater EF values for Energy StarTM rating are established by the Department of Energy. To be Energy StarTM qualified, gas storage and gas instantaneous water heaters must have EF values of 0.67 and 0.82, respectively (DoE 2015d).

Zogg *et al.* (2005) presented a brief discussion of the advantages and limiting factors of electrically-driven heat pump water heaters that are an alternative to electric resistance heaters and offer a 40-60% reduction in electricity usage. The limiting factors highlighted by them are the high installation cost, fan noise, and limited market share. Zogg *et al.* (2007) further discussed the potential of carbon dioxide heat pump water heaters by highlighting additional benefits that include the potential to heat water in a single pass, the ability to reach higher water temperatures, and possible work recovery from the expansion process.

Goodman *et al.* (2011a) experimentally and analytically investigated a transcritical carbon dioxide heat pump water heater. Component models were developed and validated experimentally for the gas cooler, evaporator, and suction line heat exchanger (*SLHX*). Using these models, Goodman *et al.* (2011b) developed a system level model for a residential application and used it to investigate the effect of the suction line heat exchanger, and compare the performance of once-through and recirculating systems. Their results showed that the once-through system outperformed the recirculating system with and without the suction line heater exchanger by an average of 15.2 and 10.2%, respectively.

Solar water heating has also been a focus of investigations into alternative water heating techniques. Much like heat pump systems, high capital costs have limited solar heating systems penetration in the water heater market (Cassard *et al.* 2011). Cassard *et al.* (2011) investigated the economic feasibility of solar water heaters for locations across the United States. They simulated system performance at each location using the Solar Advisor Model developed by the National Renewable Energy Laboratory (NREL 2010). The model allowed for the calculation of electric utility savings, and was used in the calculation of the capital cost required for the system to break even at the end of its projected life cycle. They found that these systems could reduce electric energy usage by up to 85% depending on the region, allowing for a savings of 1600 to >2600 kWh for a typical household. They found that solar water heating systems have the most potential to break even in the Northeast where electric utility costs are high, or in the Southwest where there is substantial solar irradiation.

2.1.2.2 Absorption Heat Pumps

Several studies on absorption heat pumps have been conducted by various investigators for a range capacities and configurations. Engler *et al.* (1997) showed that maximizing heat recovery within an absorption system leads to improved system *COP*. A basic single-effect cycle, a single-effect cycle with a refrigerant pre-cooler, multiple absorber heat exchange cycles, and multiple Generator-Absorber Heat Exchange (GAX) cycles were investigated in this study, with *COPs* ranging from 0.50 for the simplest cycle to 1.08 for the most complex. Cheung *et al.* (1996) evaluated 11 multistage, multi-effect absorption cycles for space conditioning applications. They found that performance degradation resulting from a changing ambient was more severe in the more complex

systems. They also noted that increased system complexity leads to higher *COPs*. Garimella *et al.* (1996) investigated a GAX cycle for space-conditioning applications. Their model showed the system achieving a cooling *COP* of 0.93 at 35°C and a heating *COP* of 1.51 at 8°C.

The above studies are all examples of absorption heat pump investigations with a focus on heating and cooling for space-conditioning applications. System capacities for those systems are larger than what is required for the residential or light-commercial water heating applications. Studies with a focus on water heating are limited, and heating mode evaluations in the space-conditioning studies do not adequately evaluate the unique aspects of absorption systems for water heating. In the water heating application, multiple passes are required to heat the water from an initial to final temperature. The absorption heat pump experiences a range of absorber, condenser, and possibly evaporator conditions during the heating process. Evaluation of each pass is required to achieve a realistic representation of the system. The present study conducts a comprehensive investigation of the performance of a direct gas-fired single-effect ammonia-water absorption heat pump for residential water heating.

The investigations discussed above offer some insight into commercially available water heating technologies and improvements to facilitate market penetration. Heat pumps have been studied by some investigators, but for water heating, these investigations have focused primarily on electrically driven vapor-compression heat pumps. On the other hand, the investigations on thermally driven heat pumps have been for space-conditioning applications. The present study focuses on the investigation of a compact single-effect absorption heat pump for water heating in residential settings.

2.2 System Description

A schematic of the direct gas-fired single-effect ammonia-water absorption heat pump water heater investigated in the present study is shown in Figure 2.1. The system consists of a main absorption loop and auxiliary coupling loops for the absorber, condenser, and evaporator. The absorber and condenser are connected to an auxiliary loop that provides heat to a water storage tank. Ammonia-water is selected as the working fluid for this investigation because the Lithium Bromide-Water pair is prone to crystallization at high temperatures and concentrations that could be experienced in the direct gas-fired desorber. Potential freezing of refrigerant water at the low ambient operating conditions is also a disadvantage of the LiBr-H₂O pair. In addition, the high specific volume of water vapor at the evaporator conditions leads to excessive pressure loss, effectively ruling it out for use in a compact system.

2.2.1 Main Loop

Referring to Figure 2.1, concentrated solution reaches saturation in the absorber at (1). The solution is then subcooled before exiting the absorber at (2). The solution is then pumped to the high-side system pressure across the pump, from (3) and (4). The rectifier is cooled by this concentrated solution stream, (5) to (6). The solution is then recuperatively heated in the solution heat exchanger, (7) to (8), before mixing with the rectifier reflux at (9). Concentrated solution enters the desorber where the generated vapor flows counter-current to the falling solution. Dilute solution exits the desorber at (11), while the generated vapor exits at (14). The dilute solution exchanges heat with the concentrated solution stream in the solution heat exchanger, (12) to (13), before flowing across an expansion device and mixing with refrigerant vapor at the absorber inlet, (27).

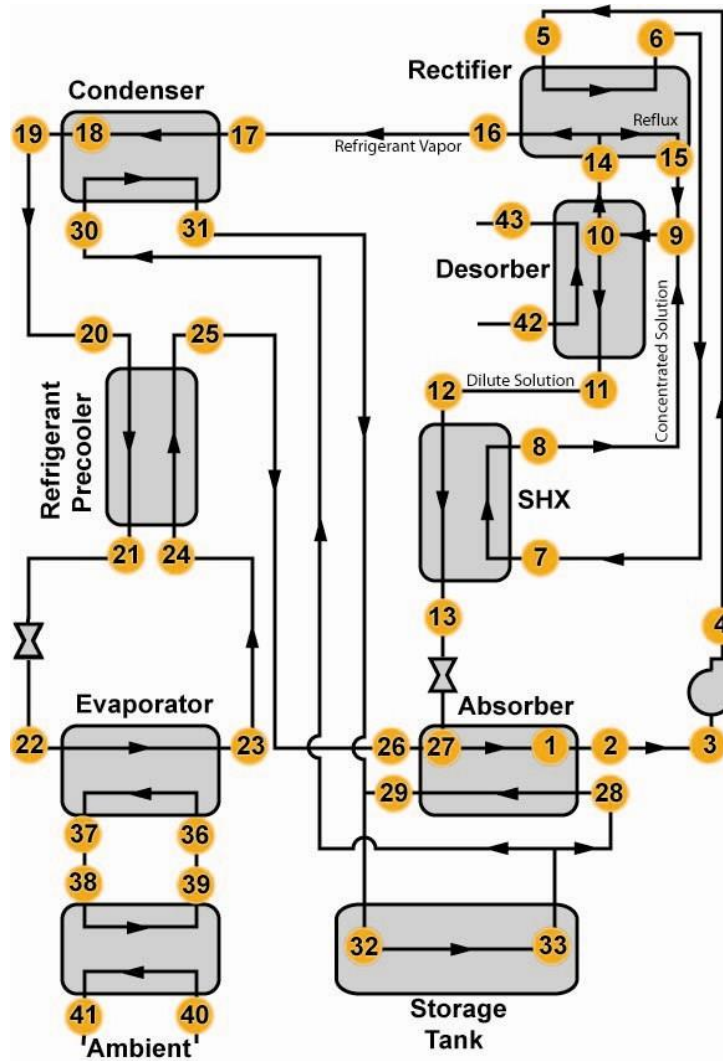


Figure 2.1: Schematic of the gas-fired single-effect absorption heat pump water heater

Vapor that exits the desorber flows to the rectifier (14), where water is selectively condensed to increase the refrigerant vapor purity. The liquid reflux exits the rectifier at (15) and mixes with the concentrated solution stream at (9). Refrigerant vapor exits the rectifier at (16) and flows into the condenser at (17). The refrigerant is condensed to a saturated liquid at (18) and exits as a slightly subcooled liquid at (19). The refrigerant is further subcooled in the refrigerant precooler, (20) to (21), before flowing through an expansion device. The refrigerant stream evaporates from (22) to (23) in the evaporator.

Upon exiting the evaporator, the refrigerant recuperatively cools the same stream exiting the condenser in the refrigerant precooler, (24) to (25). The refrigerant then enters the absorber at (26) and mixes with the dilute solution at (27). Heating is provided as the refrigerant is absorbed in the dilute solution stream to complete the cycle.

2.2.2 Auxiliary Loops

The absorber and condenser are coupled hydronically in parallel to the hot water storage tank. The hydronic fluid enters that storage tank at (32) and exits at (33) and is split with one half flowing through the absorber, (28) to (29), and the other half flowing through the condenser, (30) to (31). A parallel configuration was selected because it limits the ammonia-water high-side operating pressures while still allowing for high system performance.

The desorber is directly heated by the combustion of natural gas, which flows counter-current to the solution from (42) to (43). The stream of flue gases from combustion provides the necessary heat for the desorption of refrigerant from the ammonia-water solution. In the evaporator, the coupling fluid (propylene glycol-water) is cooled from (36) to (37) before entering a cross-flow air coupled heat exchanger, where it is heated from (38) to (39). The ambient air is cooled over the cross-flow heater exchanger from (40) to (41).

2.3 Modeling Approach

The system described above was modeled using *Engineering Equation Solver* (EES) (Klein 2014) platform. Mass, species, and energy conservation equations were used to analyze each component in the system. Because ammonia-water is a binary mixture, three independent properties were required to establish each state point. Heat transfer

resistances were taken into account with the specification of overall heat conductance, UA , for each heat exchanger. Baseline UA values for each component were calculated initially using reasonable assumptions for the closest approach temperature (CAT) or heat exchanger effectiveness for each component. The resulting UA values were then used as specifications for the system model. After analyzing the baseline system (water inlet temperature of 32°C , ambient temperature of 20°C), parametric analyses were conducted to maximize the system COP . System response to changes in UA values and other key parameters was assessed to achieve progressive improvements in COP . Each parameter was varied by $\pm 15\%$ with the remaining inputs held constant. Plots of system response to variations in each parameter were used to select the final UAs and other key parameter values. The set of parameter values selected with this process were then used to understand the effect of operating conditions and other settings such as solution and hydronic fluid flow rates. Because UA values are representative of component sizes, the UAs were used as indicators of capital cost, and components with low sensitivities were assigned relatively lower values while still not adversely affecting system performance.

For the baseline system, the ambient, exhaust inlet, and absorber and condenser coupling fluid inlet temperatures were set. The coupling fluid flow rates and the concentrated solution flow rate were also set at predetermined values to represent the operation of an actual system. Other flow rates such as the dilute solution and refrigerant flow rates were computed based on these specifications, as well as the respective mass, species, and energy balances.

The inlet temperature and flow rate for the condenser and absorber were set to 32°C and 0.047 kg s^{-1} . A 2.0 K subcooling was assumed in the absorber and condenser. The

ambient heat exchanger was supplied with air at 20°C and a relative humidity of 50%. The air flow rate was set to 0.224 kg s⁻¹. The properties of the ambient air were selected based on nominal U.S. Department of Energy residential water heater test conditions (DoE 2015a). The hydronic loop flow rate between the ambient heat exchanger and the evaporator was set to 0.096 kg s⁻¹. The temperature glide in the evaporator was set at 2.0 K; lower glides lead to substantially incomplete evaporation and lower duties, while higher glides lead to temperature pinches and poor heat extraction from the ambient. A summary of these parameters is presented in Table 2.1.

2.4 Baseline System Results

Baseline conditions were established for the absorption heat pump water heater using the design input parameters and assumptions discussed above. The concentrated solution flow rate was set to 0.0022 kg s⁻¹, and the dilute solution and refrigerant flow rates were calculated to be 0.0012 and 0.0010 kg s⁻¹, respectively. The concentrated solution, dilute solution, and refrigerant concentrations were 0.59, 0.25 and 0.998, respectively. The high

Table 2.1: Cycle model design specifications

Component	UA, W K ⁻¹	Coupling Fluid		Duty, W
		Flow Rate, kg s ⁻¹	Inlet Temperature, °C	
Absorber	140	0.047	32	1,620
Ambient Heat Exchanger	800	0.096	14	1,180
Condenser	250	0.047	32	1,170
Desorber	3.0			1,610
Evaporator	475	0.096	17	1,180
Rectifier	4.4			133
Refrigerant Heat Exchanger	20			88.2
Solution Heat Exchanger	20			448
Pump				3.00

Bold values are calculated values based on the set parameters.

and low pressures of the system were 1590 and 634 kPa, respectively. The absorber and condenser received the hydronic coupling fluid at 32°C and delivered it at 39°C. This temperature rise represents one of several passes required to heat the water from 14.5 to 57.0°C. Air exiting the ambient heat exchanger is at 14.8°C, and a relative humidity of 69.3%. Flue gas exits the desorber at 204°C. For the base case, the absorption system receives 1.6 kW of heat from the flue gases at the desorber, and provides 2.79 kW of heating, which corresponds to a *COP* of 1.74. The heating *COP* was calculated based on Equation 2.2.

$$COP_{Heating} = \frac{Q_{Absorber} + Q_{Condenser}}{Q_{Desorber}} \quad (2.2)$$

In addition to the system heating *COP*, the total heating *COP* was also calculated and is presented in Equation 2.3. This total heating *COP* accounts for the total gas input and small electrical loads. An electrical draw of 200 W is assumed for this system. Electrical loads include power to the control system, fan and pump motors, and electronic valves.

$$COP_{TOTAL,Heating} = \frac{Q_{Absorber} + Q_{condenser}}{Q_{gas} + E_{Total}} \quad (2.3)$$

The gas input was determined using $Q_{gas} = Q_{Desorber} \div \eta_{Combustion}$, assuming an 85% combustion efficiency. E_{Total} was determined based on the operating conditions of each component to be 65 W. With the above-mentioned thermal-to-electric conversion of 3.14, this corresponds to an equivalent source-based input of 200 W. With these considerations, the total heating *COP* was determined to be 1.34. It should be noted that the total *COP* provides values that are closer to expected Energy Factor values for the

system. This is because it accounts for all of the energy input to the water heating system which is used in the Energy Factor calculations.

2.5 Parametric Analyses

System performance was investigated for a range of water and ambient air temperatures. The absorber and condenser water inlet temperatures were investigated from 14.5 to 52.2°C at three different ambient air inlet temperatures of 4.4, 20 and 32°C. The base system was designed for an ambient of 20°C, and the higher and lower temperatures are representative of potential temperatures experienced by a water heater depending on installation location and time of the year.

Figure 2.2 shows a plot of *COP* and heating duty versus the water inlet temperature for the three different ambient cases investigated. The *COP* varies from 1.46 to 1.97 for the full range of water and ambient temperatures investigated. (The corresponding total heating *COP* varies from 1.12 to 1.52 for the full range of water and ambient temperatures investigated.) The *COP* increases with increasing ambient temperature and decreasing water temperature. Higher ambient temperatures allow for more heat to be transferred in the evaporator due to the greater driving temperature difference between the ambient and refrigerant streams. Lower water temperatures allow for more refrigerant to be generated because of higher solution concentrations and lower high side pressures.

The heating capacity of the system follows a trend similar to that exhibited by the *COP*. This is expected because the heating *COP* is dependent on the heating duty. The heating duty ranges from 2.33 to 3.17 kW for the ambient and water temperatures investigated.

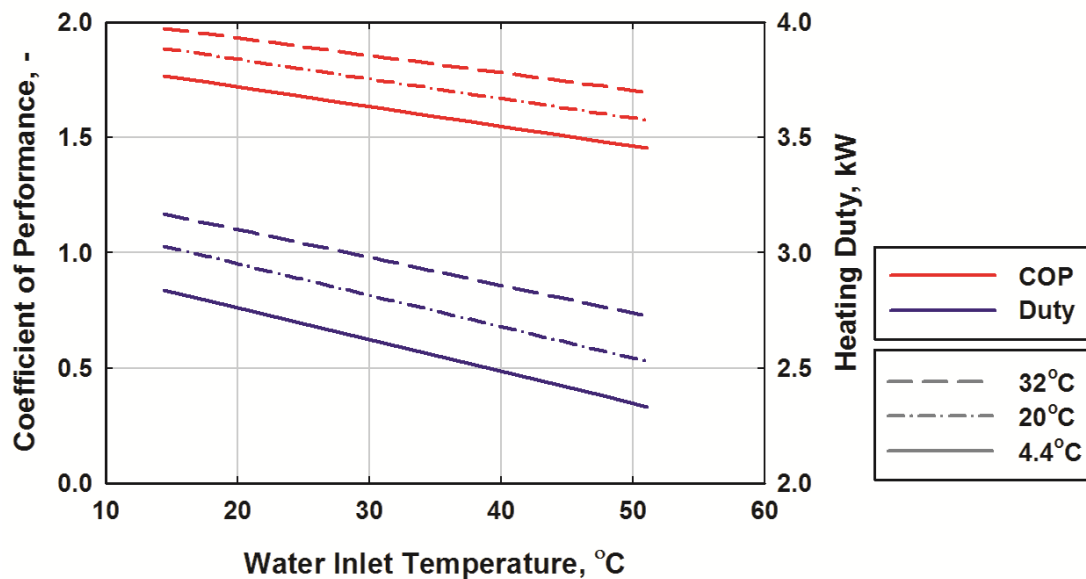


Figure 2.2: System *COP* and heating duty as a function of water inlet temperature

As water is circulated through the absorber and condenser, the operating conditions of the absorption system change at each pass. The absorption system experiences a significant change in operating pressures as a result of the change in water inlet temperature. The temperatures of absorption and condensation set the high and low pressures of the system, and are dependent on the coupling fluid temperature in the corresponding component. Figure 2.3 shows the change in pressure difference between the high and low sides of the system as a function of water inlet and ambient temperatures. The pressure difference ranges from 144 to 2011 kPa for the ambient and water temperatures investigated. During system operation, the ambient temperature is not expected to change significantly; therefore, the change in pressure difference experienced by the system will be due to increasing water temperatures. As this change happens

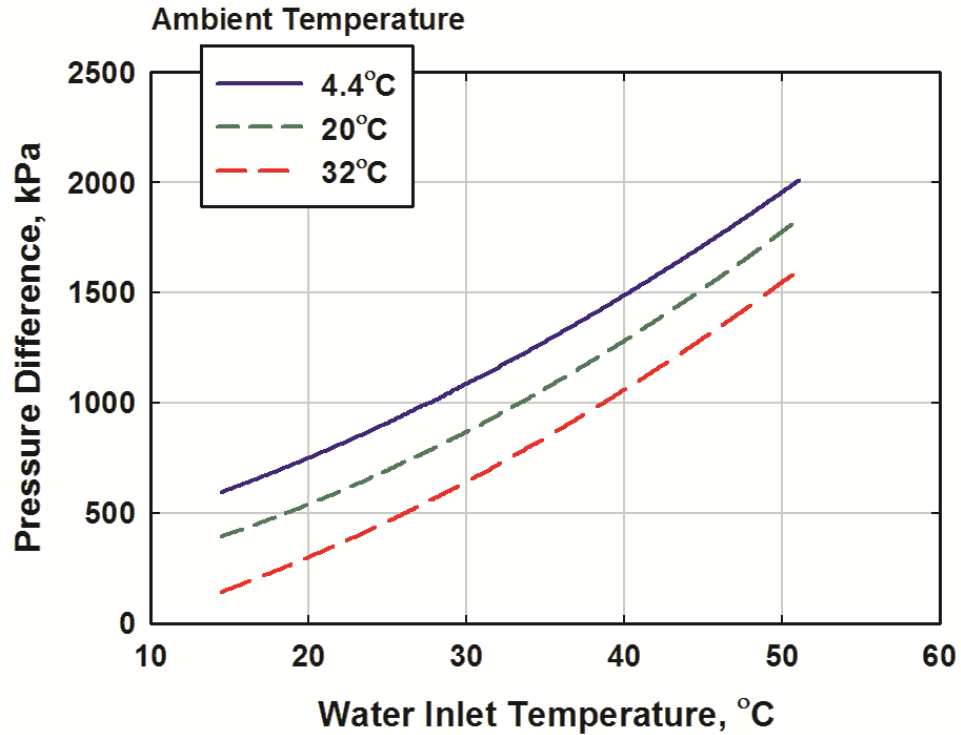


Figure 2.3: Change in high to low pressure difference

gradually during the circulation process, disruption of system operation is expected to be minimal when appropriate control strategies are applied.

In addition to the change in high to low side pressure difference, the system undergoes a significant change in solution and refrigerant concentrations. Figure 2.4 shows plots of refrigerant, concentrated solution, and dilute solution concentrations versus water inlet temperature for different ambient temperatures. For the ambient and water temperatures investigated, the refrigerant, concentrated solution and dilute solution concentrations vary from 0.9996 to 0.9615, 0.8600 to 0.3700, and 0.6800 to 0.0100, respectively. The plots show that the concentration of each stream decreases with increasing water temperatures. For higher water temperatures, the concentration of the solution exiting the absorber must be reduced to lower the low side pressure and maintain

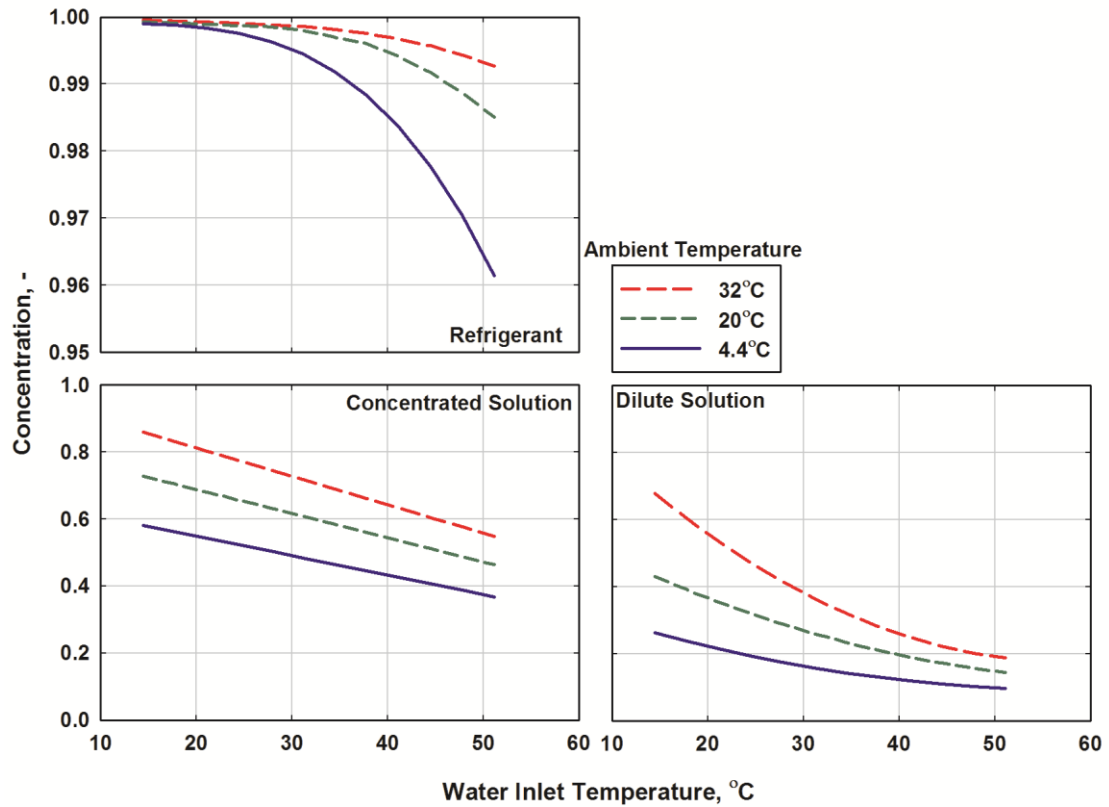


Figure 2.4: Concentration changes with water and ambient temperatures

cooling temperatures in the evaporator. The reduced concentrated solution concentration is responsible for the reduced refrigerant and dilute solution concentrations. The increase in concentration with ambient temperature is the result of a higher temperature in the evaporator. These higher temperatures allow the low side to be at higher pressures and concentrations.

Figure 2.5 shows plots of the solution and refrigerant mass flow rates for the three ambient temperatures investigated. For the ambient and water temperatures investigated, the refrigerant and dilute solution flow rates vary from 0.0013 to 0.0007 kg s⁻¹, and 0.0009 to 0.0015 kg s⁻¹, respectively. The concentrated solution flow rate was fixed at 0.0022 kg s⁻¹. The plots show that refrigerant mass flow increases with decreased water

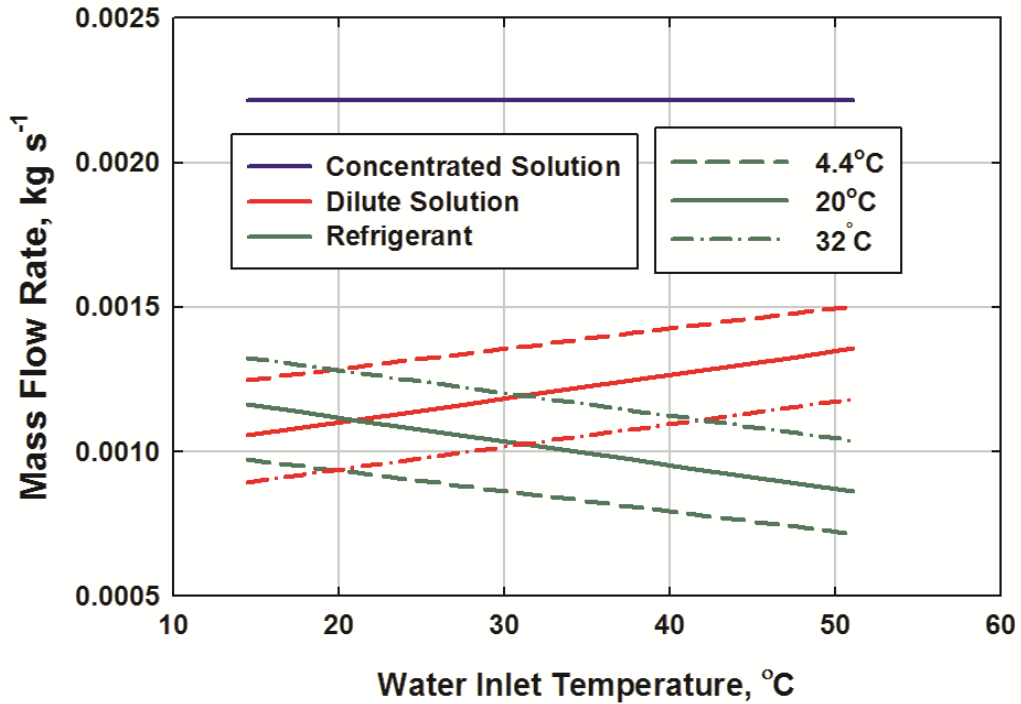


Figure 2.5: Absorption system mass flow rates

inlet temperatures. This corresponds well with the results presented in Figure 2.2, as increased refrigerant flow should correspond to increased heat duty and *COP*. Figure 2.5 further shows that increasing the ambient temperature increases refrigerant flow. This is because the increased ambient temperature allows the evaporator to operate at increased temperatures and pressures, and thus a lower lift between the low and high pressure sides of the system.

For a multi-pass water heater, the performance and heating capacity follow the trends shown in Figure 2.2. During the heating process, the absorption system experiences slowly increasing inlet temperatures because it is coupled with a large volume storage tank. The temperature change is gradual which limits disruption to system performance.

2.6 Tank Coupled Modeling

Performance of the system coupled to a residential capacity water storage tank was performed to improve understanding of the entire system. To simplify modeling efforts, a regression analysis was conducted on the absorption heat pump model results to yield equations that predict absorption system performance. These equations were used instead of the cycle model during the tank heating simulations. A 227 liter storage tank size was chosen for this study because it is representative of a residential capacity tank.

2.6.1 Heat Pump Performance Equations

Multi-axis regression analyses were performed on the modeling results presented in Figure 2.2 to yield equations for the estimation of *COP* and heat duty as a function of water inlet and ambient temperatures, as shown in Equations 2.4 and 2.5.

$$COP = a_c + b_c \cdot T_{water} + c_c \cdot T_{water}^2 + d_c \cdot T_{ambient} + e_c \cdot T_{ambient}^2 + g_c \cdot T_{ambient} \cdot T_{water} \quad (2.4)$$

$$Q_{heating} = a_d + b_d \cdot T_{water} + c_d \cdot T_{water}^2 + d_d \cdot T_{ambient} + e_d \cdot T_{ambient}^2 + g_d \cdot T_{ambient} \cdot T_{water} \quad (2.5)$$

The constants for Equations 2.4 and 2.5 are reported in Table 2.2. The R^2 values for Equations 2.4 and 2.5 are 0.9998 and 0.9995, respectively.

With the use of Equations 2.4 and 2.5, and a 227 liter water storage tank model, performance of different water heating scenarios was investigated. The scenarios included heating the tank from a cold start at 14.5°C to a minimum water temperature of 57.0°C, system response to a 76 liter draw, and response to an extended period of standby losses. For the tank model, it is assumed that the water is heated in multiple passes where the heat pump system experiences constant inlet water temperatures for extended periods of time. Water in the tank is heated from the top to the bottom allowing for the

Table 2.2: Constants for *COP* and heat duty regression analysis

Parameter	<i>COP</i>	Heat Duty
	$n = c$	$n = d$
a_n	1.8717E+00	3.0037E+00
b_n	-8.9000E-03	-1.4300E-02
c_n	3.4374E-07	2.9861E-07
d_n	5.7000E-03	9.2000E-03
e_n	3.2875E-05	5.1299E-05
g_n	3.5307E-05	5.6902E-05

maintenance of thermal stratification within the tank. The time required to heat the volume of water during the periods of quasi-steady operation was determined for each pass. The total time required to heat the water from the initial temperature of 14.5°C to above 57°C was determined from the sum of time required for each pass. Heat loss from the tank during the heating process is expected to range from approximately -15 (a gain from the surroundings) to 120 W. For the present study, it is assumed to be offset by the addition of heat from the condensation of the combusted gas exiting the desorber and passing through an in-tank heat exchanger. The heat addition from the combusted gas stream is not included in the heat duty presented above and is a function of the in-tank heat exchanger size, water temperature (10-60°C), and desorber gas outlet temperature (100-160°C) and flow rate. The heat input was estimated to be 110 W or greater for the range of expected conditions.

The tank is modeled as a cylindrical volume of water where hot water enters the top and cold water exits from the bottom. The water flows through the absorber and condenser of the absorption system where it is heated. The heated water returns to the top of the tank and thermal stratification is assumed to be maintained. A pass is considered

complete when the total tank volume has exchanged heat with the absorption system at the previous bulk inlet temperature. The water outlet temperature is determined using Equation 2.6 where Q_{heating} is a function of the water temperature into the system and the ambient temperature.

$$T_{\text{water,out}} = T_{\text{water,in}} + \frac{Q_{\text{heating}}}{\dot{m}_{\text{water}} \cdot cP_{\text{water}}} \quad (2.6)$$

This calculation provides the water outlet temperature and is used as the inlet temperature for the next pass. The total energy transferred per pass is determined using the calculated outlet temperature and Equation 2.7 where m_{water} is the mass of the water under consideration stored in the tank.

$$Q_{\text{total,step}} = m_{\text{water}} \cdot cP_{\text{water}} \cdot (T_{\text{water,out}} - T_{\text{water,in}}) \quad (2.7)$$

The energy input for each step, as well as the total energy required to heat the total volume of water to a minimum temperature of 57°C, can be determined using this procedure.

2.6.2 Cold Start

A cold start is experienced when water tanks are first installed and when all of the stored hot water has been drawn, leaving the tank completely filled with unheated water. The heating system for the tank must heat the water from the supply temperature to a minimum temperature of 57°C. Figure 2.6 shows a plot of a cold start where the water tank temperature is heated over a period of time for three ambient temperatures. The plot shows that the time required to heat a 227 liter tank to a minimum temperature of 57°C varies with the ambient temperature. This is because the higher ambient temperatures

allow for more heat to be exchanged in the evaporator component. For the data presented, the time required to heat the tank is between 3.6 and 4.3 hours, depending on the ambient conditions. This is a significant amount of time and is expected as this is a heat pump system. Evaluation of a 22 kW direct gas-fired system with a combustion efficiency of 0.85, an 11 kW electric resistance unit, and a 2.8 kW electric heat pump showed that cold-start heating times of 0.63, 1.1 and 4.2 hours would be required for the respective units. Direct heated systems are able to heat a tank more quickly but use more primary energy in the process, at a $COP < 1$. The use of a storage tank helps mitigate the risk of running out of hot water but does not eliminate the possibility of a hot water shortage. A full 227 liter tank of hot water would allow for three household occupants to shower in

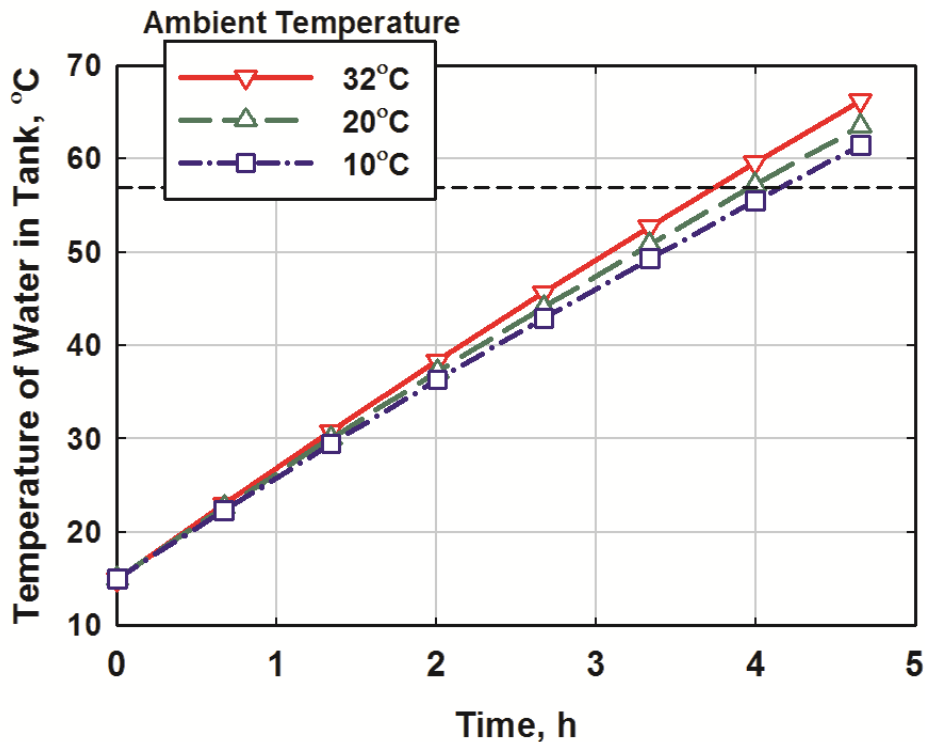


Figure 2.6: Temperature of tank during cold start

series or three loads of laundry to be completed in series with a standard washing machine. Four loads of laundry could be completed with a high-efficiency washing machine (DOE 2015b). The absorption system with the storage tank allows for this on-demand hot water and high coefficients of performance.

Figure 2.7 shows a plot of the heat pump *COP* as a function of pass number and the ambient temperature. A pass is in reference to the assumed nearly constant water inlet temperature to the heat pump system. As the water is heated in the tank, six to seven passes are required to reach the 57°C minimum for the ambient conditions investigated. The *COP* ranges from 1.97 to 1.46 for the conditions investigated. The average *COP*s for the 32, 20 and 10°C ambient cases, when heating the tank to a minimum temperature of 57°C, were determined to be 1.82, 1.73 and 1.63, respectively. The corresponding total

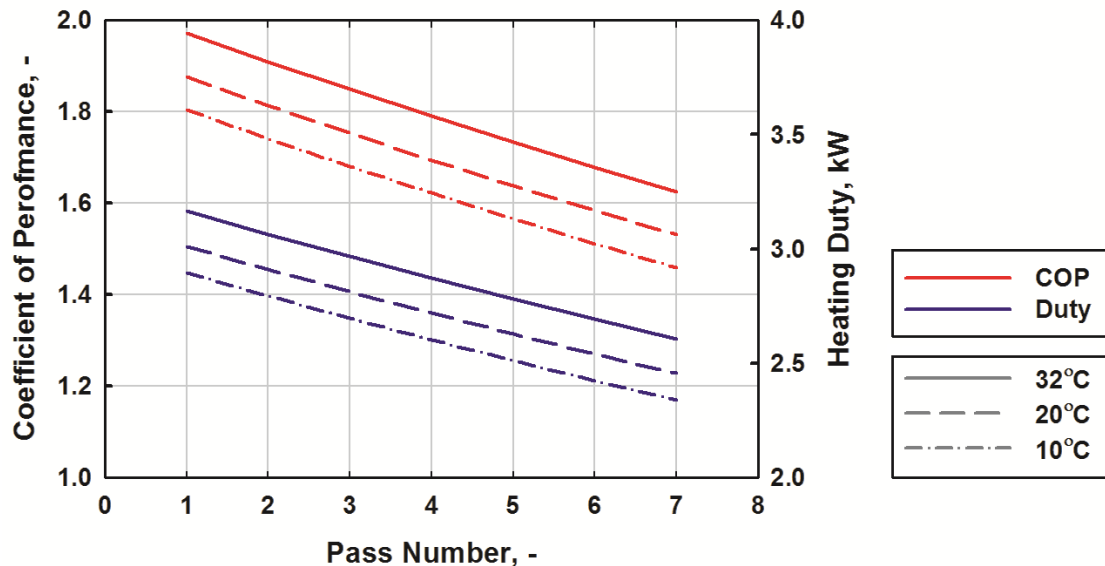


Figure 2.7: *COP* and heating duty as a function of pass number

heating *COPs* for these cases ranges from 1.52 to 1.13. These *COP* values show that there are significant gains in using a gas-fired heat pump system when compared to direct-fired systems that are limited to *COPs* below 1.

Figure 2.7 also shows the heating duty as a function of pass number and the ambient temperature. The heat duty ranges from 3.16 to 2.34 kW for the conditions investigated. The average heating duty for the 32, 20 and 10°C ambient cases, when heating the tank to a minimum temperature of 57°C, were determined to be 2.92, 2.77 and 2.61 kW, respectively. The heating capacity is inherently linked to time required to heat the water in the tank and the overall size of the system. A larger capacity heat pump would allow for the tank to be heated faster but require larger components and increased capital cost.

Figure 2.8 shows a plot of the temperature rise in the water for each pass in the water heating process for the 32°C ambient case. The step changes are representative of the temperature change experienced in each pass. The temperature rise in each pass decreases as the operating conditions for the system become less favorable and system performance decreases. Higher water temperatures into the absorption system increase operating pressures, reduce concentrated solution concentration and reduce the total heat duty. The temperature rise for the first pass is 8.0°C, while the temperature rise for the sixth pass is 6.8°C. It should be noted that each pass is the same time in length, roughly 40 minutes, as the coupling water flow rate through the absorption system and the thermal capacity are constants.

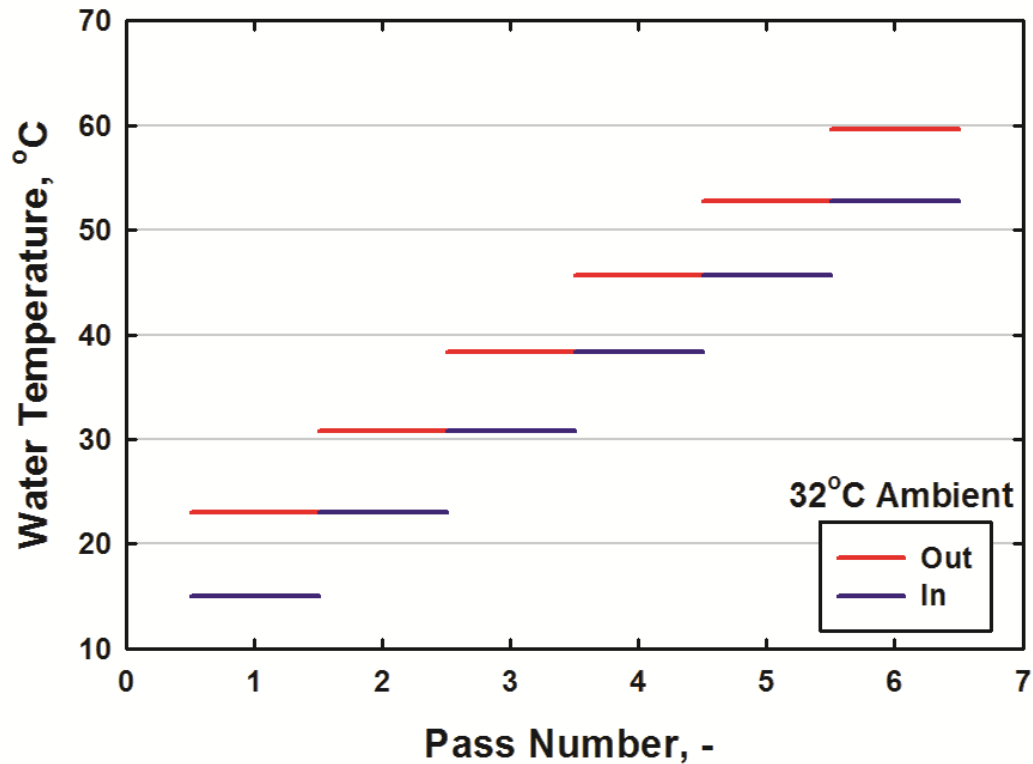


Figure 2.8: Water temperature as a function of pass number for 32°C ambient

2.6.3 Response to a 76 Liter Draw

A 76 liter draw was selected because it is approximately equivalent to a 10-15 minute shower or a cycle of standard washing machine. This draw size uses roughly 1/3 of the 227 liter storage tank. Investigating system response and performance to this draw size is important in evaluating time requirements and performance in response to typical household events. It should be noted that the water tank is assumed to have hot water drawn from the top and cold water supplied at the bottom. Thermal stratification is assumed and mixing neglected. The heat pump system is assumed to exchange heat with the bottom section of the tank, allowing it to heat the 76 liters of supplied cold water

directly. Figure 2.9 is a representative drawing of the system and tank immediately following the 76 liter draw.

Figure 2.10 shows a plot of the temperature at the bottom of the tank where 76 liters of hot water is replaced by cold water and the system response. The ambient temperature is assumed to be 20°C. The temperature drops to the cold water temperature of 14.5°C as the hot water is drawn from the top. A short stand-by period follows the draw before the heat pump starts at $t = 0$. The water is then heated in passes until it reaches at least a minimum temperature of 57°C. This is estimated to require 1.34 hours. For this case, the *COP* of the heat pump ranges from 1.88 to 1.58, with an average of 1.73. The high *COP*, in response to typical draw size, shows the potential of direct-fired heat pump water

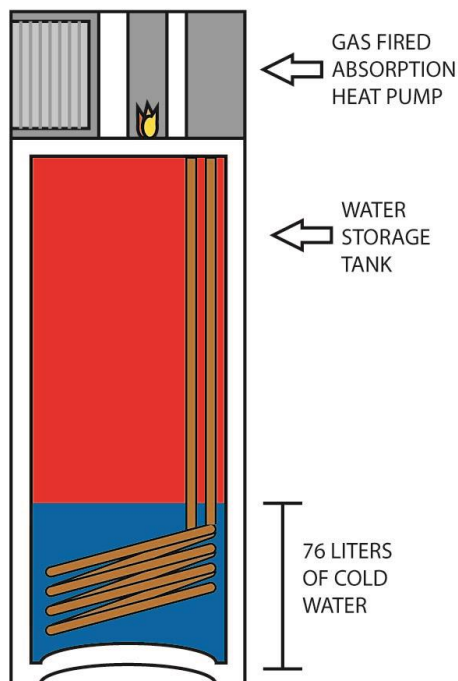


Figure 2.9: Drawing of stratified tank after 76 liter draw

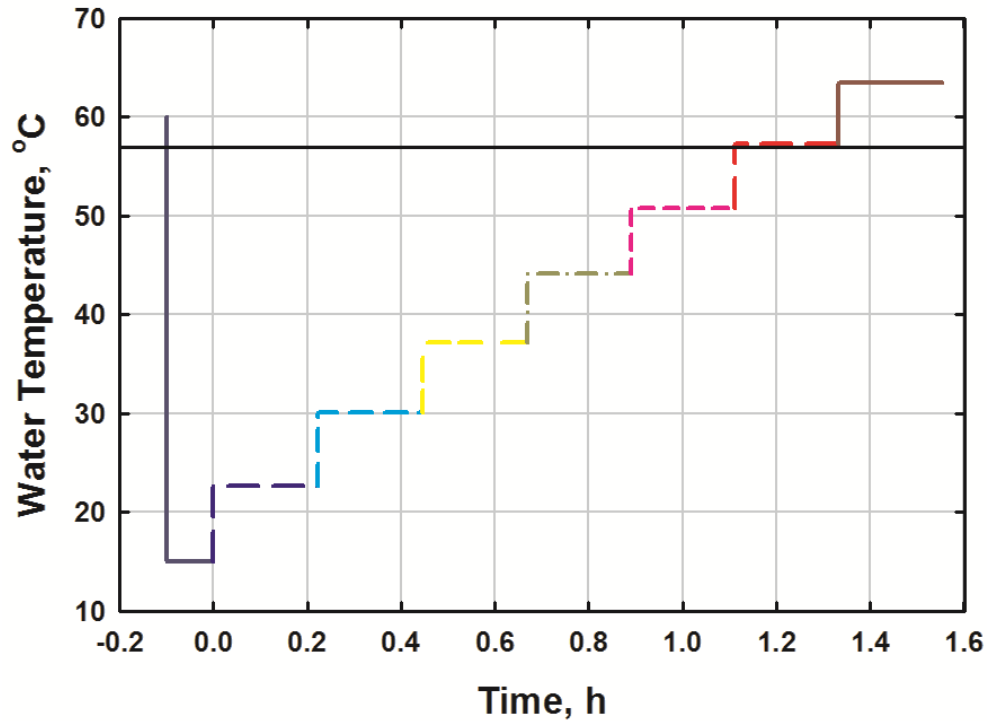


Figure 2.10: Multipass heating response to 76 liter draw

heaters under consideration in this study. The corresponding total heating *COP* ranges from 1.48 to 1.22, with an average of 1.33. In addition, the 76 liter draw scenario was evaluated for a 22 kW direct gas-fired system with a combustion efficiency of 0.85, an 11 kW electric resistance unit, and a 2.8 kW electric heat pump. Results showed that heating times of 0.21, 0.36 and 1.4 hours would be required for the respective units.

2.6.3 Stand-by Losses

The final case investigated is reheating of the tank after substantial stand-by losses have occurred. The loss of heat during periods of inactivity results in a temperature drop in the water in the tank. This heat loss is minimized by insulating the water tank. The thermal loss rate presented is representative and meant to provide context for the

reheating scenario. It should be noted that insulation type and thickness are major factors in determining this loss rate and would be selected during performance versus cost optimization of an actual installation of the overall system. The water heating system will be equipped with temperature settings that call for heat when the bulk water temperature drops below a certain value. For the case investigated, the bulk temperature limit is assumed to be 50°C. Figure 2.11 shows a plot of system in a stand-by period where the bulk tank temperature drops from 60 to 50°C at an ambient temperature of 20°C. The heat pump system is activated when the bulk tank temperature reaches the 50°C and heats the entire 227 liter tank back to a minimum of 57°C in two passes. The time required to heat the tank from 50°C to a minimum of 57°C is 0.72 hours. The average *COP* during this reheat is 1.57. The average total heating *COP* during the reheat is 1.21. Evaluation of a 22 kW direct gas-fired system with a combustion efficiency of 0.85, an 11 kW electric resistance unit, and a 2.8 kW electric heat pump showed that heating times of 0.10, 0.17 and 0.73 hours would be required to compensate for the standby losses for the respective units. The performance for this case is higher than that of a direct-fired system but is the lowest of the three scenarios investigated. Maximizing water tank insulation to reduce heat loss will minimize the need for operation in this reheat mode.

2.7 Conclusions

A detailed investigation of a direct gas-fired single-effect ammonia-water absorption heat pump water heater was performed in this study. The system was sized for a residential application and achieved much better performance compared to commercially available technologies. The system offers higher primary energy based *COPs* than direct gas-fired and electric resistance systems. It is competitive with the electrically driven heat

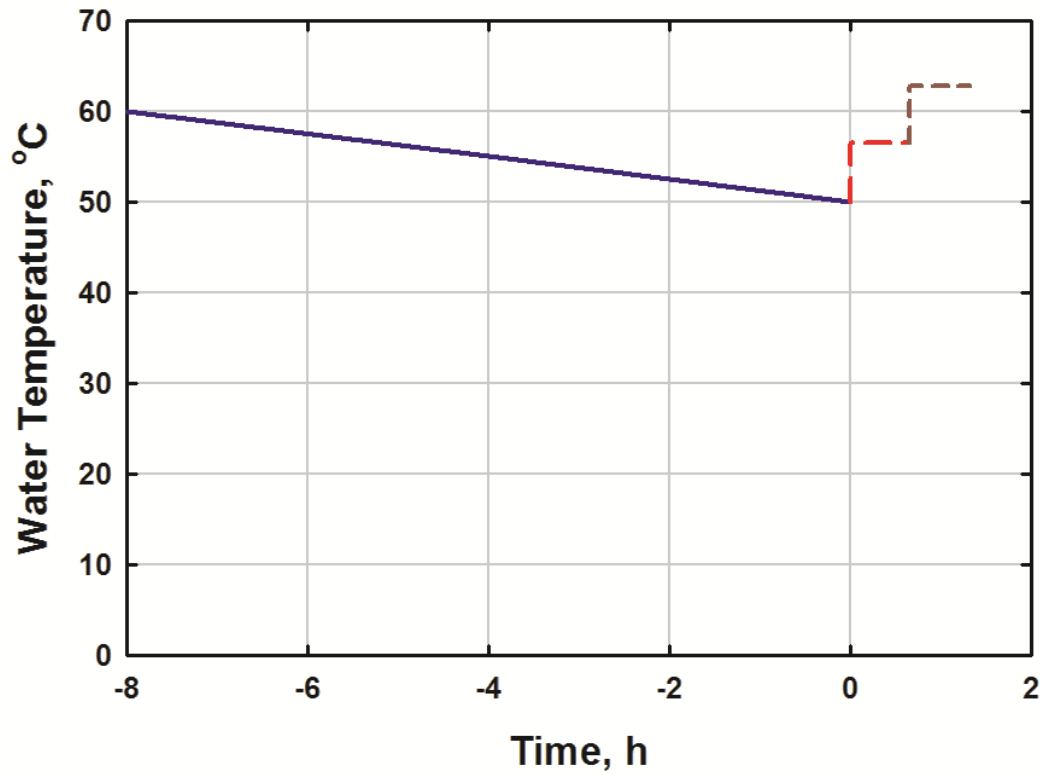


Figure 2.11: Multipass heating response to stand-by losses

pumps, particularly when accounting for thermal-to-electrical conversion efficiencies. The baseline system can achieve a heating duty of 2.79 kW and a *COP* of 1.74 at ambient and water inlet temperatures of 20°C and 32°C, respectively. The average *COP* and heating duty when heating water from 14.5 to a minimum temperature of 57°C were 1.73 and 2.77 kW, respectively. The system experiences significant pressure, concentration, and flow changes during the heating process, but this not expected to disrupt operation because the change would be gradual due to the use of the water storage tank.

The Energy Factor for this system was not determined, but the total heating *COP* was calculated for each scenario in addition to the system *COP*. This term accounts for the

total gas input and auxiliary electric requirements of the heat pump system. The system achieved a total heating *COP* of 1.34 at baseline conditions. The total heating *COP* value is more representative of a packaged unit, while the reported system *COP* is only for the absorption system.

System performance was also investigated in combination with a 227 liter storage tank model for three different heating scenarios: a cold start, response to a 76 liter draw, and response to stand-by losses. The system maintains high coefficients of performance for each case with *COP* values between 1.97 and 1.46. Minimizing stand-by losses will help maximize overall system performance. The time required for the system to heat water from cold start conditions is high compared to gas-fired and electric resistance water heaters, but decreasing this duration would require larger and more expensive components. Also, the higher *COPs* of this system compared to gas-fired water heaters compensates for this drawback, which is in fact mitigated by the thermal storage in the hot water storage tank. The system under consideration represents one of the first high-performance absorption heat pumps tailored specifically to small capacity water heating applications.

CHAPTER 3. **BREADBOARD EVALUATION OF COMPACT HEAT AND MASS EXCHANGERS FOR THE ABSORPTION HEAT PUMP WATER HEATER**

3.1 Introduction

3.1.1 Background

Absorption heat pumps are thermally driven systems that can be designed to meet cooling and heating needs of many applications. In a typical heating mode application, these systems achieve coefficients of performance (*COPs*) above one. They use natural working fluids, unlike vapor-compression heat pump systems that use synthetic refrigerants with high global warming potentials. In addition, absorption systems are thermally driven; therefore, they can reduce electrical utility demand, especially during peak hours. However, absorption systems have thus far seen limited implementation in the small-capacity residential and light commercial applications due to large conventional component size and high capital cost.

The development of more compact, mass producible heat and mass exchangers is essential to the successful implementation of absorption systems in residential and light commercial applications. Residential water heating is one area of potential success for absorption systems. Standard water heaters are limited to *COPs* less than one because they are direct heated systems. Heat pumps offer performance improvements over current systems as they achieve heating *COPs* greater than one.

This chapter presents results of an experimental investigation of an ammonia-water absorption heat pump using microchannel heat and mass exchangers for residential water heating. Discrete components are installed on a breadboard test facility and evaluated

individually and as part of a complete system. The potential success of microchannel heat and mass exchangers for residential and light commercial applications is assessed.

3.1.2 Prior Work

The success of residential and light commercial capacity absorption systems is dependent on the development of compact and cost effective heat and mass exchangers. Significant research efforts have been taken to develop components for these small capacity systems. A brief review of these research efforts follows.

While large-capacity absorption chillers have used falling-film configurations for a variety of components, novel microchannel-based configurations suitable for implementation in small-capacity absorption systems have begun to be investigated over the past few years. Garimella (1999) proposed a microchannel array with an alternating lattice structure of nominal 1 mm diameter tubes for use as an absorber for a residential capacity absorber. Vapor was introduced at the bottom of the array, and exchanged heat and mass with the dilute solution flowing over the microchannel array and the heat of absorption being removed by coolant flowing in multiple passes through the tubes. This configuration was first demonstrated experimentally by Meacham and Garimella (2003) and subsequently by Meacham and Garimella (2004) with an improved design based on insights from flow visualization that accounted for potential maldistribution in the distribution tray above the tube array. Using a heat transfer area of 0.456 m^2 with a tube array envelope of $0.162 \times 0.157 \times 0.15 \text{ m}$, the revised absorber transferred absorption duties as high as 15.1 kW. Heat transfer coefficients of up to $1650 \text{ W m}^{-2} \text{ K}^{-1}$ were achieved on the working fluid absorption side. With minor modifications to the design first tested by Meacham and Garimella (2003), i.e., simply replacing the distributor tray

with one that allowed vapor escape routes, and flowing hot coupling fluid through the microchannel tubes, Determan and Garimella (2011) demonstrated the use of this same geometry as a desorber for a residential capacity absorption heat pump. This component, with a tube array envelope of $0.178 \times 0.178 \times 0.508$ m and a surface area of 1.9 m^2 transferred up to 17.5 kW and yielded desorption-side heat transfer coefficients between $659 \text{ W m}^{-2} \text{ K}^{-1}$ and $1795 \text{ W m}^{-2} \text{ K}^{-1}$. Lee *et al.* (2012) incorporated a small diameter tube absorber into a full absorption chiller breadboard test facility and demonstrated its effectiveness in facilitating absorption over a wide range of heating mode and cooling mode conditions with absorber pressures of 150, 345 and 500 kPa at varying desorber outlet concentrations (5-40%) and solution flow rates ($0.019\text{-}0.034 \text{ kg s}^{-1}$). Garimella *et al.* (2011) used the insights gathered from these studies to propose such microchannel array components as a uniformly effective miniaturization technology for all components of an absorption chiller. Essentially, the same falling-film tube array configuration could be used for a desorber, absorber, condenser and evaporator, and even for recuperative components within the system. Their system level design and fabrication analyses showed that compact absorption systems could be achieved with similar component designs and also reported design options and techniques to reduce manufacturing costs for operations such as brazing of tube arrays and headers. The modular and versatile nature of this technology enables implementation over a range of heating and cooling modes and cooling and heating capacities.

Hu and Chao (2008) designed, fabricated, and experimentally investigated a 40 W cooling capacity lithium-bromide water absorption cooling system with a micro-evaporator, micro-condenser and expansion channel. The components were fabricated by

photo-chemically etching features on silicon wafers including channels with a hydraulic diameter of 0.131 mm. An individual etched wafer was then bonded to machined plastic sheets. The top sheet incorporated ports for the working fluid, while the bottom sheet incorporated a flow passage for the coupling fluid. The desorber and absorber of the system were more conventional flooded column designs. It should be noted that each flooded column required a significant liquid inventory, partially negating the benefits of the compact condenser and evaporator. System *COP* varied from 0.465 to 0.479 over a range of elevated evaporator temperatures (11 to 19°C) that are much higher than typical cooling conditions of approximately 8°C, and a fixed condenser temperature (45°C). They note that an “ideal cycle” with an evaporator temperature of 19°C and condenser temperature of 45°C should achieve a *COP* of 0.8. Potential limitations for reduced system performance include the ingress of non-condensable gases, ambient heat loss/gain and poor control. In addition to the limitations mentioned by the authors, pressure loss (and saturation temperature drop) due to the large specific volume of water vapor at such low operating pressures is a significant limitation. Also, most significantly, miniaturization of the absorber and desorber components would still be needed to achieve a compact system.

Pence (2010) presented an investigation of microscale fractal flow networks for heat and mass exchange. The design was developed with the consideration of increasing vapor/solution flow area as vapor generation occurs; helping to minimize pressure loss. The author notes that the design could be used for many of the absorption components. Functioning as the desorber component, vapor and solution would flow in the same direction and spread through the fractal flow networks. The co-flowing solution/vapor

would result in reduced refrigerant vapor purity when compared to counter-flow designs, and would require a larger rectification section.

Convective flow components in microchannel heat and mass exchangers have also received attention in recent years. Nagavarapu and Garimella (2011) reported a detailed design methodology for designing heat and mass exchange components consisting of adjacent sheets of metal with etched microchannel passages that carry coupling fluid and working fluid in alternating channels in counterflow. They accounted for the respective heat and mass transfer resistances and also analyzed flow distribution across the headers in detail to develop configurations that would yield nominally uniform flows through the microchannels. For a nominal absorption system cooling duty of 10.55 kW corresponding to an absorber duty of 19.28 kW, they showed that an absorber could be fabricated in an envelope of $0.167 \times 0.140 \times 0.092$ m using 80 pairs of metal sheets with microscale passages. Determan and Garimella (2012) used these photochemically etched and diffusion bonded sheets to develop a novel integrated monolithic unit containing all of the heat and mass exchangers of a single-effect ammonia-water absorption system. Within an envelope of $0.200 \times 0.200 \times 0.034$ m and a total weight of 7 kg, the unit provided 300 W of cooling at a *COP* of 0.375. The system served as a proof of concept and demonstrated feasibility of this compact integrated design. In addition to the use of microscale concepts, the integration of multiple heat and mass exchangers into one pair of metal sheets enabled modular fabrication, with the number of such pairs and their internal dimensions being determined by the desired cooling capacity. Also, because connections between components can also be accomplished within these same sheets, overall system mass can be reduced considerably, and the absence of complex plumbing

and connections between components substantially reduces pressure drops and pumping power requirements, and also minimizes parasitic heat gains and losses. The compact system also results in lower thermal masses and short startup and shutdown times, and enables fast responses to changes in operating conditions. Finally, the compact integrated envelope requires a very small working fluid inventory, and also minimizes assembly and shipping requirements.

Garimella *et al.* (2015) used the proof-of-concept unit of Determan and Garimella (2012) and developed a complete packaged cooling system that provided 3.3 kW of cooling at a *COP* of 0.47. Two integrated monolithic units were used to allow for more favorable geometries for counter-flow vapor generation conditions. The desorber, analyzer and rectifier were integrated into one unit, and the absorber, condenser, evaporator, solution heat exchanger and refrigerant heat exchanger were integrated in the second unit. The integrated heat and mass exchangers showed the scalability of the monolithic concept by Determan and Garimella (2012) with a more than 10 times increase in cooling capacity. In addition, system *COP* at space cooling conditions was improved by more than 30 percent. The packaged unit dimensions were $1.06 \times 0.813 \times 0.66$ m. The primary absorption system occupied only 35% of the volume of the packaged unit.

Hoysall *et al.* (2015) addressed the issue of potential maldistribution of two-phase flows in such microscale components. Using a combination of flow measurements and analysis of high speed flow visualization techniques, they studied the distribution of overall mass fluxes and those of the individual gas and liquid flow rates across the different parallel channels in a microchannel array. High resolution video frames enabled

the computation of the distribution of the respective phase flow rates, void fractions, and interfacial areas available for heat and mass transfer. They used these insights to provide guidance for the effects of maldistribution on heat and mass transfer in absorption heat pump components, and also suggested mitigation strategies.

The above discussion shows that there has been some recent progress on using microscale configurations for developing compact residential space heating and cooling systems. Compact falling-film and convective flow heat and mass exchangers have both been developed. The present study investigates the application of compact convective flow heat and mass exchangers for application in thermally driven (gas-fired) absorption heat pumps for residential water heaters. The development of an absorption cycle and its performance when coupled to a water storage tank was investigated in Chapter 2, and predicted to provide 2.78 kW of heat at a *COP* of 1.74. That investigation is used as a starting point for Chapter 3, in which attention turns to the individual components required to implement a gas-fired residential heat pump water heater. Discrete heat and mass exchangers required for this compact heat pump application are designed and fabricated using methods similar to those presented by Determan and Garimella (2012), and experimentally investigated after installation in an absorption heat pump water heating test platform developed for this purpose. The results from Chapter 3 are used to design, fabricate and evaluate a monolithic microchannel heat and mass exchanger as part of a packaged prototype in Chapter 4.

3.2 System and Component Description

3.2.1 System Description

An overall schematic of the direct gas-fired single-effect ammonia-water absorption heat pump under consideration here is shown in Figure 3.1. Details of the analysis of cycle performance at design conditions as well as at different water storage tank temperatures are presented in Chapter 2. The system consists of a main loop and auxiliary coupling loops for the absorber, condenser, desorber and evaporator. The absorber and condenser are connected to auxiliary loops that serve as a medium temperature sink. The evaporator is coupled to an auxiliary loop that serves as the low temperature source. The desorber is direct gas-fired, with flue gases from combusted natural gas serving as the high temperatures source.

Referring to Figure 3.1, concentrated solution exits the absorber as a subcooled liquid at (1). The solution is pumped to the high pressure side of the system, (1) to (2). Heat is removed from the vapor side of the rectifier by the concentrated solution stream, (2) to (3). Water is preferentially condensed on the vapor side to increase refrigerant purity. The concentrated solution exchanges heat in the solution heat exchanger with the dilute solution stream exiting the desorber, (3) to (4). Concentrated solution enters the desorber where it mixes adiabatically with vapor exiting the desorber. The solution flows through the desorber, counter-current to generated vapor as it is heated by combusted gas, (4) to (5). The heat addition process generates refrigerant vapor from the solution stream decreasing the ammonia concentration within the solution. Dilute solution exits the desorber and exchanges heat in the solution heat exchanger, (5) to (6). Dilute solution flows through an expansion device and enters the absorber where it mixes with

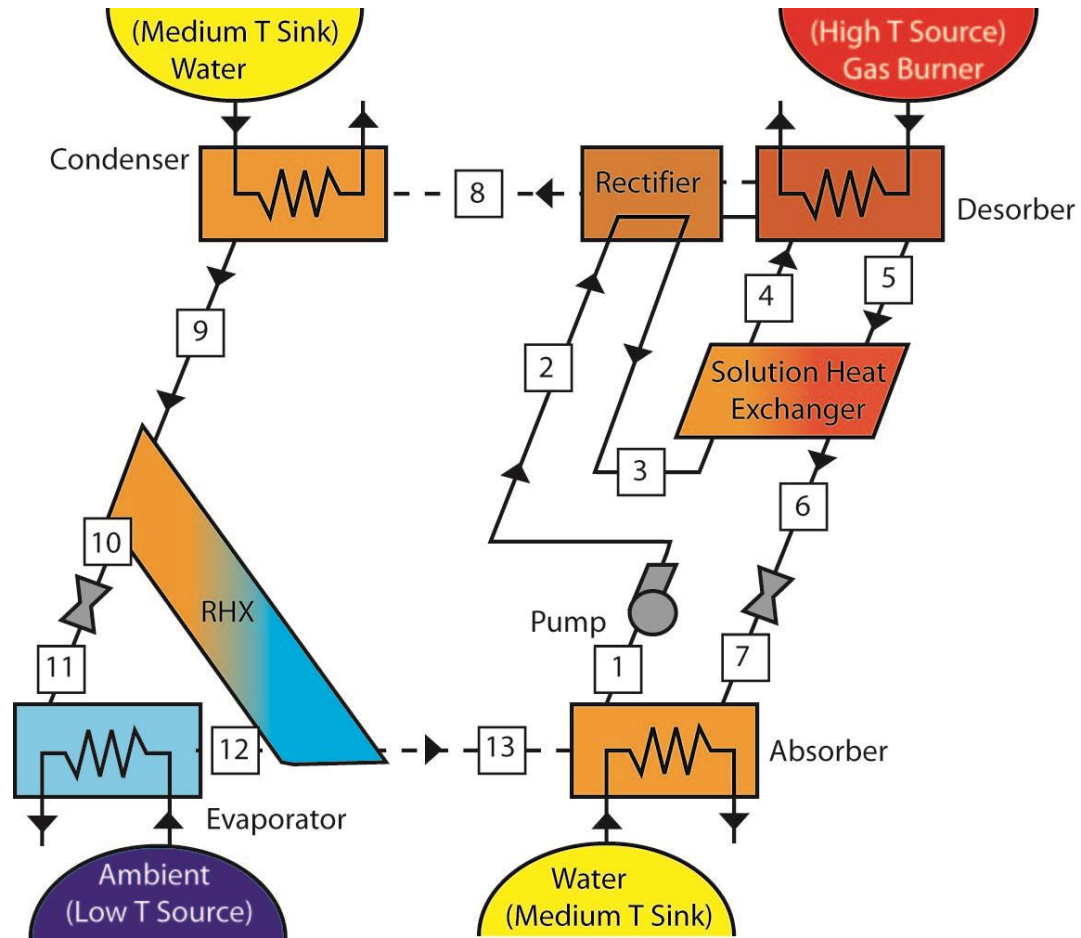


Figure 3.1: Schematic of absorption heat pump

refrigerant vapor, (6) to (7). Heat is rejected to the medium temperature sink as the mixture reaches liquid saturation and is further subcooled.

Refrigerant vapor exiting the desorber is purified in the rectifier where water is preferentially condensed from the vapor stream. The rectifier condensate returns to the desorber while high purity refrigerant exits the rectifier and flows to the condenser. Refrigerant exits the condenser as a slightly subcooled liquid, (8) to (9). The refrigerant is further subcooled in the refrigerant heat exchanger, (9) to (10), before flowing through an expansion device, (10) to (11). The refrigerant enters the evaporator where heat is

exchanged with the low temperatures source, (11) to (12). Vapor refrigerant flows through the refrigerant heat exchanger, (12) to (13), where it is heated further by the high temperature refrigerant stream. The vapor flows into the absorber where it mixes and is absorbed by the dilute solution stream to complete the cycle.

Thermodynamic modeling of the gas-fired ammonia-water heat pump water heater using the *Engineering Equation Solver* (EES) (Klein 2014) software platform was presented in Chapter 2. The absorption heat pump delivered 2.79 kW of heat at system *COP* of 1.74 at baseline ambient and water inlet temperatures of 20 and 32°C, respectively. The system was investigated over a range of ambient (4.4-32°C) and water inlet temperatures (14.5-57°C). Performance in combination with a 227 liter storage tank model was also investigated. The thermally driven system was able to maintain high coefficients of performance for the conditions investigated. The design and fabrication of compact heat and mass exchangers is the next step in investigating the potential of this system. The inlet and outlet conditions for each component of this baseline model were used to design the heat and mass exchangers in the present study, as described below.

3.2.2 Heat and Mass Exchangers

Several of the heat and mass exchangers required for the implementation of this system are designed using microscale geometries similar to those reported by Determan and Garimella (2012). Thus, the microchannel heat and mass exchangers are fabricated using an array of stainless steel sheets containing microscale features, with the assembly of sheets being bonded between endplates. Each component assembly uses sets of two sheets stacked in an alternating fashion. These sets of sheets provide flow paths for the working fluid and coupling fluids streams that exchange heat within the component.

Figure 3.2 shows an exploded assembly drawing of a representative discrete microchannel heat exchanger on the left. The image on the right shows an enhanced view of the headers on one side of the component. Solution flows directly into the channels through an open header while the coolant exits in a direction perpendicular to the channel flow.

Each microchannel component was designed using models developed specifically for the fluid composition, flow regime, and thermodynamic conditions of each component. Models for single-phase heat transfer in components with microscale features are reported in Determan (2008). These models were modified to account for condensation and evaporation mechanisms, and were used to design the condenser and evaporator. The design and modeling of the microscale absorber is based on the model developed by Nagavarapu and Garimella (2011) for coupled heat and mass transfer in ammonia-water

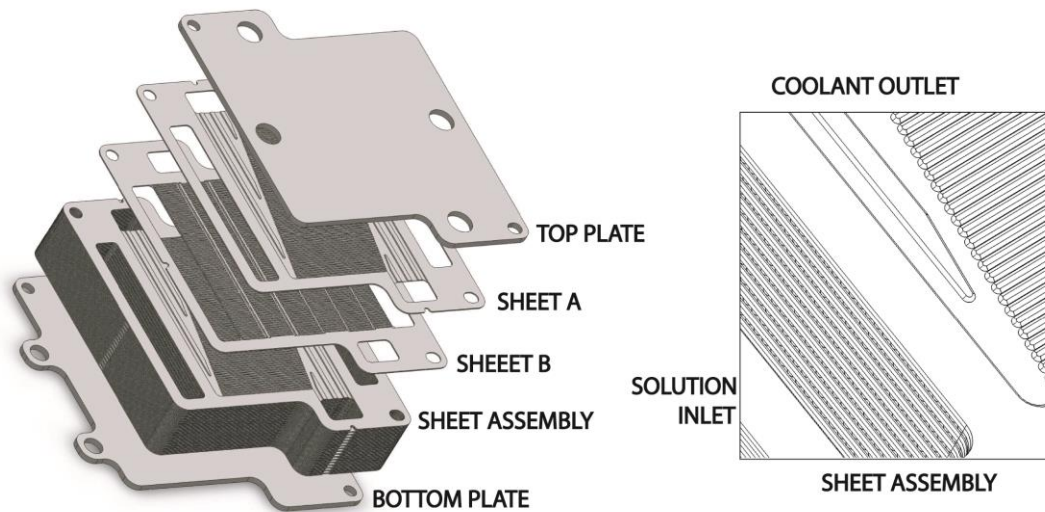


Figure 3.2: Discrete microchannel heat exchanger assembly

absorbers with microscale features. In all cases, the component models use a segmented architecture that iteratively computes the relevant fluid stream parameters at multiple locations along the length of the heat and mass exchange components. Output parameters include temperatures, concentrations, qualities, flow rates and other thermodynamic data for the solution, refrigerant and coupling fluid streams within each component (as applicable). Parameters adjusted in the design of individual components to satisfy design requirements and constraints include channel length, number of channels per sheet, and number of sheets per heat exchanger. All but one of the heat exchangers was designed to require the same number of sheets to allow for integration into a monolithic structure without significant redesign. Table 3.1 contains the key dimensions of the discrete components fabricated and tested on the breadboard facility. In addition to the information presented in Table 3.1, it should be noted that all of the components were designed to have channel hydraulic diameters of 0.442 mm.

These discrete microchannel components were fabricated using a two-step process. Individual sheets were chemically machined using a photo-chemical etching process. The

Table 3.1: Breadboard component sizing

Component	Number of shims	Channels per Shim	Channel Length (m)	HX Width (m)	HX Length (m)
Absorber	30	55	0.156	0.081	0.232
Condenser	30	55	0.152	0.081	0.222
Evaporator	30	55	0.102	0.081	0.176
Solution Heat Exchanger	20	55	0.102	0.081	0.176
Refrigerant Heat Exchanger	30	25	0.088	0.044	0.164

sheets were then stacked between cover plates and then brazed in a vacuum furnace to form individual components. Each component was pressure tested to ensure the absence of leaks across passages on the same side as well as cross leaks between the two sets of fluid passages.

In addition to the microchannel components, a direct gas-fired desorber was designed and fabricated. The desorber component was designed to minimize pressure loss of the combusted gas stream and avoid flooding on the solution side of the component. A vertically oriented shell-and-tube heat and mass exchanger with a diameter and height of 0.051 and 0.432 m, respectively, was designed to meet these requirements. In the component, concentrated solution enters the shell side at the top and is heated as it flows downward (counter-current to generated vapor.) The solution exits as a dilute liquid at the bottom of the component via a downward oriented tube to prevent the exit of generated vapor. Vapor generated in the component flows upwards in a serpentine path and exchanges heat and mass with the falling liquid solution. This interaction reduces the vapor temperature and increases the ammonia concentration. Vapor exits at the top of the component. Natural gas is combusted in an enclosed chamber at the bottom of the component and combusted gas flows through flue tubes counter to the falling ammonia-water solution. Combusted gas exits the top of the component above the condensation temperature of water vapor. All components were installed on the test facility for the assessment of component and system performance.

3.3 Experimental Approach

A schematic and photographs of the breadboard and combustion room facilities used for the investigation of the absorption heat pump water heater are shown in Figures 3.3

and 3.4, respectively. In the schematic, the components located within the combustion room are enclosed by a red box. The remaining components are located on the breadboard test facility. Temperature, pressure and flow rate measurement locations are shown in Figure 3.3.

3.3.1 Instrumentation and Data Acquisition

Temperature measurements are taken at the inlet and outlet of every main and auxiliary loop component using calibrated T-type thermocouples (accuracy $\pm 0.25^{\circ}\text{C}$). Two absolute pressure transducers (accuracy $\pm 0.03\%$ of range) are used to measure the condenser outlet and absorber outlet pressures. A third absolute pressure transducer (accuracy $\pm 0.25\%$ of range) is installed at the evaporator inlet. Coriolis flow meters (accuracy $\pm 0.1\%$) are used to measure the concentrated and dilute solution, refrigerant, and condenser and evaporator coupling fluid flow rates. A magnetic flow meter (accuracy $\pm 0.5\%$) is used to measure the absorber coupling fluid flow rate. A National Instruments data acquisition system with LabVIEW as the interface records all measured data for real-time data analysis. Real time plots of the temperatures, pressures and flow rates are used to confirm steady state operation before data are recorded at any desired test condition.

A diaphragm flow meter (accuracy $\pm 0.01 \text{ ft}^3$) is used to measure the natural gas flow rate to the direct-fired desorber. The gas line pressure and fuel-air mixture pressure are measured by well-type manometers. Barometric pressure and ambient temperature are measured with a digital barometer (Model EW 90080-02, Cole Parmer). Combusted gas exiting the desorber is periodically analyzed with a combustion gas analyzer (Fyrite® InTech®, Bacharach Inc.) The higher heating value (HHV) of the natural gas is tracked

using published data from the local utility provider. These measurements are taken to allow for the calculation of the combustion rate and heat input to the desorber component.

Flow rates of the absorber, condenser and evaporator coupling fluids are controlled by adjusting metering valves. Temperatures of the absorber and condenser coupling fluid are controlled by auxiliary heat exchangers coupled to chilled water. The temperature of

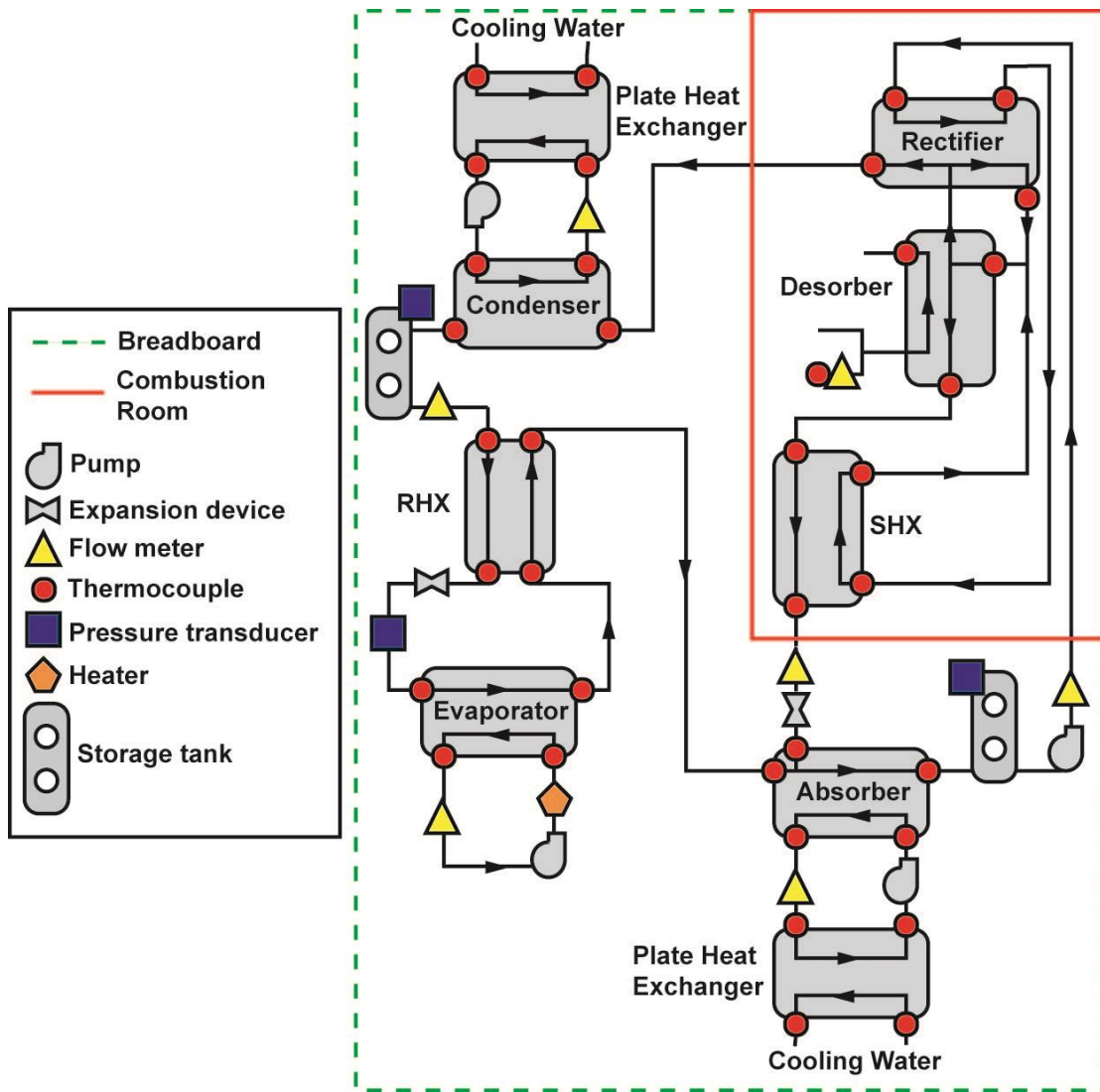


Figure 3.3: Test facility schematic

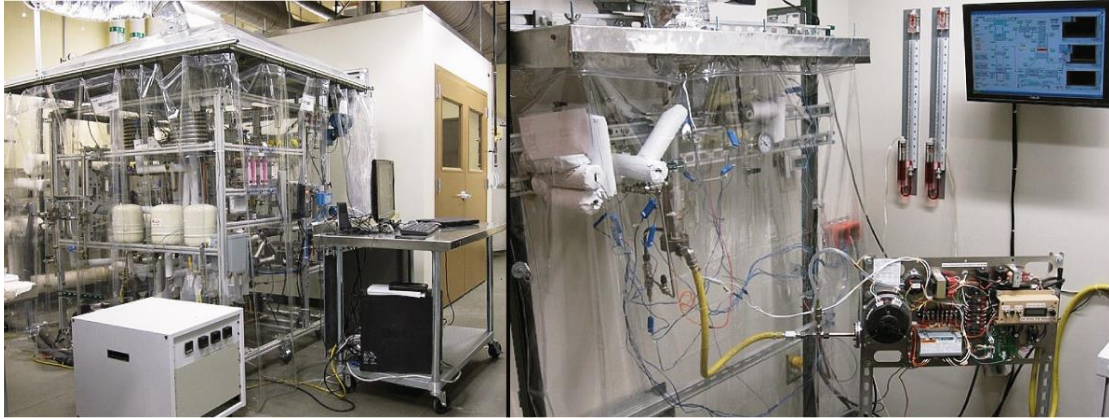


Figure 3.4: Test facility; breadboard (left), combustion room (right)

the evaporator coupling fluid is controlled by varying the current supplied to the resistance heater that serves as the cooling load in the loop. The flow of natural gas and air to the combustion chamber at the bottom of the desorber is regulated by a custom designed electronic control module that interfaces with a hot surface ignition control module (Model S8910U1000, Honeywell) and a variable speed blower (NRG118/0800-3612, EBM Papst).

Additional details for the breadboard instrumentation are included in Appendix A.

3.4 Data Analysis

Experiments were conducted with the focus of maximizing system performance at conditions as close to the water heater design conditions as feasible. During operation, steady state was determined using real-time plots. Once steady state was achieved; temperature, pressure, and flow rate measurements were recorded, and these data were analyzed to determine the state of the solution and refrigerant at various locations in the loop, estimate component duties, and analyze their performance.

3.4.1 System-level State Points

The working fluid, a binary mixture of ammonia-water, requires three independent properties to define its state at any location in the system. The temperatures and pressures measured at various locations in the test loop serve as two of the three independent properties. The third property used for defining the state is concentration or quality. Because of the uncertainty associated with obtaining samples of vapor and liquid at various locations during operation in such a compact system with a small working fluid inventory, appropriate assumptions of expected quality (e.g., saturated liquid or saturated vapor) at certain locations around the test loop are made for the third property to define the state of the mixture. In this study, these saturation assumptions are made at the dilute solution exit of the desorber and the refrigerant vapor outlet of the rectifier. Mass and species balances are conducted in the rest of the test loop to define the state at locations where such assumptions of quality cannot be made. The concentrated solution concentration is determined from mass and species balances on the desorber-rectifier component. This is performed because the amount of subcooling at the outlet of the absorber is unknown, making an assumption of saturated phase inappropriate. Other properties such as enthalpy and specific volume can be estimated once the state of the mixture is completely defined. A step-by-step procedure describing data reduction analyses is provided by Lee *et al.* (2012).

3.4.2 Component Level Analysis

Once the state of the solution and vapor is known at all locations around the test loop, the relevant component duties are estimated. Component duties are estimated by using both fluid sides. The working fluid side heat duty is estimated using the measured mass flow rates and calculated enthalpies of the solution and/or vapor for the respective

component. The coupling-fluid side heat duty is calculated using the measured flow rate and temperatures at the inlet and outlet of the component. The average of the measured working- and coupling fluid duties is used to determine the overall heat transfer conductance using the following equation.

$$UA = \frac{Q}{LMTD} \quad (3.1)$$

In Equation 3.1, *LMTD* is the logarithmic mean temperature difference, which is defined using measured working and coupling fluid temperatures. It should be noted that such single-point assessments of components with coupled heat and mass transfer and the respective resistances, and thermal capacity rates varying along the length of the components, are approximate indicators of performance. Due to the objective of the present study being validation of component performance while installed in a complete absorption system, internal measurements within the components were not performed. For the design of such components, the segmented iterative approach to calculating the varying transport resistances and driving gradients should be followed; however, the *UA* values calculated here provide an overall measure of component performance while operating in an absorption system, and also help identify areas that limit overall system performance.

Once components heat duties are calculated, the total heating load and coefficient of performance can be calculated. The delivered water heating duty is estimated as the combined heating load of the absorber and condenser components.

$$Q_{\text{heating}} = Q_{\text{absorber}} + Q_{\text{condesner}} \quad (3.2)$$

The coefficient of performance is estimated as the total heating duty divided by the heat input to the desorber component.

$$COP = \frac{Q_{\text{heating}}}{Q_{\text{desorber}}} \quad (3.3)$$

A sample calculation is provided in Appendix A.

3.5 Results and Discussion

Based on the analyses described above, the performance of the individual components and the overall system are discussed here. It should be noted that due to the closed loop nature of an absorption system, with multiple vapor and liquid streams connected in series and parallel, and coupled to external conditions or within the closed loop system, conditions supplied to individual components around the system cannot be precisely and independently specified or controlled. This is especially true when performance at off-design system conditions is being tested. The analysis of the performance of the individual components presented below acknowledges this interdependence while assessing component-level performance.

3.5.1 Absorber

The absorber component is the location where the refrigerant vapor and dilute solution combine to form the concentrated solution. During this process sensible heat and the heat of absorption are removed by a coupling fluid. The coupling fluid flows counter-current to the solution flow in adjacent microchannels. This component is often referred to as the ‘bottleneck’ of absorption system (Beutler *et al.* 1996) because of its crucial role in governing system performance, and the fact that an absorber must transfer large heat duties across adverse concentration gradients and small driving temperature differences.

For this investigation, the absorber was in fact found to be the limiting component. Figure 3.5 shows a plot of the absorber UA and heat duty as a function of the concentrated solution flow rate. The UA and heat duty values were found to range from 25.0 to 38.1 W K^{-1} and 0.97 to 1.4 kW, respectively. The design values for UA and heat duty are 136.9 W K^{-1} and 1.62 kW, respectively. The heat duty is shown to increase with increased solution flow rate while the UA is relatively constant. The UA and heat duty are below the target levels at the design concentrated solution flow rate. This is partly due to the use of a reduced desorber firing rate and solution concentration. At design concentration, the low-side pressure was significantly higher than design because of poor absorber performance. To provide appropriate system level conditions, the heat duty of the absorber was decreased so that it would operate at the needed lower system pressure. The solution concentration and desorber firing rates were decreased so that the absorber heat duty was lower. These adjustments decrease the load on the absorber and allow the low-side to operate at pressures closer to design due to the lower than design driving temperature difference across the absorber.

The target concentrated solution concentration and low-side pressure were 0.593 and 634 kPa, respectively. The concentrated solution concentration and low-side pressure of provided to the absorber on the breadboard facility were in the range of 0.45 ± 0.05 and $670 \text{ kPa} \pm 20 \text{ kPa}$, respectively. These adjustments affect performance of some of the other components also, which is be discussed for specific heat and mass exchangers in the following sections.

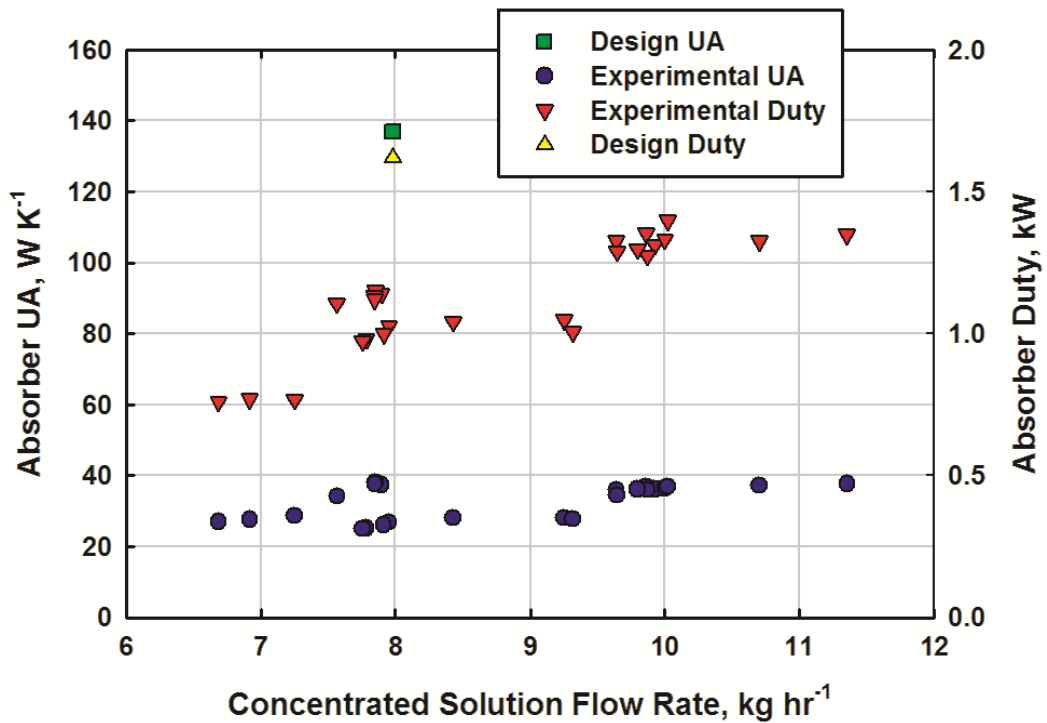


Figure 3.5: Absorber *UA* and heat duty

Minimizing the approach temperature difference between the saturated concentrated solution and coupling fluid inlet is also critical to ensure an optimal balance between a heat rejection temperature that is adequate for water heating on the one hand and a low enough heat extraction temperature at the evaporator on the other, because both components operate at the same nominal pressure. Figure 3.6 shows a plot of the approach temperature difference at the solution-side outlet of the absorber, which ranges from 12.6 to 25.7°C for the experimental results, while the desired design approach temperature is 2.3°C. This further indicates that the component is significantly limiting to the overall system performance.

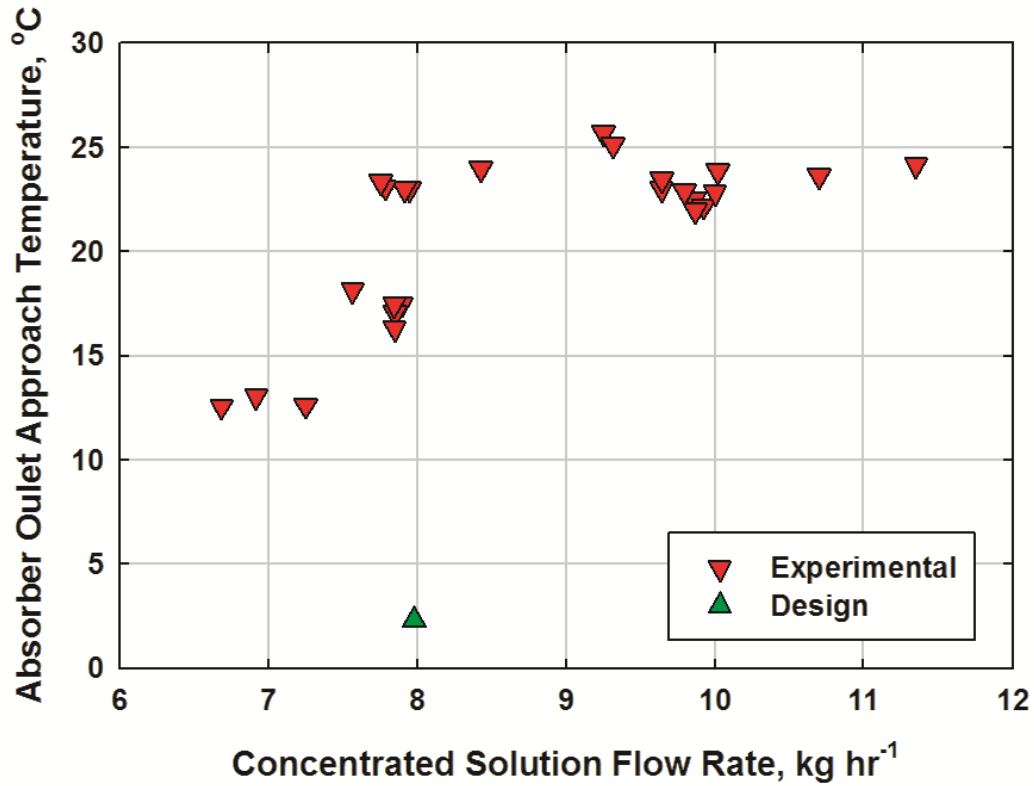


Figure 3.6: Absorber solution outlet approach temperature difference

3.5.2 Condenser

The condenser functions to condense refrigerant vapor generated by the desorber, with the heat of condensation removed by a coupling fluid flowing counter-current to the refrigerant stream in adjacent microchannels. The high-side pressure of the absorption system is established the pressure at which condensation occurs, which is in turn determined by the coupling fluid inlet temperature and flow rate.

Figure 3.7 shows a plot of the Condenser UA and heat duty as a function of refrigerant flow rate. The UA and heat duty values were found to range from 140 to 323 $W K^{-1}$ and 0.52 to 0.94 kW, respectively. The design values for the UA and heat duty are 250 $W K^{-1}$ and 1.17 kW, respectively. The plot shows that the experimental UA values are near design values, while the refrigerant flow rates are below the design values. The

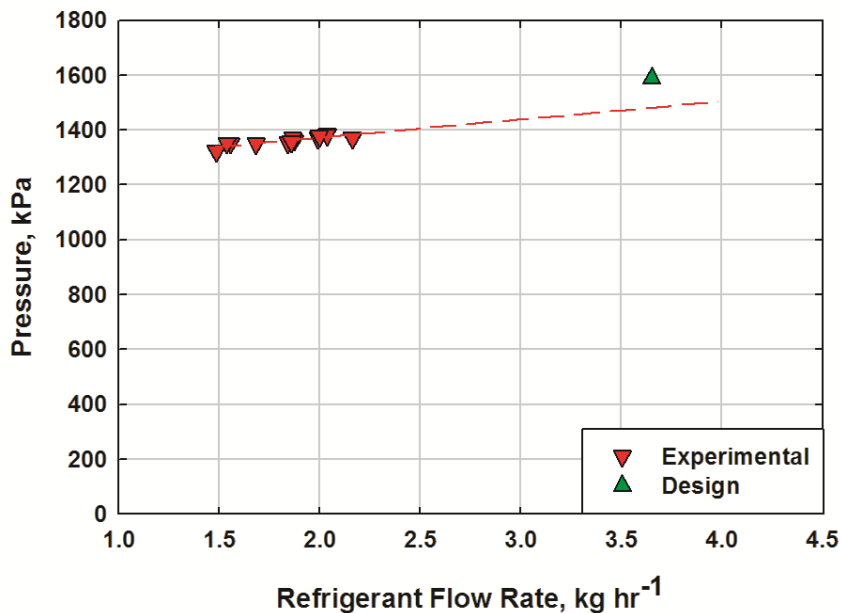


Figure 3.8: High side pressure of breadboard system

between the condensing fluid and the coupling fluid, thereby requiring a lower high-side pressure.) A curve fit to the experimental data is included to estimate system pressure, if the system were to achieve the design refrigerant flow rate. The curve fit shows that the high-side pressure would still be lower than the design values. This lower pressure requirement and the measured UA values indicate that the condenser operates as designed or better.

3.5.3 Desorber

Heat input is provided to the desorber through the combustion of natural gas, with an electronic control module used to regulate the flow of the fuel-air mixture to the burner. Combustion products heat the concentrated solution, leading to the generation of ammonia-water vapor and the correspondingly lower concentration dilute solution.

Figure 3.9 shows a plot of the desorber heat duty and the dilute solution outlet temperature as a function of concentrated solution flow rate. The heat duty and dilute

solution outlet temperature were found to range from 1.32 to 1.55 kW and 103 to 121°C, respectively. The design heat duty and dilute solution outlet temperature are 1.61 kW and 136°C, respectively. The plot shows that the heat duty and dilute solution temperature are lower than the design values. This is primarily due to the need to decreased desorber duty by decreasing the natural gas firing rate so that the absorber could reject its heat to the coupling fluid at or near the necessary operating temperatures. The lower dilute solution exit temperature is also due to the reduced firing rate.

3.5.4 Evaporator

The refrigerant enters the evaporator downstream of the expansion valve as a low quality mixture. The coupling fluid provides the heat of vaporization while flowing counter-current to the evaporating refrigerant in adjacent microchannels. The low-side

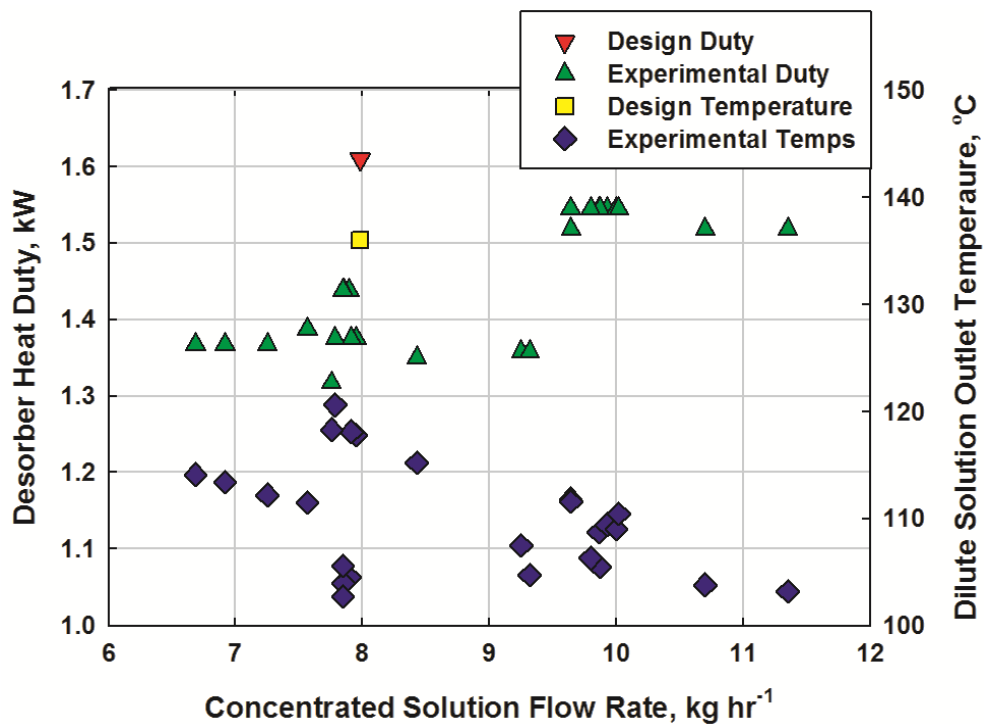


Figure 3.9: Desorber heater duty and dilute solution outlet temperature

pressure and temperature of the evaporator coupling fluid are important factors in determining the heat addition to the system in the evaporator. A low-side pressure that allows a refrigerant temperature 5-10°C lower than the coupling fluid inlet temperature is desirable.

Figure 3.10 shows a plot of the evaporator UA and heat duty as a function of refrigerant flow rate. The measured UA and heat duty values ranged from 48.5 to 91.7 $W K^{-1}$ and 0.45 to 0.62 kW, respectively, while the design UA and heat duty values are 475 $W K^{-1}$ and 1.18 kW, respectively. The UA and heat duties values are lower than the design values because the refrigerant flow rate supplied is lower than the design value. The curve fits to the data shown here indicate that the component will also be undersized

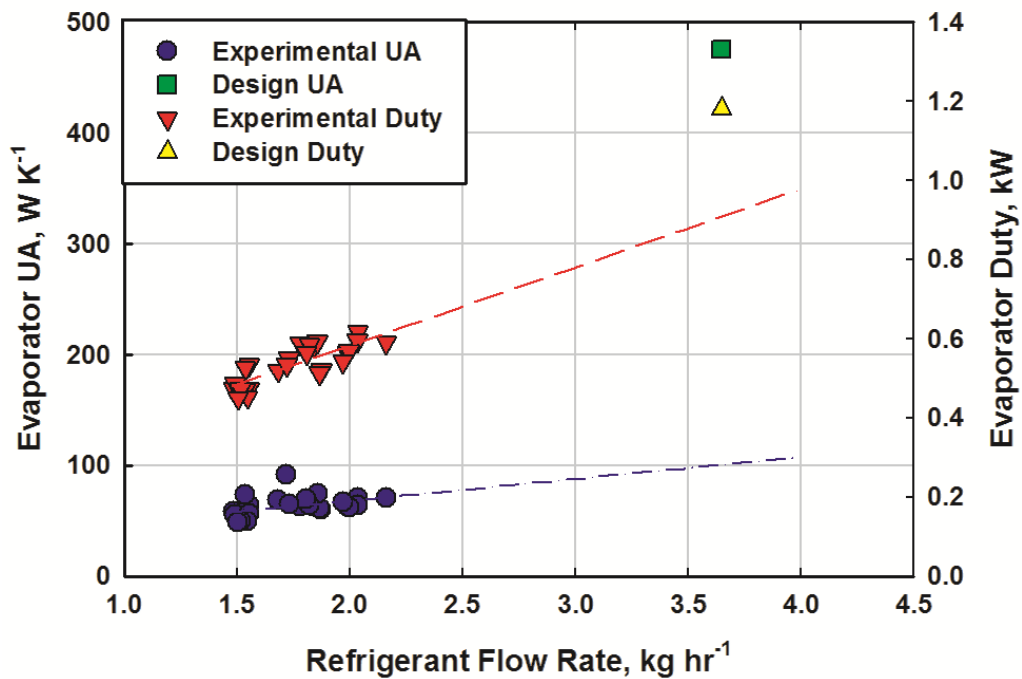


Figure 3.10: Evaporator UA and heat duty

at design conditions.

Figure 3.11 shows a plot of the evaporator temperature glide ($T_{ref,out} - T_{ref,in}$), refrigerant inlet, and coupling fluid inlet temperatures as a function of the refrigerant flow rate. The evaporator temperature glide, refrigerant inlet temperature, and coupling fluid inlet temperature ranged from 0.5 to 12°C, 12 to 17°C, and 25 to 31°C, respectively. The design evaporator temperature glide, refrigerant inlet temperature, and coupling fluid inlet temperature were 3, 12 and 17°C, respectively. These results indicate lower than required performance. The decreased refrigerant flow rate and larger temperature difference between the inlet streams of the component required to achieve refrigerant temperature glide near the design value implies poorer than expected performance.

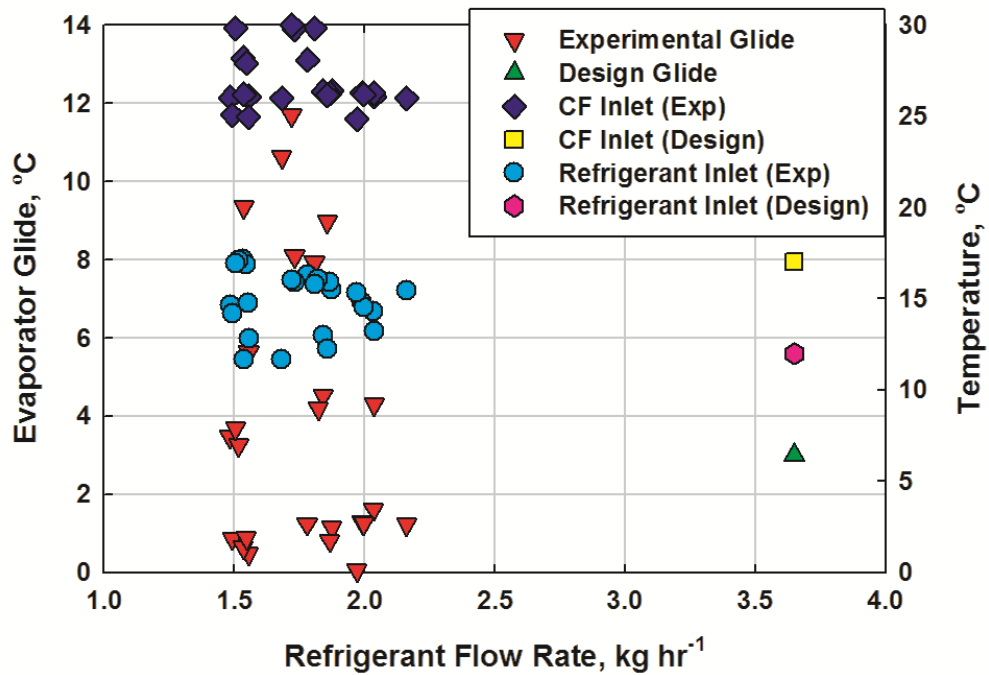


Figure 3.11: Evaporator glide and coupling fluid inlet temperatures

Maldistribution of the incoming two-phase mixture of refrigerant across the microchannel passages is identified as one contributor to this suboptimal performance.

3.5.5 Rectifier

The rectifier component purifies the refrigerant vapor exiting the desorber by selectively condensing water from the vapor stream, with vapor exiting as a high purity refrigerant. High purity refrigerant is essential to minimize the temperature glide experienced by the refrigerant in the evaporator. A larger temperature glide due to lower purity causes temperature pinches and decreases evaporator duty. However, over rectification can result in the condensation of valuable refrigerant vapor and also decrease system performance. Therefore, a properly sized rectifier is important in optimizing system performance.

Figure 3.12 shows a plot of the rectifier UA and heat duty values as a function of concentrated solution flow rate. The UA and heat duty values ranged from 2.43 to 4.78 $W K^{-1}$ and 65 to 127 W , respectively. The design UA and heat duty values are 4.4 $W K^{-1}$ and 130 W , respectively. (It should be noted that the rectifier operates in a region of steep changes in saturation temperature of the ammonia-water mixture with very small changes in concentration, making the respective LMTD values sensitive to such small changes. Therefore, the reported UA values can be quite sensitive to small changes in inlet conditions.) The plot shows that UA and heat duty values are near design values. As noted previously, the refrigerant flow rate was below the design value. An increased refrigerant flow rate should result in an increase in heat exchange between the concentrated solution and vapor in the rectifier.

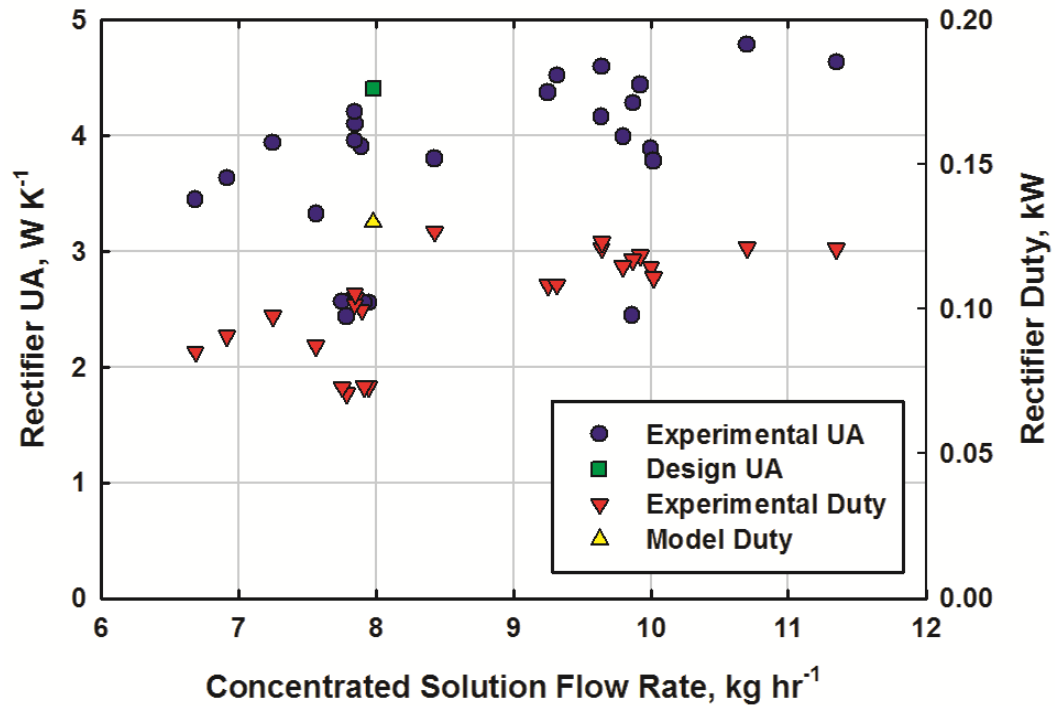


Figure 3.12: Rectifier UA and heat duty

3.5.6 Refrigerant Heat Exchanger

The refrigerant heat exchanger is a recuperative heat exchanger that transfers heat from the high pressure refrigerant stream to the low pressure refrigerant stream. Cooling the high pressure refrigerant stream to a lower enthalpy minimizes flashing across the expansion valve and increases evaporator cooling duty. In addition, heating of the low pressure refrigerant exiting the evaporator adds to the sensible cooling load in the absorber, which in turn increases the possible water heating duty.

Figure 3.13 shows a plot of the refrigerant heat exchanger effectiveness and heat duty as a function of the refrigerant flow rate. The effectiveness and heat duty values ranged from 68 to 100 percent and 11 to 43 W, respectively. The design effectiveness and heat duty are 93 percent and 88 W, respectively. The lower-than-design refrigerant flow rates

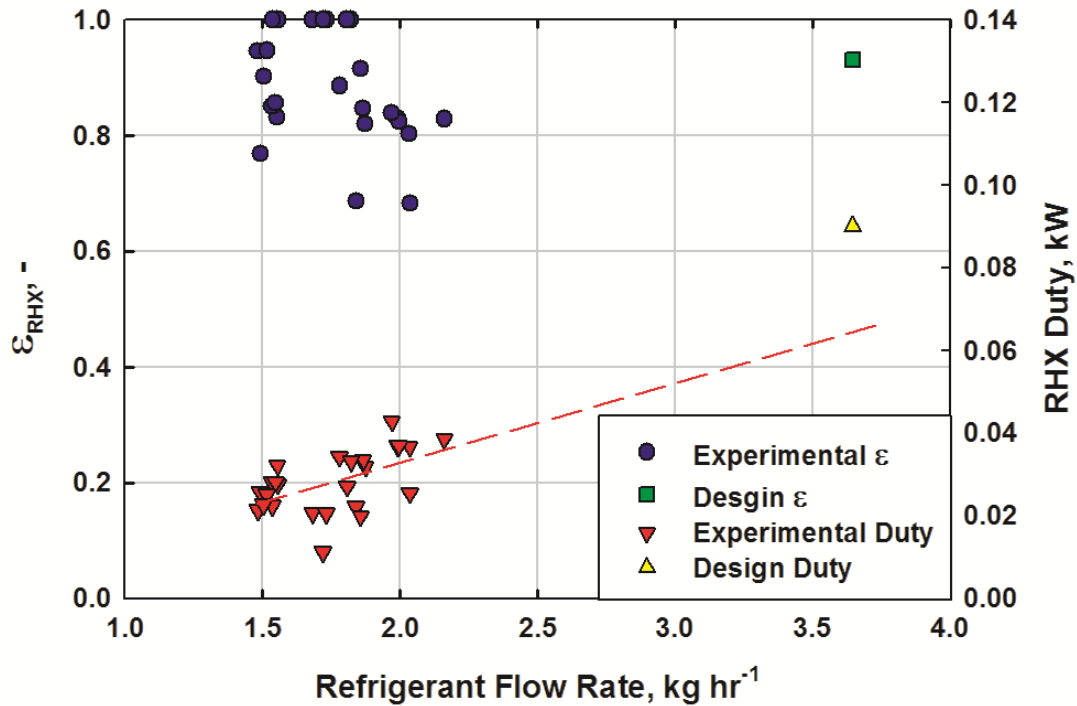


Figure 3.13: Refrigerant heat exchanger effectiveness and heat duty

result in higher effectiveness values due to the lower thermal capacity rate of the refrigerant stream. Estimates of the heat duty at design flow rates based on these results shows that the component would be undersized.

3.5.7 Solution Heat Exchanger

The solution heat exchanger transfers heat from the dilute solution exiting the desorber to the concentrated solution stream. Preheating the concentrated solution decreases the external heat input required in the desorber to generate vapor. Cooling the dilute solution decreases the sensible cooling load in the absorber. An effective solution heat exchanger allows a system to achieve higher *COPs* compared to similar systems without this recuperative component.

Figure 3.14 shows a plot of the solution heat exchanger UA and heat duty values as a function of the concentrated solution flow rate. The UA and heat duty values range from 6.14 to 13.5 W K^{-1} and 240 to 360 W , respectively. The design UA and heat duty values are 18 W K^{-1} and 450 W , respectively. Experimental effectiveness values ranged from 49 to 71 percent, whereas at design conditions, the desired heat exchanger effectiveness is 92 percent. This lower-than-design performance impacts the performance of the absorber, desorber, and the system as a whole.

3.5.8 Overall System

The design system conditions of 32°C coupling fluid inlet to the absorber and condenser, 17°C coupling fluid inlet to the evaporator, and a desorber heat input of 1.61

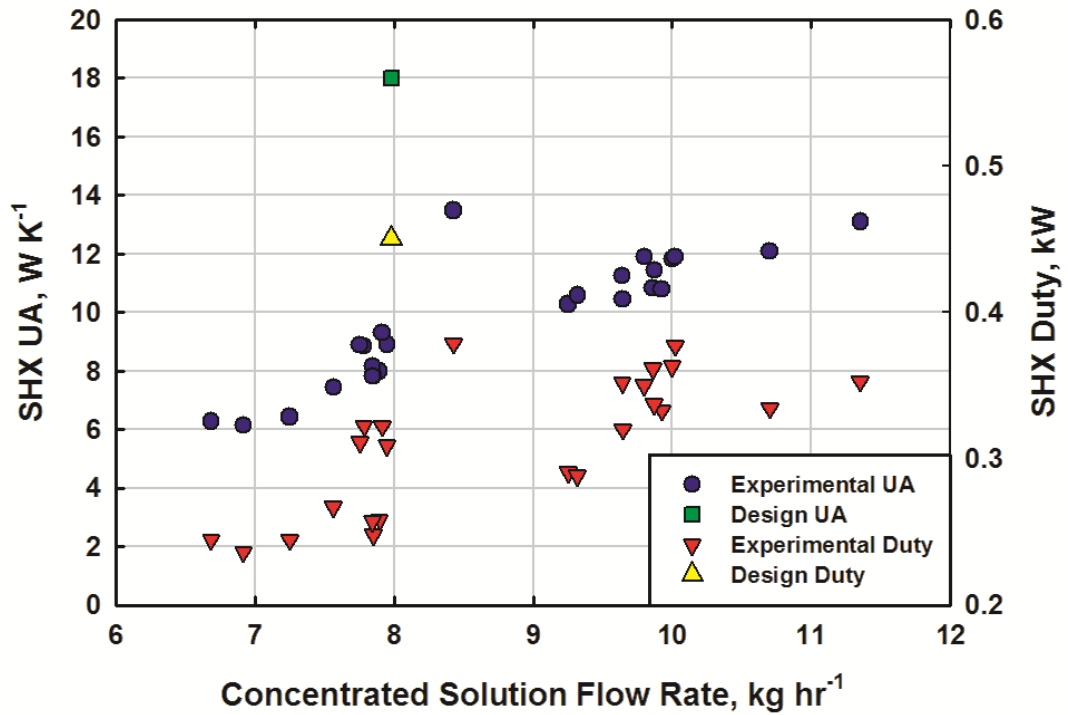


Figure 3.14: Solution heat exchanger UA and heat duty

kW were targeted during the presented study. Component limitations resulted in testing at modified conditions. The absorber and evaporator were operated with off-design coupling fluid temperatures to allow for improved low side pressures and evaporator heat duties.

Figure 3.15 shows a plot of the system heating duty and *COP* as a function of concentrated solution flow rate. The plot shows that duty and *COP* increase with increasing solution flow rate. The heating duty and *COP* values ranged from 1.54 to 2.06 kW and 1.12 to 1.36, respectively. The design heating duty and *COP* values are 2.79 kW and 1.74, respectively. The deviations in heat exchanger performance from design values lead to this lower system performance. Resizing several of the components and

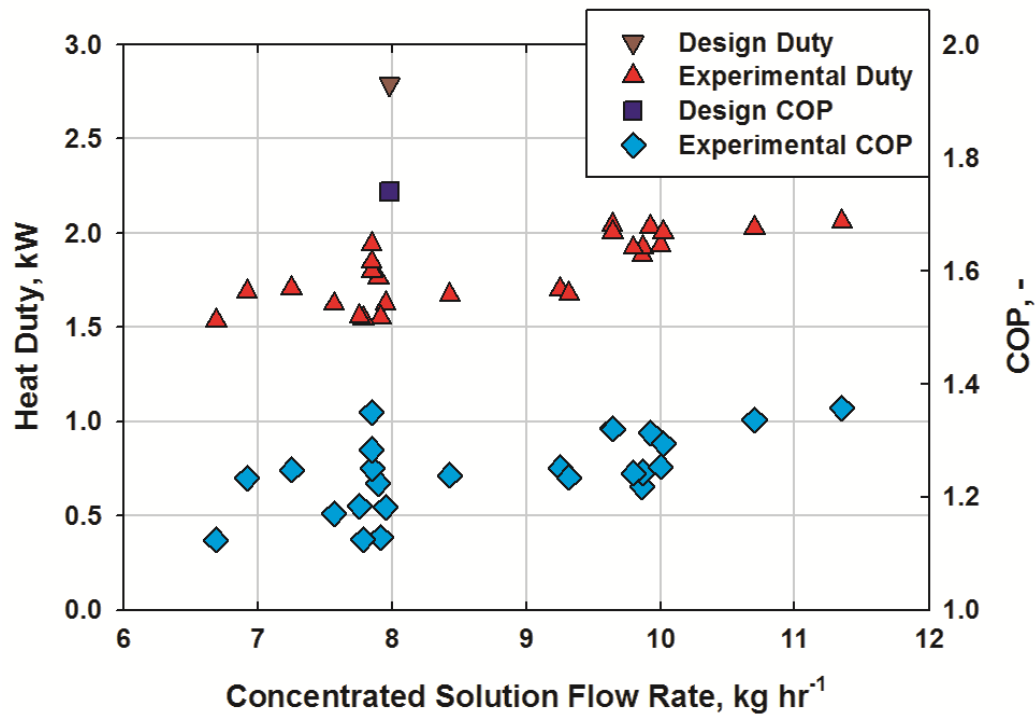


Figure 3.15: System heating duty and *COP*

redesigning the absorber should result in system performance closer to the design heating duty and *COP* of 2.78 kW and 1.74, respectively.

3.5.9 Heat and Mass Exchanger Refinement

The experiments showed that several of the components, e.g., the evaporator, refrigerant heat exchanger and solution heat exchanger, were undersized. The absorber was found to be significantly undersized and was the ‘bottle-neck’ of the system. The condenser, rectifier, and desorber were determined to be sized appropriately, and performed near design.

The evaporator, refrigerant heat exchanger, and solution heat exchanger were resized based on the experimental results, with the inclusion of an additional safety factor. The condenser size was increased with just the inclusion of a safety factor. Table 3.2 contains the dimensions of the resized microchannel components. The redesigned components were also sized to require the same number of shims to allow integration into a monolithic unit.

The absorber limited system performance considerably, probably due to maldistribution of the vapor-liquid flows across the channels that hindered species

Table 3.2: Resized microchannel components

Component	Number of shims	Channels per Shim	Channel Length (m)	HX Width (m)	HX Length (m)
Condenser	40	55	0.152	0.081	0.222
Evaporator	40	55	0.152	0.081	0.222
Solution Heat Exchanger	40	55	0.102	0.081	0.176
Refrigerant Heat Exchanger	40	55	0.102	0.081	0.176

transfer across phases. A more in-depth study is needed to clearly understand techniques to ensure better flow distribution while maintaining the advantages of microscale passage geometries. For the present system, until such refined designs are ready, a small conventional heat and mass exchanger configuration, such as a shell-and-tube absorber demonstrated by Garrabrant *et al.* (2013b), may be used to augment absorption capacities.

3.6 Conclusions

The results from an experimental investigation of a residential ammonia-water absorption heat pump water heater using discrete microchannel heat and mass exchangers were presented in this chapter. The system achieved a maximum heating duty and *COP* of 2.06 kW and 1.36, respectively. Refined heat exchanger designs, based on the results of this study are used in Chapter 4 to bring system performance closer to the design heating duty and *COP* of 2.78 kW and 1.74, respectively.

The condenser, rectifier and desorber components were found to operate near-design. However, the evaporator, refrigerant heat exchanger, and solution heat exchanger were found to require increases in size to operate near their respective design values, with maldistribution of the two-phase at the inlet being one potential reason for the lower performance. The absorber component did not perform well, again most probably due to maldistribution of the vapor-liquid flows, which in this component heavily dependent on coupled heat and mass transfer, would led to performance deterioration, making this the ‘bottle-neck’ of the system. An independent investigation of the microchannel absorber designs is needed to improve understanding of the absorption process in microchannels and allow for refined component designs.

The study showed the potential of small capacity absorption systems using microchannel heat and mass exchangers for implementation as thermally driven heat pump water heaters. With the proposed increase in heat exchanger sizes, and an alternative but already established absorber design, an extremely compact system can be achieved. As a result, this study helps address barriers that have previously prevented the implementation of small capacity absorption systems. The compact components could easily fit within the package envelope of current mechanically driven heat pump water heater systems. Integration of the microchannel components into a monolithic unit will further decrease the packaged unit size. Such packaged systems are currently under development by the present authors. In addition, the advancement of cost-effective mass production techniques for the microchannel heat exchangers will allow these small capacity systems to be economically viable.

CHAPTER 4. **INTEGRATED PACKAGED HEAT PUMP WATER HEATER PROTOTYPE USING COMPACT HEAT AND MASS EXCHANGERS**

4.1 Introduction

4.1.1 Overview

In this chapter, attention turns to the integration of these components into a residential capacity system for multi-pass water heating. Components designed in Chapter 3 function as the core components of the absorption heat pump system. Integration of these components into a compact heat pump water heater is an important step towards achieving the reduction of residential energy use for water heating.

Water heating accounts for 18 percent of total energy usage in homes, second only to space-conditioning, yet the majority of homes in United States use direct heated units, which are limited to coefficients of performance (*COPs*) less than one (DOE 2014). In 2009, eight million water heaters were purchased in the U.S. and only one million were Energy StarTM rated (Ryan *et al.* 2010). It should be noted that the Energy StarTM rating includes a wide range of technologies, many of which have only marginal improvements in *COP* relative to conventional direct-heated systems. Heat pumps offer greatly improved coefficients of performance when compared to direct heated systems. Electrically driven heat pumps are commercially available and serve as drop-in replacements for electric resistance heated units. There is currently no drop-in replacement heat pump for gas-fired water heaters. This is significant because of the eight million water heaters sold in 2012, 52 percent were gas-fired units (AHRI 2014). The

development of a gas-fired heat pump water heater could serve as a high efficiency replacement for roughly half of the U.S. domestic market.

This chapter presents the design, fabrication and experimental evaluation of a packaged prototype ammonia-water absorption heat pump water heater that uses compact microchannel heat and mass exchangers. The use of such heat and mass exchangers limits system size, and their modular design could allow for low cost mass production. The gas-fired prototype system is designed to be tank mounted, similar to commercially available electrically driven heat pump water heater designs.

4.1.2 Prior Work

The prior work discussed in Chapter 3 focused on the development of compact heat and mass exchangers for absorption heat pump applications, including for this application. In this chapter, a discussion of prior work on the development of electrically and thermally driven heat pump water heaters is presented first.

Residential capacity electrically driven heat pump water heaters have been the focus of many investigations over the past few decades. Thermally driven heat pump investigations at this capacity have been limited but have garnered more interest in the past five to ten years. Zogg *et al.* (2005) studied the advantages and limiting factors of electrically driven heat pump water heaters. They found that electrically driven heat pumps yield a 40-60% reduction in electricity usage when compared to direct heated units. They highlighted the high installation cost, fan noise, and consumer acceptance as the limiting factors. Zogg *et al.* (2007) further discussed the potential of carbon dioxide heat pump water heaters by highlighting additional benefits, including the potential to

heat water in a single pass, to reach higher water temperatures, and the potential to take advantage of work recovery from the expansion process.

Goodman *et al.* (2011a) developed a transcritical carbon dioxide heat pump water heater. Component models were developed and validated experimentally for the gas cooler, evaporator, and suction line heat exchanger (*SLHX*). Using these models, Goodman *et al.* (2011b) developed a system-level model for a residential application. The system-level model was used to investigate the effect of a suction line heat exchanger and compare once-through and recirculating systems. Their results showed that the once-through system outperformed the recirculating system with and without the suction line heater exchanger by an average of 15.2 and 10.2%, respectively.

Hepbasli and Kalinci (2009) conducted a review of the literature on heat pump water heating systems. They highlight the significant energy consumption for water heating in the US and note that 60% of households in the US do not use electricity to heat water. Their review focused on electrically driven heat pump water heaters, with no mention of thermally driven heat pumps. They reviewed investigations of ground source, air source, thermoelectric, solar-assisted, and gas-engine heat pumps. They found that many of the studies focused on increasing system complexity to increase system performance.

Chua *et al.* (2010) conducted a review of the literature on heat pump systems. They reviewed different investigations with applications specific to residential and commercial space heating, cooling, water heating, and refrigeration. Studies to enhance heat pump performance were reviewed and included multi-stage, ejector, hybrid desiccant, and

hybrid solar variations. Thermally driven heat pumps were mentioned but not discussed in detail.

Garrabrant *et al.* (2013b) presented the investigation of two absorption heat pump systems for residential water heating applications: a single-effect and a Generator Absorber Heat Exchange (GAX) device. The systems were modeled to investigate performance over a range of potential water temperatures. Component models were then used to design heat and mass exchangers that were investigated as part of a full system on a breadboard test facility. Testing at baseline design conditions in the single-effect cycle configuration resulted in a system *COP* within 3 percent of the model predictions. Testing at baseline design conditions of the GAX cycle resulted in a system *COP* that was more than 20 percent less than the model predictions. A major limitation was the performance of the solution cooled absorber (SCA/GAX). It was determined that the component size required with their heat exchanger design would be prohibitively large. They also noted that the additional plumbing and measurement devices associated with the breadboard system resulted in ambient heat loss of 9 to 10 percent of the total system heat. In addition to system and component evaluation, burner and chamber designs for the direct-fired desorber were investigated with the goal of meeting emissions targets.

Garrabrant *et al.* (2014) reported the results from performance testing of three prototype direct gas-fired ammonia-water absorption heat pump water heaters. Steady state performance was investigated for the range of temperatures experienced when heating water for residential use and was indicative of an Energy Factor (*EF*) of 1.2-1.3. They discussed the importance of intelligent controls and the ability to operate over a significant range of high-to-low side pressure differences. They also presented a

comparison of primary energy consumption and operating cost between the gas-fired heat pump and commercially available units. This comparison showed that a gas-fired heat pump would minimize primary energy use and operating costs compared to other designs.

Wu *et al.* (2014) performed a detailed literature survey of absorption heating technologies for residential, industrial and rural applications. A range of absorption technologies was reviewed, including heat pumps, heat storage systems, heat transformers, compression-absorption heat pumps, and others. In the review of systems for residential applications, the majority of the studies were modeling investigations and focused on space-heating applications. The investigation presented by Garrabrant *et al.* (2013a) was highlighted as a study that focused specifically on domestic water heating and involved modeling and experimental work. Wu *et al.* (2014) noted that the adoption of absorption systems in civil applications has been limited because of the historical dependence on conventional heating systems and the popularity of vapor-compression systems.

The heat and mass exchangers discussed in Chapter 3 were sized based on the modeling study presented in Chapter 2 using the *Engineering Equation Solver* (EES) platform (Klein 2014). The absorption heat pump system was nominally sized to provide 2.79 kW of heat at a coefficient of performance (*COP*) of 1.74. In addition, performance was investigated over a range of ambient (4.4-32°C) and water inlet conditions (14-57°C).

The review of prior work above shows that in the past decade, interest in residential capacity thermally driven heat pump water heaters has increased. This chapter focuses on the design, demonstration and evaluation of a prototype heat pump water heater. The system is designed to be in the same capacity range as commercially available electric heat pumps.

4.2 System and Component Description

A schematic of a direct gas-fired single-effect ammonia-water absorption heat pump is shown in Figure 4.1. The system consists of a main loop and auxiliary loops for the absorber, condenser, desorber and evaporator. The absorber and condenser are coupled in parallel to a medium temperature sink (the water being heated). The evaporator is coupled to the ambient, which serves as the low temperature source. The desorber is direct gas-fired and flue gases from the combustion of natural gas serve as the high temperature source. The single-effect absorption heat pump is a two-pressure system where the solution heat exchanger, desorber, rectifier and condenser operate at the high system pressure. The evaporator and absorber operate at the low system pressure. The working fluid pair of the system is an ammonia-water mixture in which ammonia is the refrigerant and water is the absorbent. More details of the absorption system are provided in Chapters 2 and 3.

The system was designed to heat water from 14.5°C to a minimum of 57°C using a multi-pass heating approach. The multi-pass heating approach allows the system to be reasonably sized, in both footprint and capacity, and take advantage of higher coefficients of performance at lower temperature lifts. Also, extended periods of operation are favorable to offset losses associated with start-up and shut-down.

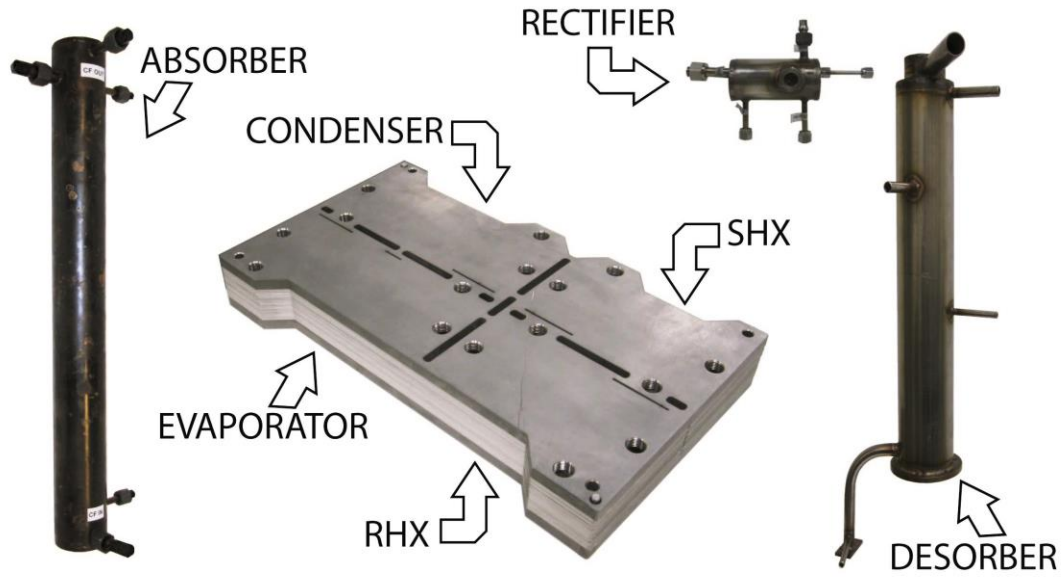


Figure 4.2: Images of packaged unit heat and mass exchangers

originally presented by Determan (2008) and Nagavarapu and Garimella (2011). Specific sizing of these components is presented in Chapter 3.

A shell-and-tube desorber-rectifier design was used to accomplish heat exchange between high temperature flue gases and the liquid solution. Liquid solution flows downward on the shell side of the component while combusted gas flows upward on the tube side. Refrigerant vapor generated on the shell side flows upward through the desorber and its purity is increased in the rectifier.

A shell-and-tube configuration was also used for the absorber in this study, based on results presented in Chapter 3. This component can be replaced by microchannel based designs once refinements of the absorber discussed in Chapter 3 are achieved, to further reduce the size of the packaged unit. In the shell-and-tube absorber, premixed solution

and vapor flow downward on the shell side while the coupling fluid flows upward on the tube side.

Figure 4.3 contains an image of the heat and mass exchangers integrated into the complete packaged prototype unit. The 0.51-meter high packaged unit consists of the main and auxiliary components that are required for the heat pump system. The system includes heat exchangers, pumps/fans, storage tanks and plumbing. It is mounted on a 0.61 meter diameter platform that is representative of commercially available water heater tanks. The unit contains three closed loops: the main ammonia-water loop, the

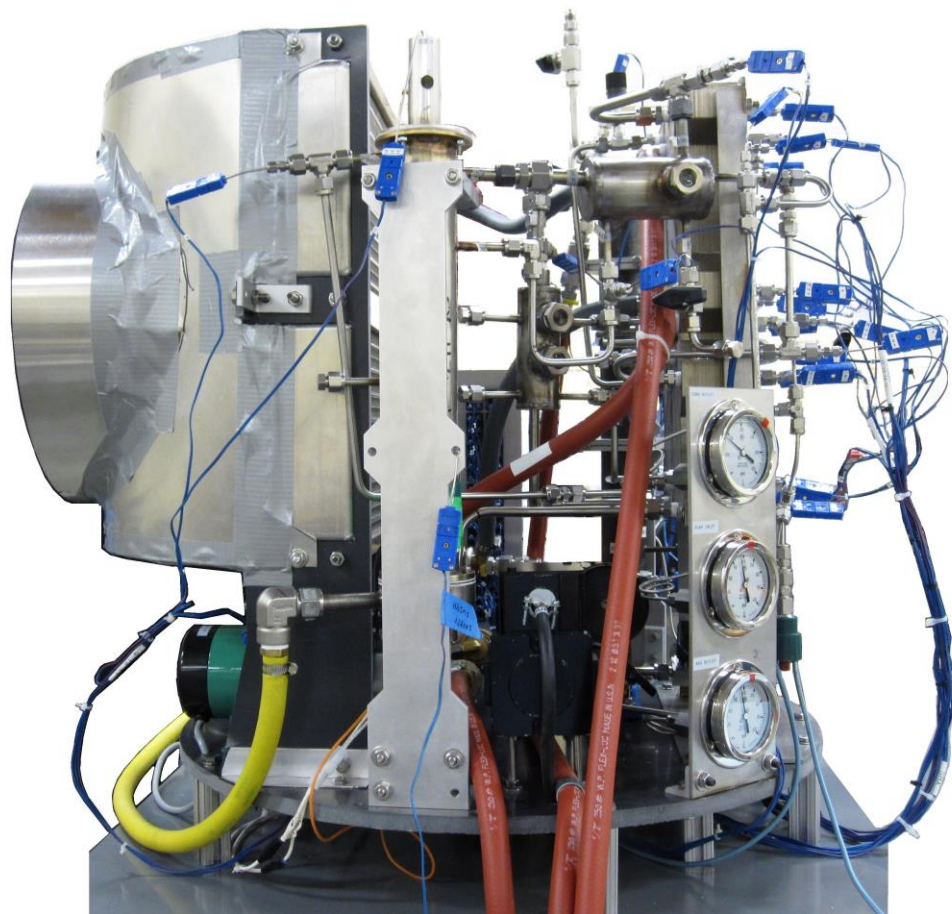


Figure 4.3: Packaged prototype heat pump

ambient-evaporator loop, and the absorber-condenser-tank loop. The evaporator is coupled to an ambient air heat exchanger with a coupling fluid circulating between the components with a centrifugal pump. Coupling fluid flows through the absorber and condenser in parallel and is circulated with a centrifugal pump.

To the author's knowledge, this is the first reported packaged prototype residential capacity absorption heat pump systems using microchannel heat and mass exchangers for multi-pass water heating.

4.3 Experiments

A schematic and photographs of the packaged direct gas-fired ammonia-water absorption heat pump water heater and auxiliary support facilities are shown in Figures 4.4 and 4.5, respectively. In the schematic, the auxiliary components are enclosed by a red box. The auxiliary facilities serve as the heat sink for the system and represent the storage tank of a complete system. The remaining components are located within the envelope of the packaged heat pump water heater. Temperature, pressure and flow rate measurement locations are noted in Figure 4.4.

4.3.1 Instrumentation and Data Acquisition

Temperature measurements are taken at the inlet and outlet of every main and auxiliary component using calibrated T-type thermocouples (accuracy $\pm 0.25^\circ\text{C}$). Three absolute pressure transducers (accuracy $\pm 0.03\%$ of range) are used to measure the condenser outlet, evaporator inlet, and absorber outlet pressures. A Coriolis flow meter (accuracy $\pm 0.1\%$) is used to measure the combined coupling fluid flow rate to the absorber and condenser. A National Instruments data acquisition system with LabVIEW as the interface records all measured data for real-time data analysis. Real-time plots of

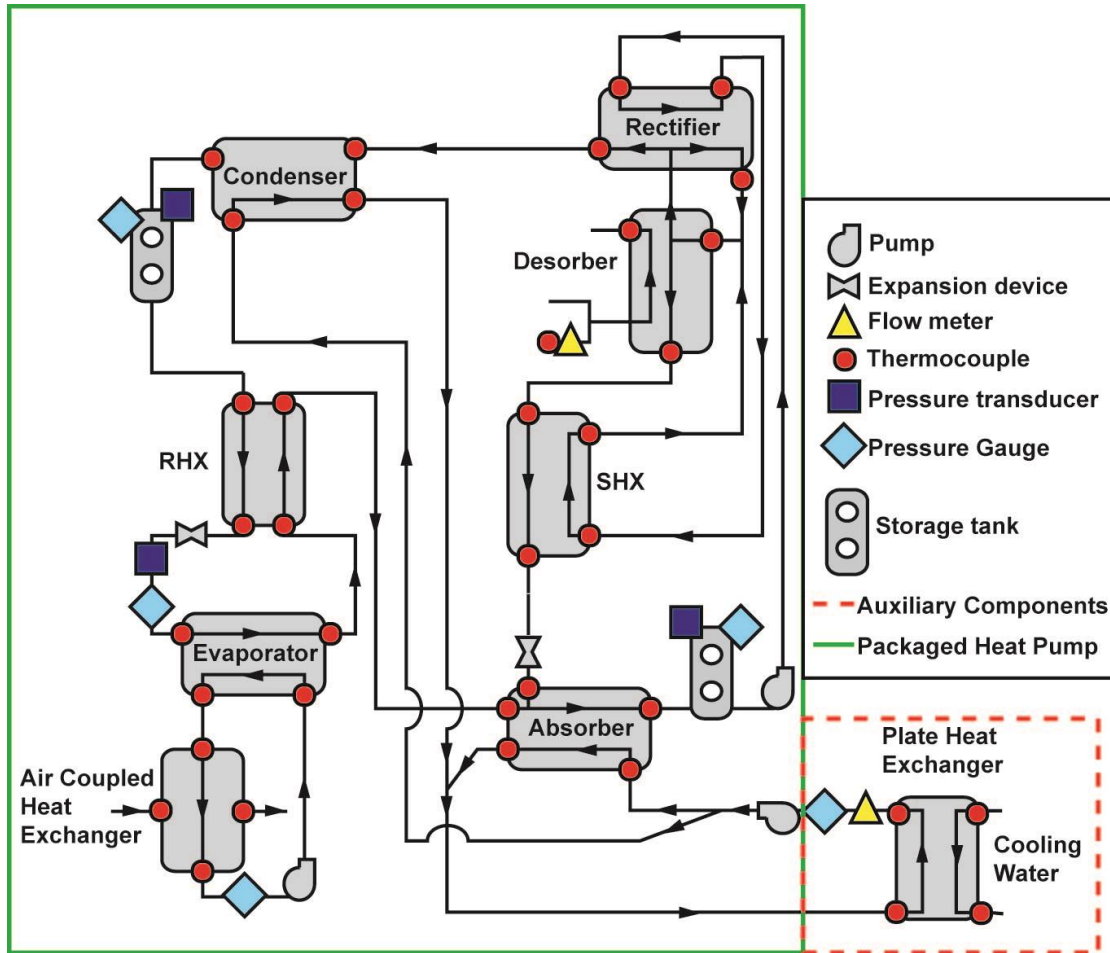


Figure 4.4: Schematic of packaged unit and auxiliary components

the temperatures and pressures are used to verify steady state operation before data are recorded at any desired test condition.

A diaphragm flow meter (accuracy $\pm 0.01 \text{ ft}^3$) is used to measure the natural gas flow rate to the direct gas-fired desorber. The natural gas line pressure and fuel-air mixture pressure are measured by Well-type manometers. Barometric pressure and ambient temperature are measured with a digital barometer (Model EW 90080-02, Cole Parmer). Flue gases exiting the desorber are periodically analyzed using a combustion gas analyzer (Fyrite® InTech®, Bacharach Inc.) The higher heating value (HHV) of the natural gas is

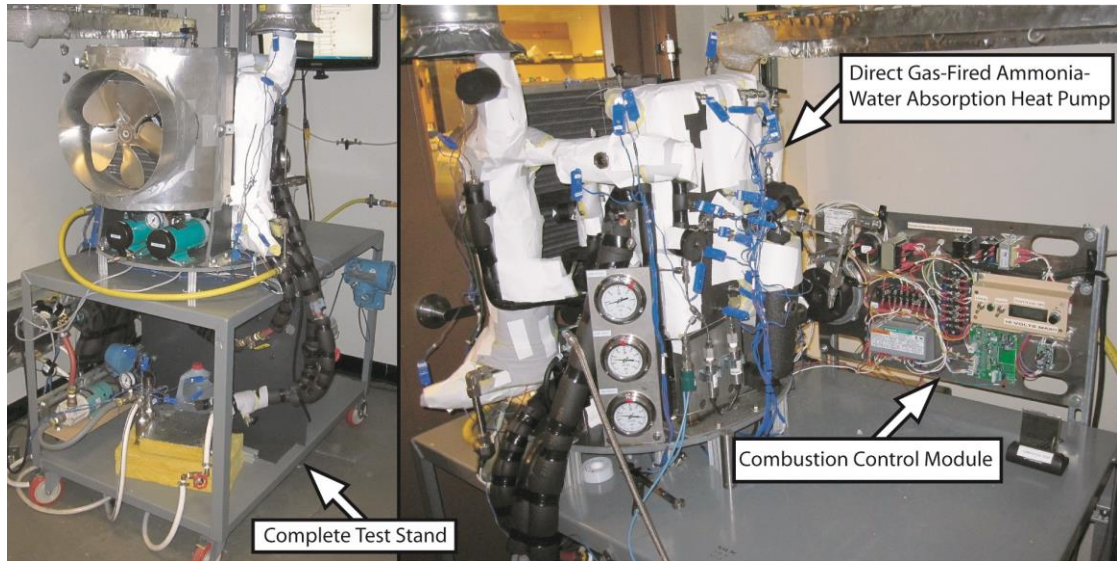


Figure 4.5: Photographs of the packaged unit and supporting facilities

determined using published data from the local utility provider. These measurements enable calculation of the combustion rate and heat transfer rate to the desorber component.

Coupling water flow to the absorber and condenser is controlled by a set of manual valves. The inlet temperature of the absorber-condenser coupling fluid is controlled by an auxiliary plate heat exchanger coupled to the building chilled water. The temperature of the evaporator coupling fluid is dependent on the ambient air temperature and heat exchanger performance. Temperature of the room was controlled with an auxiliary air handler unit. The flow of natural gas and air to the combustion chamber at the bottom of the desorber is regulated by a custom-designed electronic control module that interfaces with a hot surface ignition control module (Model S8910U1000, Honeywell) and a variable speed blower (NRG118/0800-3612, EBM Papst).

Additional details for the packaged unit instrumentation are included in Appendix B.

4.4 Data Analysis

Experiments were conducted in two stages. The first was to maximize system performance at the baseline design conditions. The second was to investigate system performance over a range of water temperatures (10-60°C) and ambient temperatures (10-32°C). During operation, steady state was determined using real time plots. After the system had maintained steady state operation for 15 to 20 minutes; temperature, pressure, and flow rate measurements were recorded. These data were analyzed to determine the state of the solution and refrigerant at various locations in the loop, estimate component duties, and analyze system performance.

The working fluid, a binary mixture of ammonia-water, requires three independent properties to define its state at any location in the system. The temperatures and pressures measured at various locations in the ammonia-water loop serve as two of the three independent properties. The third property used for defining the state is concentration or quality. Appropriate assumptions of expected quality (e.g., saturated liquid or saturated vapor) at certain locations around the ammonia-water loop are made for the third property to define the state of the mixture. In this study, the dilute solution exit of the desorber ($q = 0$), the refrigerant vapor outlet of the rectifier ($q = 1$), and the concentrated solution outlet of the absorber ($q = 0$) are the locations of these saturation assumptions. Species balances are conducted in the rest of the loop to define the state at locations where such assumptions of quality cannot be made. Other properties such as enthalpy and specific volume can be estimated once the state of the mixture is completely defined.

It should be noted that a species balance on the desorber-rectifier component would be the preferred method for determining the concentration of the concentrated solution.

This is because subcooling of solution in the absorber can occur but is difficult to measure directly. Assuming saturation when the mixture is actually subcooled impacts the state point concentration estimation and calculations that depend on this value. This technique was necessitated by the objective of minimizing intrusions into the system and maintaining a standalone packaged unit size as close to a commercial prototype as possible. Therefore, flow rates in the working fluid were not directly measured.

The heating duty is calculated using the total mass flow rate of coupling water to the absorber and condenser and the change in temperature across the auxiliary plate heat exchanger, as shown in Equation 4.1. The specific heat of the water is determined based on the average water temperature. Redundant temperature measurements are collected to ensure the accuracy of the measurement.

$$Q_{\text{heating}} = \dot{m}_{\text{water, total}} \cdot c_{p, \text{avg, water}} \cdot \Delta T_{\text{water}} \quad (4.1)$$

The desorber duty is calculated from the heating rate of the natural gas and the combustion efficiency, as shown in Equation 4.2. The measured combustion efficiency ranged from 0.84 to 0.89.

$$Q_{\text{desorber}} = Q_{\text{natural gas}} \cdot \eta_{\text{combustion}} \quad (4.2)$$

The coefficient of performance is calculated from the total heating and desorber heating duties, shown in Equation 4.3.

$$COP_{\text{heating}} = \frac{Q_{\text{heating}}}{Q_{\text{desorber}}} \quad (4.3)$$

At the component level, heat duties and UA values were estimated based on the available instrumentation on the packaged unit, although the uncertainties were understandably high due to the lack of direct working fluid flow rate measurements. For example, the average uncertainty in the evaporator heat duty was 50 percent. The heat duty of the evaporator is determined based on measured temperatures and an estimated refrigerant flow rate. The refrigerant flow rate is determined from an energy balance between the coupling fluid and refrigerant sides of the condenser. The condenser coupling fluid flow rate is not measured. Instead, the combined heated water flow rate through the absorber and condenser is measured. Individual component coupling fluid flow rates are calculated from mass and energy balances. This is further complicated by the fact that in most cases, the water temperature rise across both components is comparable, which increases uncertainty associated with individual component flow rates. As a result, measured inlet and outlet temperatures for each component, with uncertainties of $\pm 0.25^\circ\text{C}$, are presented in the results section and assessed to evaluate component performance.

A sample calculation is presented in Appendix B.

4.5 Results and Discussion

Results of system and component performance are presented in this section. First, performance at the baseline design condition is evaluated. Second, performance over a range of water inlet ($10\text{-}60^\circ\text{C}$) and ambient temperatures ($10\text{-}32^\circ\text{C}$) is presented.

4.5.1 Operation at baseline design conditions

The system model and state points used in the design of each component of this system targeted operation at absorber and condenser water inlet temperatures of 32°C , an

ambient temperature of 20°C, and a desorber heat duty of 1.61 kW. The model of Keinath *et al.* (2015) predicted a heating duty and *COP* of 2.78 kW and 1.74, respectively, at these conditions.

The first set of experiments focused on maximizing packaged system performance at the baseline design conditions. Adjustments were made to the system to optimize performance, including changes to the refrigerant and solution charge. The optimized packaged system was determined to operate near predicted performance levels at the baseline conditions. Table 4.1 contains key parameters for comparison between the theoretical model and the prototype system. The prototype system achieved a heating duty and *COP* of 2.58 kW and 1.6, respectively, at baseline conditions. The table shows that most operational parameters were within 10 percent of design. The high-side pressure was found to be lower than design and is the result of an over performing condenser unit.

Table 4.1: Theoretical model and experimental comparison at baseline conditions

	Modeling	Experiments	% difference
COP, -	1.74	1.6	8.0
Heating Duty, kW	2.79	2.58	7.5
High-side pressure, kPa	1588	1351	15
Low-Side Pressure, kPa	634	593	6.5
Concentrated Solution Concentration	0.593	0.576	2.9
Dilute Solution Concentration	0.251	0.261	4.0
Refrigerant Concentration	0.998	0.997	-

It should be noted that the integrated system achieved significant improvements over the breadboard system described in Chapter 3 due to the use of the refined components developed based on the results of the experiments reported in Chapter 3; further highlighting the potential of small-capacity absorption systems using microchannel heat and mass exchangers. The delivered capacity and COP, coupled with the compact system footprint, show that this system could be a viable high efficiency alternative to direct-heated systems on the market today.

4.5.2 Water and Ambient Temperature Sweeps

The packaged unit was investigated over a range of water inlet (10-60°C) and ambient (10-32°C) temperatures (Table 4.2). This study is performed to characterize system performance at expected, but off-baseline, design conditions.

4.5.2.1 System Level Performance

Figure 4.6 shows a plot of heating *COP* as a function of water temperature into the absorber and condenser, and the ambient air temperature. Reducing the water temperature and increasing the ambient temperature increases system *COP*. The plot shows that the data follow the expected trend where performance increases with increased ambient temperature for a set water inlet temperature. The lines on the plot are theoretical model

Table 4.2: Experimental test matrix

Water, °C \ Amb °C	10	15	20	25	30	35	40	45	50	55	60
32											
20											
14											
10											

predictions for the heat pump water heater developed in Chapter 2. They show that performance degradation as the water temperature is increased is more severe for the experimental system. Several factors contribute to this, including heat exchanger effectiveness, concentration shifts, and pressure shifts of an actual system versus the theoretical design model.

It is important to note that below an ambient temperature of 20°C, performance levels out and even decreases for the presented data. This is a result of adjustments to the system that were required to allow continuous operation at these conditions. The low water inlet temperature reduces the system pressures as well as the desorber temperature. Non-optimal control strategies were required to keep the water vapor in the combustion

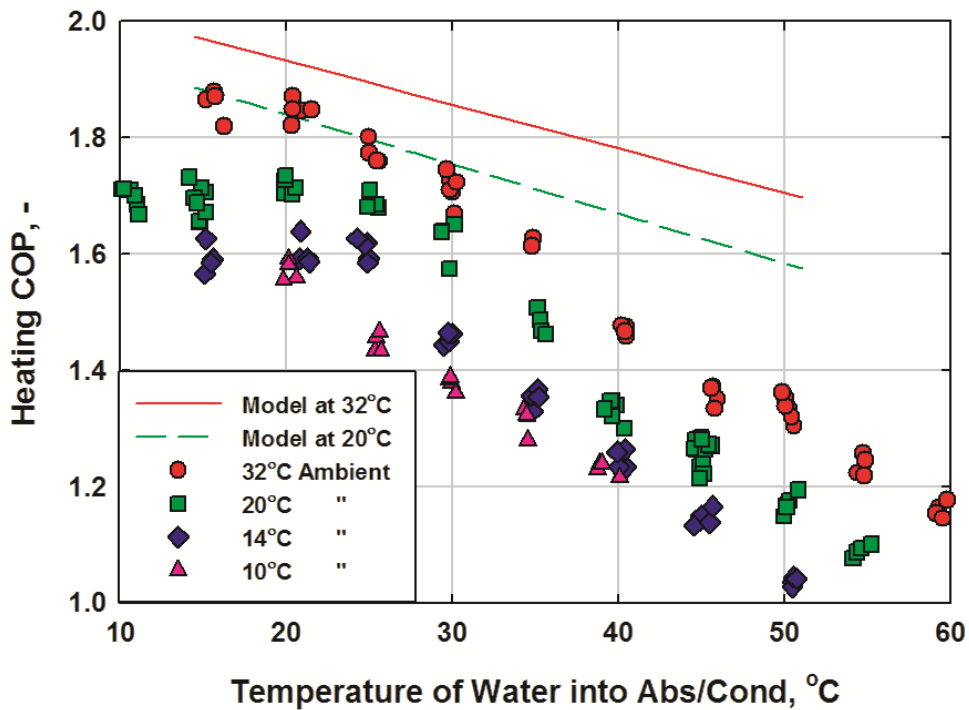


Figure 4.6: Heating *COP* as a function of water and ambient temperatures

gas stream from condensing in the flue tubes and extinguishing the burner. In an actual system, extended operation at these low temperatures would typically not be necessary. If necessary, a control strategy could be used to avoid extinguishing the burner, even if it may reduce the *COP*.

Figure 4.7 shows a plot of the heating duty as a function of water temperature into the absorber and condenser, and ambient air temperature. Reducing water temperature and increasing ambient temperature increases the total heating duty. At higher ambients, the evaporator is able to extract more heat from the ambient. Reduced water temperatures allow the system to operate at higher concentrations, which increases the refrigerant flow rate. In addition to the experimental data, the plot contains results from the system level

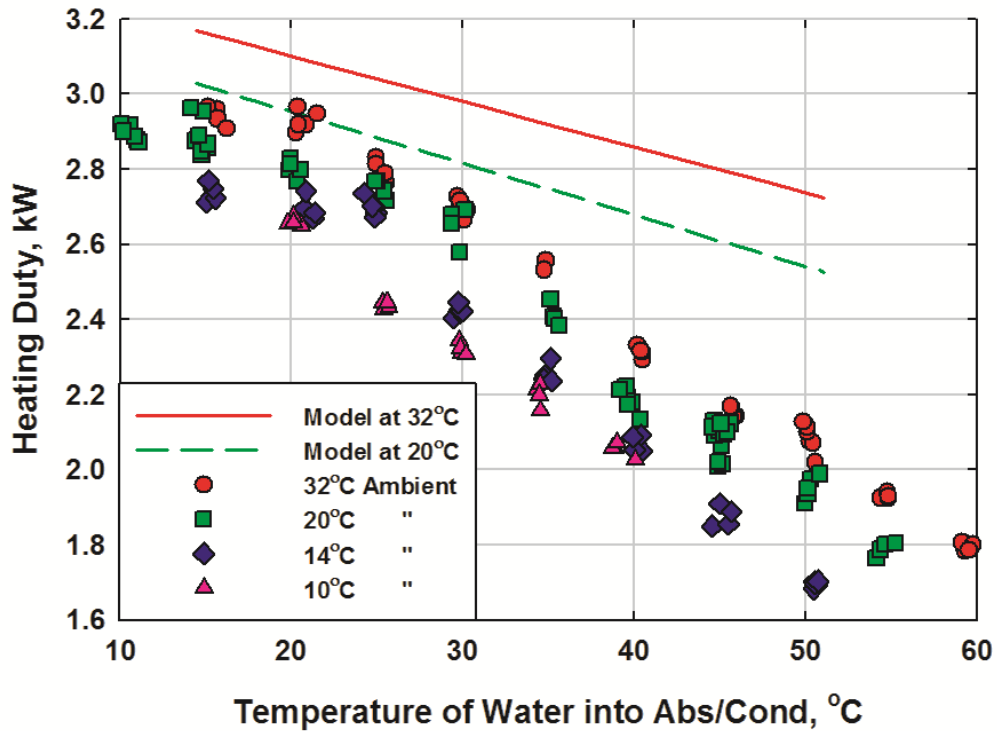


Figure 4.7: Heating duty as a function of water and ambient temperatures

model. A comparison shows that performance degradation is more severe for the experimental system as water temperature is increased. Heat exchanger limitations are experienced as temperatures and flow rates change with the inlet water temperatures. In the solution heat exchanger, concentrated and dilute solution temperatures, and flow rates change with increased inlet water temperatures. Heat exchanger performance at these conditions decreases because of these changes, with its impact propagating throughout the system. A more detailed discussion of the factors contributing to the differences between the model predictions and the measured values is presented in Section 4.6.

Figure 4.8 shows a plot of the high-to-low side pressure difference as a function of water temperature into the absorber and condenser and ambient air temperature. The pressure difference decreases with decreasing water temperature and increasing ambient temperatures. This is because the high side pressure decreases as colder temperatures are experienced in the condenser. The low-side pressure is less affected as solution concentration changes with the colder temperatures. The low-side pressure is higher at increasing ambient temperatures, which leads to the spread of the data points at the same water inlet temperature. More heat can be gained in the evaporator, which increases the load on the absorber, thereby increasing the low-side pressure. The experimental pressure difference is below model predictions. This is because the condenser is over performing, which results in lower than predicted high-side pressures.

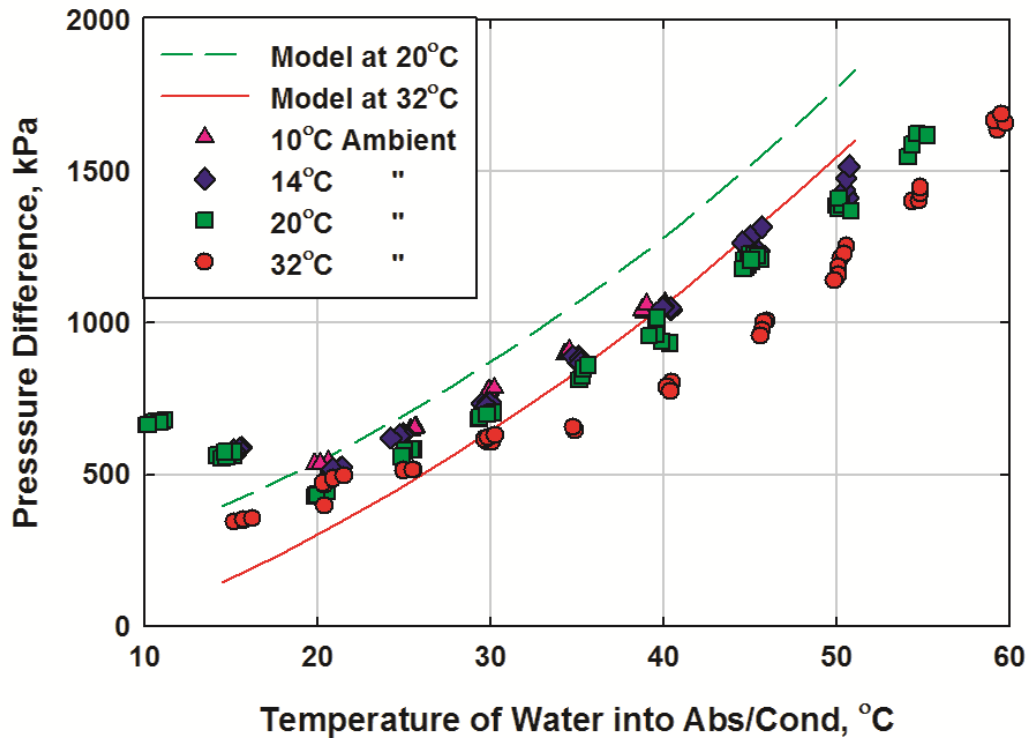


Figure 4.8: High to low side pressure difference

Figure 4.9 shows three plots of solution and refrigerant concentrations as a function of water temperature into the absorber and condenser and ambient air temperature. The top left plot shows that refrigerant concentration decreases with higher water temperatures and lower ambient temperatures. The general trend of the experimental data agrees with model predictions, although there is some variation. In experiments, the refrigerant concentration is determined using the measured temperature and pressure and an assumed quality of one at the outlet of the rectifier. The bottom left plot shows that the concentrated solution concentration increases with lower water temperatures. The lower absorber temperatures allow for increased solution concentrations. The concentrated solution concentration predicted by the theoretical model is found to vary more

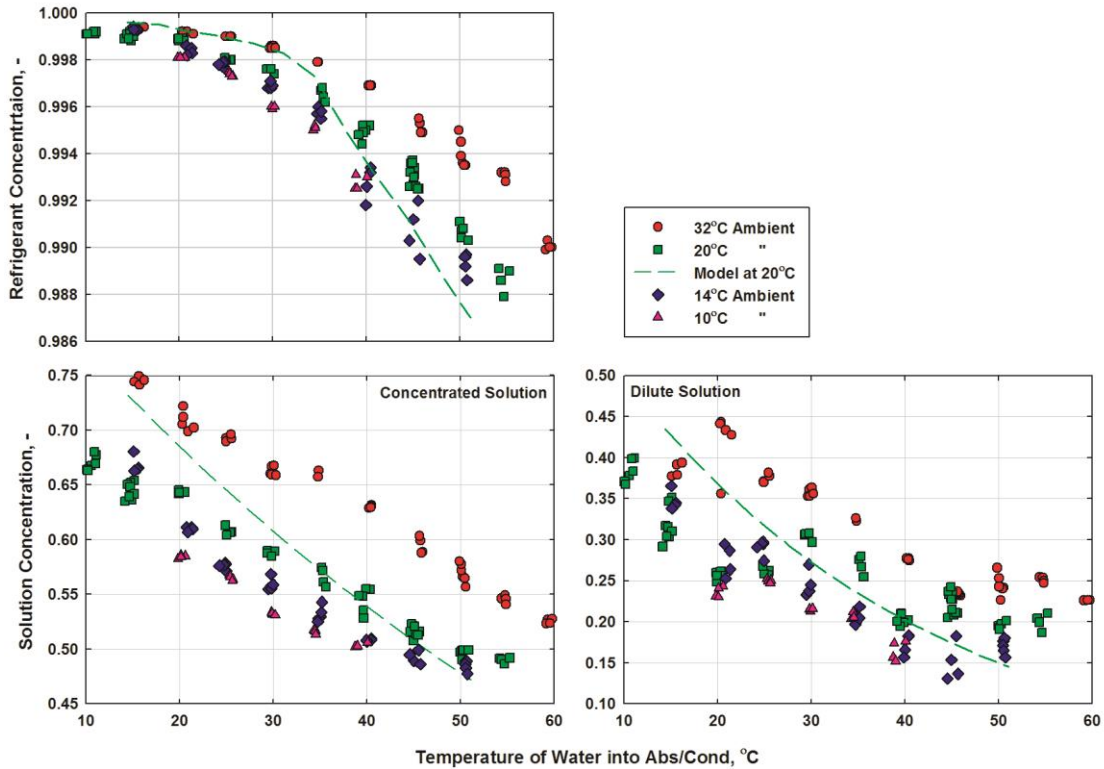


Figure 4.9: Solution and refrigerant concentrations

significantly with the change in water temperature than the experimental data. The bottom right plot shows that the dilute solution concentration increases with lower water temperatures. This agrees with the trend of increased concentrated solution concentrations. The higher solution concentrations lead to the desorber generating more refrigerant, but also operating at lower temperatures. Dilute solution exiting the component is cooler and has a higher concentration of ammonia.

It should be noted that the packaged system uses refrigerant and solution storage tanks that allow for shifts in concentration over the range of water inlet and ambient temperatures investigated. Without these refrigerant and solution storage tanks, the system would not be able to operate over such a wide range of water inlet temperatures.

In the baseline ambient and water temperatures case, the refrigerant and solution storage tanks are approximately half full. This allows refrigerant to be stored without backing up into the condenser (artificially raising the high side pressure) or discharged without running the refrigerant tank dry (resulting in vapor flow to the refrigerant heat exchanger). The solution storage tank helps to maintain liquid flow to the pump in the case of significant solution and refrigerant storage on the high pressure side, and prevents solution back up into the absorber (artificially raising the low-side pressure) in the case of increased storage on the low pressure side. The volumes of the refrigerant and solution storage tanks are $2.43 \times 10^{-4} \text{ m}^3$ and $1.45 \times 10^{-4} \text{ m}^3$, respectively.

4.5.2.2 Component Performance

Individual component performance is also evaluated for the range of water and ambient temperatures investigated here. Estimated heat duties and UA values are, however, not presented because the uncertainty of the predicted values is significant and trends can be observed from more the accurate temperature data.

Figure 4.10 shows four plots of measured absorber component temperatures for the four ambient cases investigated. The plots show that the temperature difference between the concentrated solution outlet and water coupling inlet is minimal. This is an indication of good absorber performance. The temperature difference between the solution outlet and coupling fluid inlet increases with decreasing water temperature. This is expected as the load on the component is increasing. The increased load is a result of increased refrigerant flow. The concentrated solution concentration increases and the low-side pressure decreases as part of this shift in performance. The increased concentration allows for more refrigerant to be generated in the desorber and the lower pressure

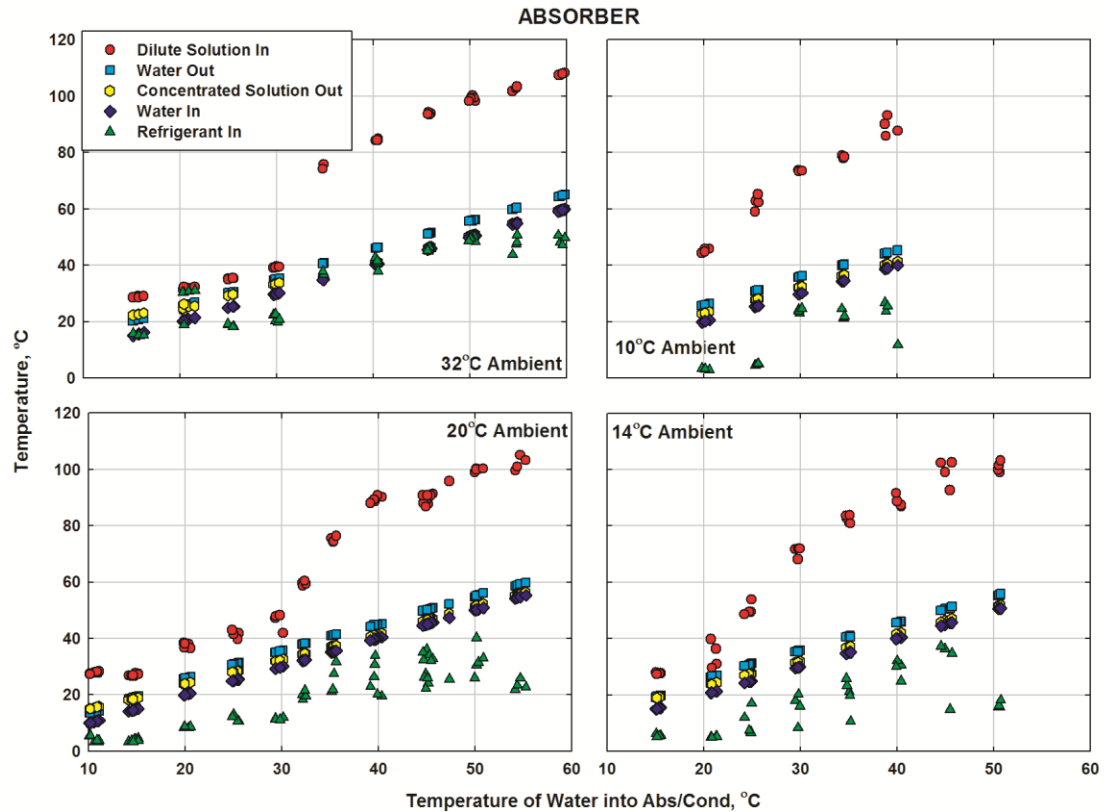


Figure 4.10: Absorber temperature profiles

increases the inlet temperature differences in the evaporator. It is also important to note the inherent link between components in the system: the solution and refrigerant inlet conditions are a result of solution and refrigerant heat exchanger performance.

Figure 4.11 shows four plots of measured condenser temperatures for the four ambient cases investigated. The plots show that the temperature difference between the refrigerant outlet and water coupling outlet is minimal. This is an indication of a well performing condenser. The high-side pressure of the system is dependent on this temperature difference and the amount of subcooling. Minimizing both allows the system to operate at lower high-side pressures and potentially allow for increased refrigerant generation. The plots also show that for a given hot water inlet temperature, the

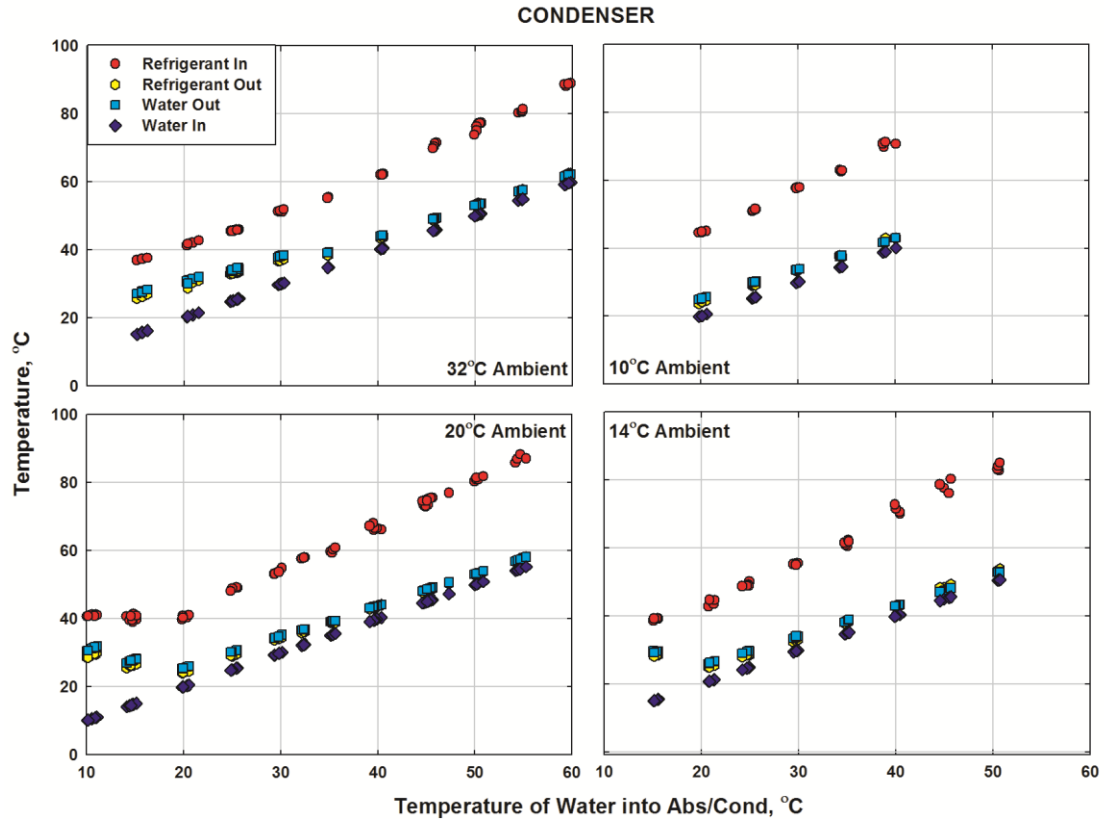


Figure 4.11: Condenser temperature profiles

temperature of the refrigerant entering the condenser is higher at lower ambients. This is because the concentrated solution concentration is lower and the refrigerant generated is at a lower purity for lower ambients.

Figure 4.12 shows four plots of measured desorber component temperatures for the four ambient cases investigated. The plots show that higher dilute solution outlet temperatures are achieved at lower ambients, which is due to lower solution concentrations. The plot also shows that the exhaust gas temperature decreases with decreased coupling water temperatures. At the lowest exhaust temperatures, condensation of water vapor in the flue gas becomes more likely. If condensation of the flue gas occurs

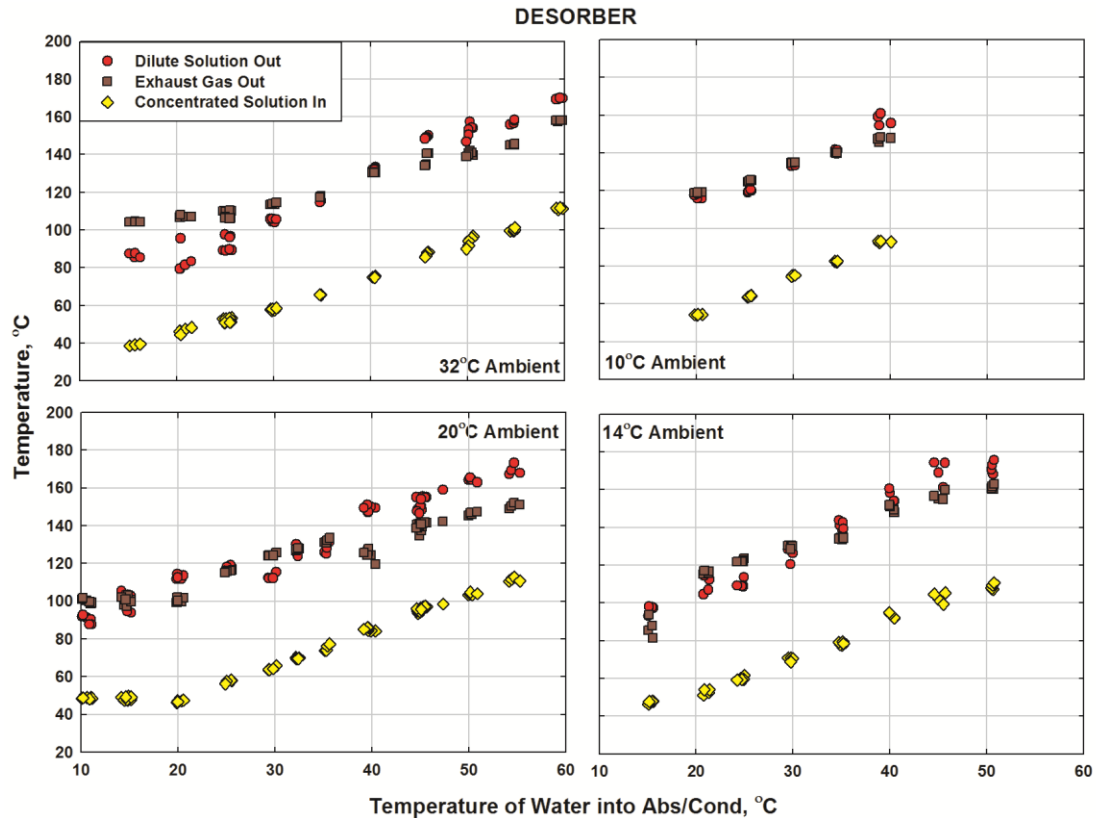


Figure 4.12: Desorber temperature profiles

and enough accumulates in the component, the burner would be extinguished. During testing, this occurred on several occasions. It is important to note that tests conducted in this study required operation at these conditions for extended periods of time (e.g., several hours). However, an actual production unit would likely not experience these low water temperatures for extended time periods. A control strategy could be devised to maintain exhaust gas temperatures above the temperature of condensation of water vapor to account for such situations. The system would have operational security at the cost of a reduced *COP* during such brief periods of operation in this mode.

Figure 4.13 shows four plots of measured evaporator temperatures for the four ambient cases investigated. The plot shows that the refrigerant inlet temperature

decreases with decreasing water temperature. This is because the lower water temperature results in reduced low-side pressure. The temperature change in the coupling fluid increases with decreased hot water inlet temperatures. This is because the effectiveness of the ambient heat exchanger decreases as the heat load of the evaporator is increased. At the high water temperatures, the cooling provided by the evaporator is minimal, and all temperatures approach the ambient air temperature.

Figure 4.14 shows four plots of measured rectifier temperatures for the four ambient cases investigated. The plots show that temperatures increase with increasing coupling water temperatures. Refrigerant outlet temperatures increase with reduced ambient

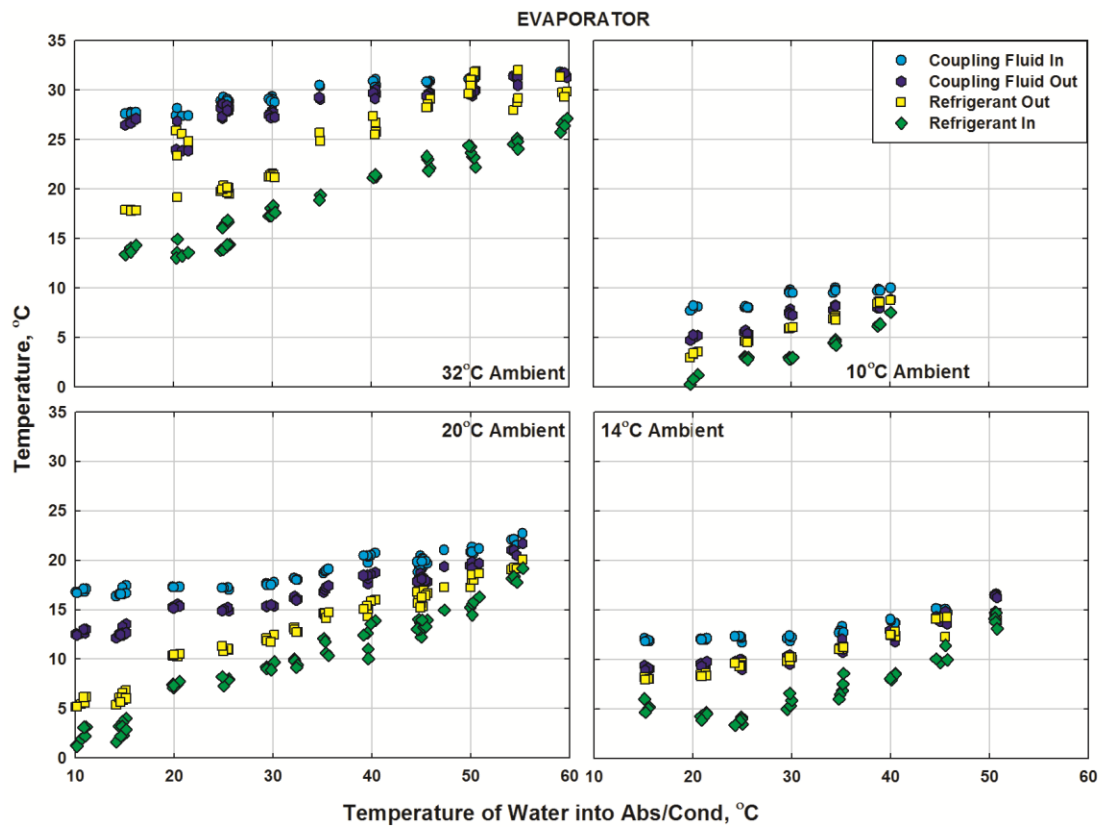


Figure 4.13: Evaporator temperature profiles

temperatures for a given water temperature. The higher temperatures correspond to lower refrigerant purities. Refrigerant temperature and purity are a function of solution concentrations, system pressures and the effectiveness of the rectifier. It is important to note that the difference in concentration between ambient cases for a given water temperature is minimal. Overall, the rectifier produces high purity refrigerant for the points investigated.

Figure 4.15 shows four plots of measured refrigerant heat exchanger temperatures for the four ambient cases investigated. The plots show that the temperature change between the low side inlet and outlet is greater than the high side in most cases. This is expected

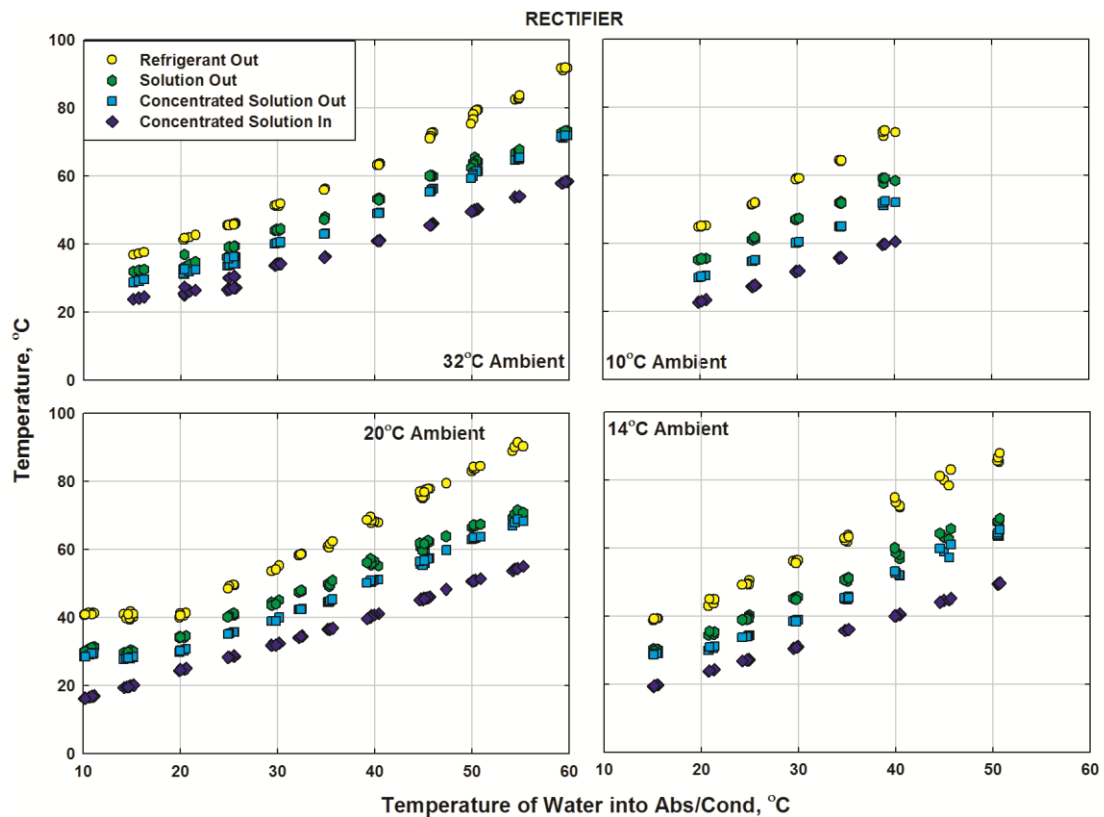


Figure 4.14: Rectifier temperature profiles

as refrigerant enters the heat exchanger near vapor saturation for most cases. The spread in low side outlet temperatures for a given water temperature is the result of varying outlet qualities. Because the refrigerant is a mixture, it experiences a significant temperature rise as the fluid mixture approaches the saturated vapor state.

Figure 4.16 shows four plots of measured solution heat exchanger temperatures for the four ambient cases investigated. Several non-obvious factors contribute to the temperature plots, including phase change of the concentrated solution near the outlet, changing heat exchanger effectiveness and changing solution flow rates. As the concentrated solution is heated, it reaches saturation and begins to vaporize. This limits

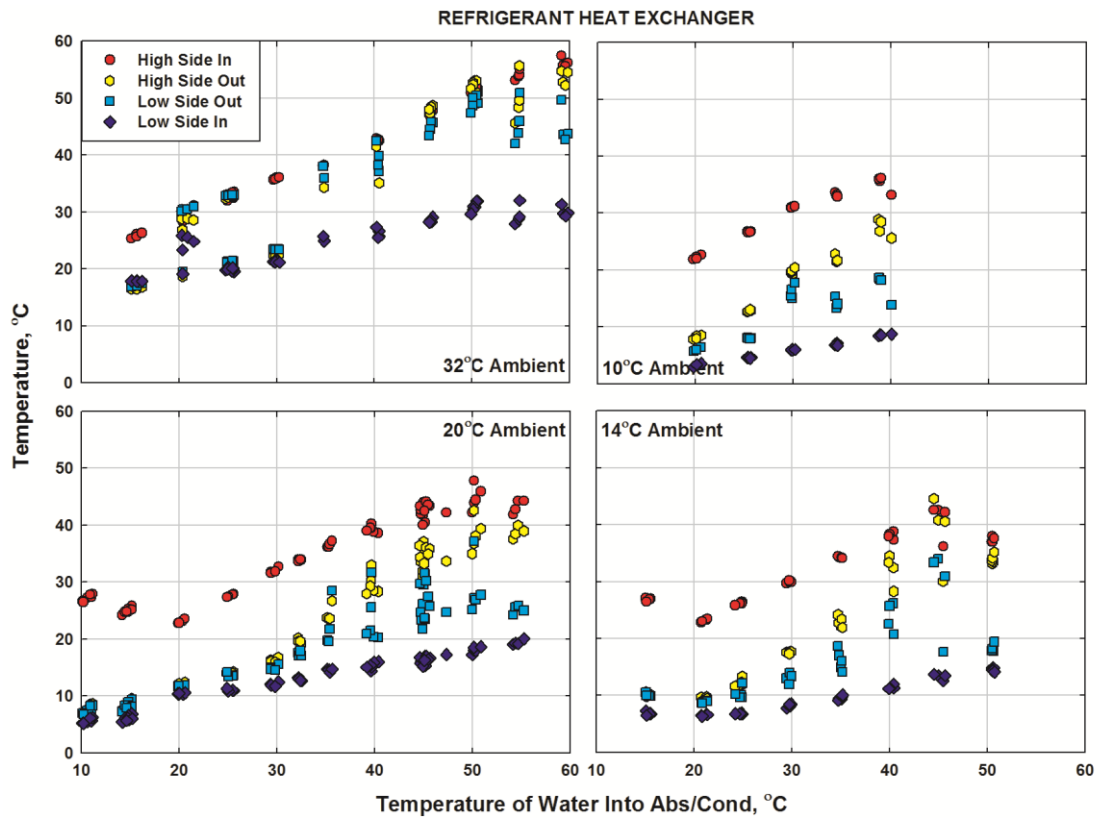


Figure 4.15: Refrigerant heat exchanger temperature profiles

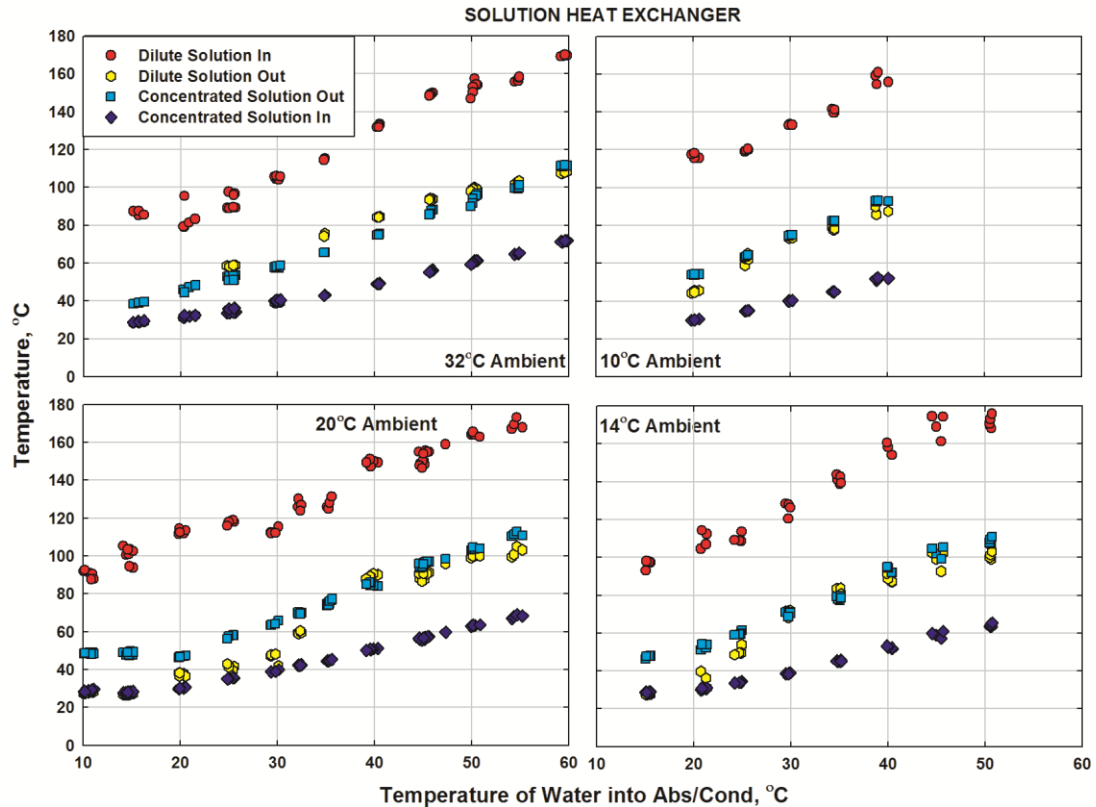


Figure 4.16: Solution heat exchanger temperature profiles

the concentrated solution outlet temperature. At lower water temperatures, the refrigerant flow rate increases and, as a result, the dilute solution flow rate decreases. The decreasing temperature difference between the dilute solution outlet and the concentrated solution inlet shows the impact of decreasing dilute solution flow.

4.6 Model and Experiment Comparison

Some differences between measured performance and modeled results can be seen in Figures 4.6 and 4.7. Adjustments to the model were explored to explain the differences between the data and model predictions presented in Chapter 2. Changes to the model included the addition of a variable ambient heat loss term, a variable evaporator glide,

reduced solution and refrigerant heat exchanger effectiveness values, and setting closest approach temperatures in place of UAs for the condenser and absorber.

The system was well insulated to minimize thermal loss, but operation in a confined space where circulation of air is increased by the ambient fan resulted in some thermal loss. In addition, the temperature difference between several components and the ambient was substantial. For example, the temperature of the dilute solution exiting the desorber ranged from 80 to 180°C, while the ambient temperature ranged from 10 to 32°C. A function that varied linearly was implemented to account for this thermal loss. For the 20°C ambient cases, the loss ranged from 10 to 300 W for water temperatures of 32 to 60°C.

Experimental results showed that the desired evaporator glide of 3°C could not be maintained at higher water inlet temperatures. Based on this result, a linear function was implemented in the cycle model to allow for variation of the evaporator glide with water inlet temperatures. The glide was allowed to range from 3 to 1°C as the water temperature increased from 32 to 60°C.

The solution and refrigerant heat exchanger effectiveness values at the baseline design conditions were reduced to bring model state point and system values into agreement with experimental results. The baseline model predictions of 0.92 and 0.93 for the solution and refrigerant heat exchangers were reduced to 0.72 and 0.80, respectively, implying that the heat recovery in these components is lower than desired.

The remaining changes reflect observations during the tests, and improved model stability. The approach temperature to the condenser was set to 1°C. The condenser

performed well and a minimal approach temperature was maintained throughout. Similarly, the absorber performed well and an approach temperature of 3°C was implemented in the model. Using approach temperatures in place of heat exchange conductance UAs improved model stability and allowed for operation over a larger range of conditions.

These changes brought the model COP and heat duty predictions within 5 percent of the corresponding measured values for the baseline case of a 20°C ambient and 32°C water inlet temperature. The agreement between predicted and measured values was also high throughout the water and ambient temperature range investigated, as shown in Figure 4.17. Improvements in the recuperative heat exchanger, evaporator glide control,

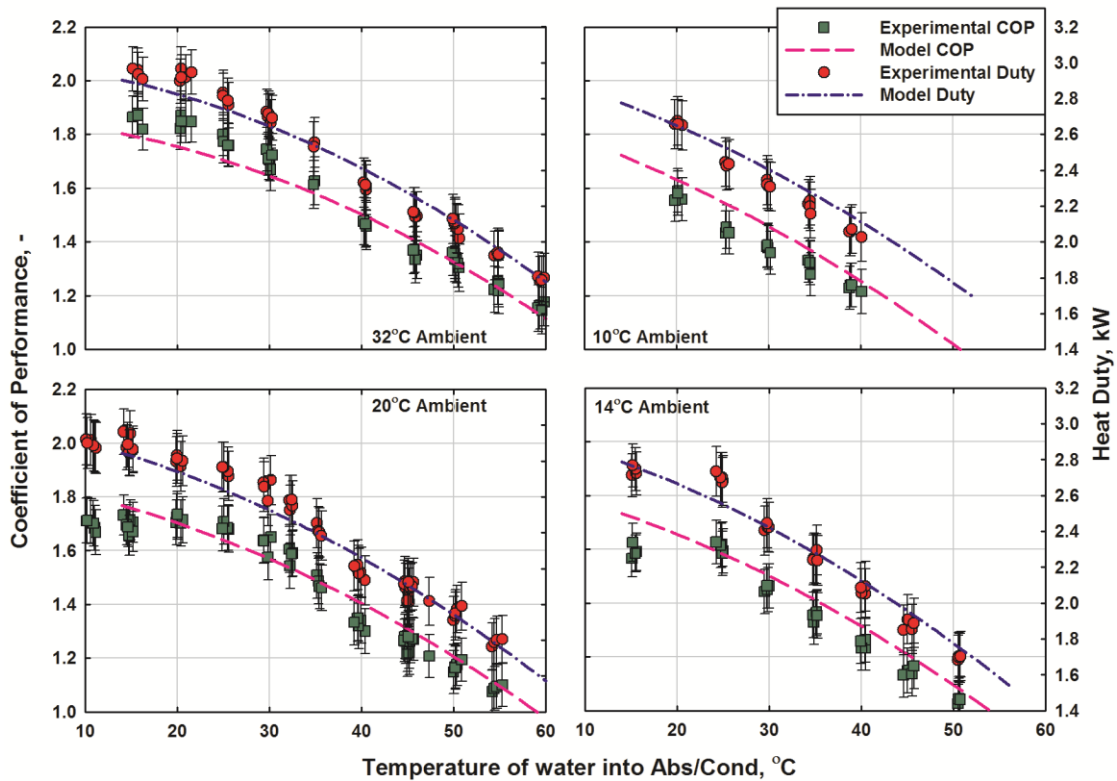


Figure 4.17: COP and heat duty, refined model and experiment comparison

and minimization of heat loss will further improve system performance to the model predictions of Chapter 2.

4.7 Conclusions

In this chapter, compact heat and mass exchangers for an absorption heat pump water heater were developed, with the design and performance of individual components discussed in detail in Chapter 3. Insights from the results of Chapter 3 were used to successfully integrate and demonstrate a refined monolithic heat and mass exchanger into a residential capacity multi-pass water heater prototype in this chapter. The compact heat and mass exchangers enabled a small overall system footprint while maintaining a high level of performance.

The system achieved performance within eight percent of model predictions presented by in Chapter 2 at baseline conditions, delivering a heat duty of 2.58 kW at a *COP* of 1.6. Performance of the system was investigated over a wide range of water (10 – 60°C) and ambient conditions (10 – 32°C). The unit maintained stable operation over this wide range of operating conditions. It maintained a high coefficient of performance for the majority of the conditions. Performance of individual heat and mass exchangers was also interpreted from the measured parameters. Less than expected internal heat recovery, lower than design evaporator glide, and thermal losses may have contributed to the performance not being as high as the model predictions. Addressing these factors will improve system performance further.

The packaged prototype demonstrated here is a significant step forward in the development of high efficiency thermally driven heat pumps for residential capacity water heating.

CHAPTER 5. ENERGY AND COST COMPARISON OF RESIDENTIAL WATER HEATING TECHNOLOGIES

5.1 Introduction

5.1.1 Background

Water heating is the second largest user of energy in households, accounting for up to 18% of total energy costs (DoE 2015c). As a result, focus on the development of more efficient water heaters has increased over the past decade. More efficient water heater designs, like heat pump systems, are being developed to offer Energy Factors (*EF*) above current designs. The Energy Factor is a rating based on a representative daily energy usage test to allow for comparison between different water heating technologies. Direct heated systems are limited to Energy Factors of one or less and have been approaching this theoretical limit for some time. The Energy Factor is one of the criteria considered in the ENERGY STARTM rating of water heaters.

In 2009, manufacturers shipped 8 million water heaters in the United States, one million of which were ENERGY STARTM rated (Ryan *et al.* 2010). Increasing the number of units shipped that meet this rating criterion is important in reducing residential energy consumption. This is more likely to happen if there are more ENERGY STARTM rated water heaters available. The life expectancy of a water heater is 10-15 years (DoE 2015c), which makes increasing the availability and number of these products more pressing because the opportunity to replace these units is infrequent. To address this, two approaches should be taken. First, the number of already commercially proven and available ENERGY STARTM systems should be increased. Second, the development and commercialization of new ENERGY STARTM qualifying water heaters is needed. In

combination, more energy efficient water heaters will be available to consumers and increase market share.

The present study considers both of the steps mentioned above. A survey is performed to determine the overall state and availability of ENERGY STAR™ water heaters. Current water heater technologies are discussed. A recently developed gas-fired absorption heat pump water heater that offers *EF* values greater than one is also discussed. Energy and cost analyses are performed to evaluate the current state of water heaters from a consumer's perspective and the cost of a gas heat pump to allow for a reasonable payback period is estimated.

5.1.2 Prior Work

The studies discussed in this section investigate the cost implications of changes to water heater insulation and parts, as well as the implementation of new water heater designs. Changes in designs to meet US Department of Energy (DOE) standards, and the implementation of heat pump, gas instantaneous or tankless, and condensing gas storage units are also discussed.

Lekov *et al.* (2000) performed a study to estimate the energy savings potential and associated costs for water heaters driven by three different energy sources: a 190 liter electric heated unit, a 150 liter gas-fired unit, and a 120 liter oil-fired unit. Baseline models with current technology and future models that incorporate new mandated features were assessed. Variation in future models included different thicknesses of water blown and HFC-245a blown insulation (to be used in place of HCFC-141b blown insulation), heat traps, plastic tanks, improved flue baffles, side arm heaters and several other potential improvements. The study showed that for the water heaters investigated,

energy-efficiency can be increased by 4% for electric units, 9% for gas-fired units and 2% for oil fired units. The importance of the blowing agent and insulation thickness to reduce standby losses was highlighted. A payback period threshold of less than four years was used to determine acceptable designs. The study concluded that electric and gas-fired water heaters offer a much higher and cost-effective efficiency level with an acceptable payback than oil-fired units.

Tomlinson and Murphy (2004) investigated the performance of 17 integrated electric heat pump water heaters installed at homes in the United States over a period of 18 months. Eleven of the units were installed in the South East Region. The units were equipped with electric resistance heaters for back up heating. Units were switched between heat pump and electric resistance heating to allow for comparison of operational performance. The average coefficient of performance (*COPs*) values in resistance and heat pump mode were calculated to be 0.86 and 2.00, respectively. Consumers experienced an average energy savings of 55% with a heat pump water heater. This shows that there is the potential for significant energy and monetary savings for an end user. Other important findings from this study were that hot water draw patterns varied significantly from 87 to more than 417 liters per day, compressor runtimes were expectedly long (multiple hours and up to 11.5 hours per day) and the use of the heat pump did not aggravate hot water run-outs as might be expected. They defined hot water run-outs as a draw that ended with a tank outlet temperature of 40.5°C or lower. Run-outs were typically experienced less than 5 times a day and were not dependent on the mode of operation (resistance heater or heat pump).

Schoenbauer *et al.* (2011) investigated the use of gas-fired storage water heaters, instantaneous water heaters, and condensing instantaneous water heaters for residential applications by performing field tests at ten households. The 15-month study showed that instantaneous water heaters allowed for a reduction in energy use and operational cost when compared to the standard gas-fired storage unit. Non-condensing instantaneous units used 22-54% less energy than the storage units. Condensing instantaneous units used 23-63% less energy than storage units. However, the high installation cost, in addition to a lengthy payback period, makes the instantaneous units economically undesirable.

Lekov *et al.* (2011) conducted a life-cycle cost and payback period analysis for gas and electric storage water heaters. The study was motivated by new energy efficiency standards for residential water heaters by the US Department of Energy set to take effect in 2015. Gas storage (condensing and non-condensing), electric storage and electric heat pump storage water heaters were assessed. Capital, installation and operational costs were considered for each unit. The study showed that efficiency improvements to the baseline units reduce the life-cycle cost in most cases for gas and electric water heaters. They found that electric heat pump and condensing gas units provided lower life-cycle cost for homes with large volume water heaters.

The studies discussed above highlight different aspects of different water heating technologies. Some valuable findings about heat pump water heaters were reported. The first is that the use of a heat pump did not result in hot water run-outs as is a concern of many evaluating the viability of this technology. The second is that the high-efficiency

units are most suited for homes with large volume water heaters where they provide lower life cycle costs.

5.2 Rating Systems

Several rating systems have been instituted to allow for the evaluation and comparison of different water heater designs on an equivalent basis. The Energy Factor allows for comparison of performance across all designs and is a U.S. Department of Energy test that evaluates energy usage throughout a representative day. Test conditions, instrumentation, installation, test procedure and calculation requirements can be found at DoE (2015a).

Technology-specific ratings have also been developed, and include the First-Hour Rating (*FHR*) for storage water heaters, and the Liters-per-Minute (*LPM*) flow rating for instantaneous water heaters. The *FHR* is the maximum volume of hot water that a storage water tank can supply within an hour where the tank is initially fully heated. The *LPM* is the maximum flow rate that can be provided by an instantaneous water heater while maintaining a temperature rise of 43°C (DoE 2015d). The U.S. Department of Energy uses these tests to benchmark technologies. The *EF* and other tests are used to set lower limits to the ENERGY STAR™ rating. These values have increased and continue to increase as technologies are improved. For electric storage units, a minimum *EF* and *FHR* of 2.0 and 189 liters per hour are required, respectively. For gas storage units, a minimum *EF* and *FHR* of 0.67 and 254 liters per hour are required, respectively. For gas instantaneous units, a minimum *EF* of 0.82 and *LPM* of 9.5 liters per minute are required.

Another aspect relevant to the comparison of fossil fuel and electric heated units is the accounting of the inefficiencies related to the generation and transmission of

electricity. When accounting for these inefficiencies, the word Primary is typically used as a prefix for the variable of interest, e.g., Primary *EF*. The penalty associated with this added cost for grid electricity is a factor of 3.14 (DoE 2013). Similarly, source penalties associated with natural gas, propane and heating oil No. 2 are 1.05, 1.01 and 1.01, respectively.

5.3 Water Heater Designs

Water heating technologies investigated in the present study are briefly described here, along with their advantages and limitations. The majority of these technologies are commercially available and information on them was gathered from nationwide distributors (HomeDepot 2015), manufacturers (Rheem, Electrolux, Westinghouse), and energy related agencies (ACEEE 2015; DoE 2015d). Gas storage (non-condensing, condensing and heat pump), electric storage (direct heated and heat pump), tankless (non-condensing, condensing and electric) and heating oil water heaters are reviewed below. Figures 5.1 and 5.2 show schematics of the water heating technologies under consideration here.

5.3.1 Gas Storage

These systems use the combustion of natural gas or liquid propane to directly heat stored water. Natural gas systems are more common in areas with local natural gas utilities. Propane systems are more common in areas where on-site gas storage is required. The combustion of gas to heat water is simple, effective and reliable, making it a widely adopted technology for residential water heating.

Standard gas storage water heaters (Fig. 5.1a) are available with a range of system parameters. For the units surveyed, these parameters include heating rate (9-23 kW), tank

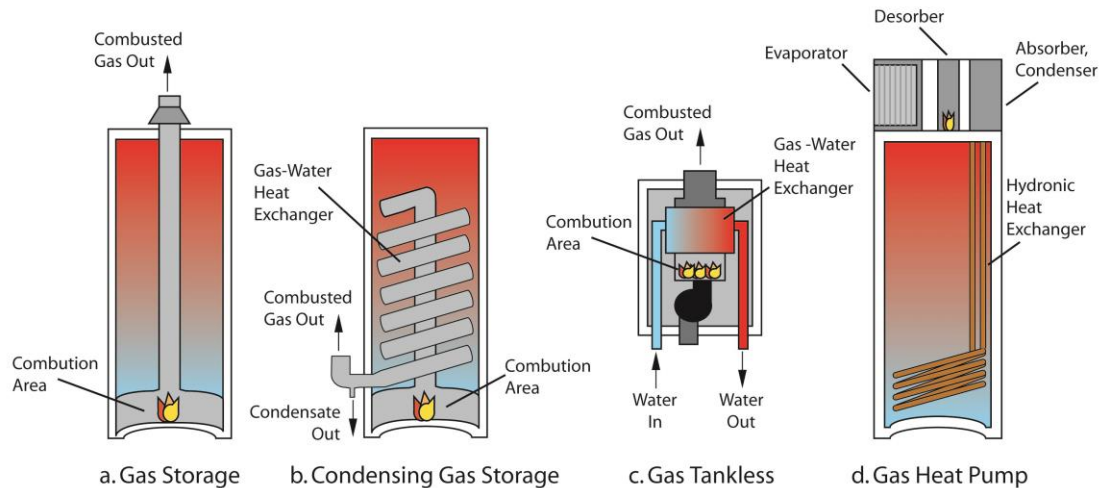


Figure 5.1: Schematics of gas water heaters

volume (110-370 L), *EF* rating (0.48-0.69), height (1.3-1.9 m), and diameter (0.4-0.7 m). The *FHR* for these systems ranged from 185-511 liters. It should be noted that the higher *EF* rated units are power damper and power vent systems. The large number of options cater well to the selection of a gas water heater for any residential capacity and space constraint. Few parts and a long product life make these units inexpensive and worry-free for most users. However, direct heating and combustion losses for the non-condensing systems lead to low *EF* values. The theoretical limit for a direct heated unit is 1, with these systems operating well below this value.

A more efficient gas storage technology is one where the combusted materials are cooled to the point of water vapor condensation (Fig. 5.1b). This allows for almost all of the heat of combustion to be transferred to the water tank. The *FHR* for the systems surveyed ranged from 529-583 liters with storage tank volumes of 227-303 liters. Storage volume sizes align with the idea that these higher efficiency systems are cost effective in high water usage installations. Energy Factor values are not reported but are expected to

be 0.77 or higher. This increase in efficiency comes with increased system complexity, size and cost, and as a result, this technology is targeted at households of 5 or more to help reduce its payback period.

5.3.2 Gas Tankless

Gas tankless units allow for on demand hot water use without a water storage tank and the stand-by losses associated with a tank (Fig. 5.1c). Many of these units are ENERGY STAR™ rated and they are a good option where space is a significant constraint. Although these systems maintain high *EF* values, they are direct heated and limited to *EF* values below 1. Also, the achievable temperature of delivered hot water is a function of water flow rate, and simultaneous water draws may limit the temperature of water delivered to each user. High installation cost and lengthy payback periods, as highlighted by Schoenbauer *et al.* (2011), are other drawbacks of these systems.

Non-condensing gas tankless units are available for a range of system parameters. The heating rate and *EF* of these units range from 22-59 kW and 0.82, respectively. The Liter-per-Minute rating ranges from 12.5-16.3 LPM.

Condensing gas tankless units are available for the larger heating capacities (46-58 kW.) The Energy Factor of the surveyed systems ranged from 0.91-0.98. The Liter-per-Minute rating ranged from 14.4-21.2 LPM. Similar to condensing gas storage units, the added costs of these systems result in them being targeted to large draw households. The *EF* values achieved show that this technology is approaching its *EF* limit and alternative technologies will be required for gas-fired systems to achieve higher *EF* values.

5.3.3 Gas Heat Pump

At present, there are no commercially available gas heat pump water heaters at the residential capacity. However, studies conducted by a number of researchers (Garrabrant *et al.* 2013b; Garrabrant *et al.* 2014) and the present study have shown the potential of such systems. Garrabrant *et al.* (2014) presented experimental results from three absorption heat pump storage water heater systems (284 liter tank) that were indicative of *EF* values of 1.2-1.3. Chapter 4 presented experimental results for a compact packaged prototype absorption heat pump using microchannel heat and mass exchangers. The system was designed to be tank mounted, similar to current electric heat pump water heaters and provided 2.58 kW at a COP of 1.6. These systems used the combustion of natural gas to drive an absorption heat pump system (Fig 5.1d). This system is more complex than a direct heated system, is larger and more costly, but with benefits of lower energy use and operating costs. These emerging compact and cost competitive gas-fired absorption heat pump systems enable a commercially viable gas-fired storage water heater to achieve *EF* values greater than 1. This is significant because gas water heating technologies are currently limited to *EF* values less than 1, while electric heat pump systems are advancing electric water heating options to *EF* values greater than 1.

5.3.4 Heating Oil-fired Units

Oil-fired water heater units operate in a manner similar to the gas-fired units. A mixture of oil and air is combusted to heat stored water. These units have a high capital cost and relatively low *EF* values in the 0.53-0.55 range. High fuel costs are another drawback of these systems.

5.3.5 Electric Storage

Similar to non-condensing gas storage units, electric storage water heaters are available with a range of system parameters (Fig. 5.2a). These parameters include heating rate (7.6-11 kW), tank volume (110-435 L), *EF* rating (0.86-0.95), height (0.66-1.8 m), and diameter (0.45-0.8 m). The range of water heating options makes selecting an electric storage unit for a desired size and space constraint straightforward. Few parts and long product life make these units inexpensive and maintenance free for most users.

The high *EF* values appear to make these units attractive. However, based on the ENERGY STAR™ rating system, none of these units qualify as ENERGY STAR™ products. This is because electric storage units are required to have *EF* values greater than 2.0. This is in part to account for electricity production and transmission losses. If the *EF* is adjusted to account for these losses (DoE 2013), the Primary *EF* values for the surveyed electric storage units range from 0.27-0.31.

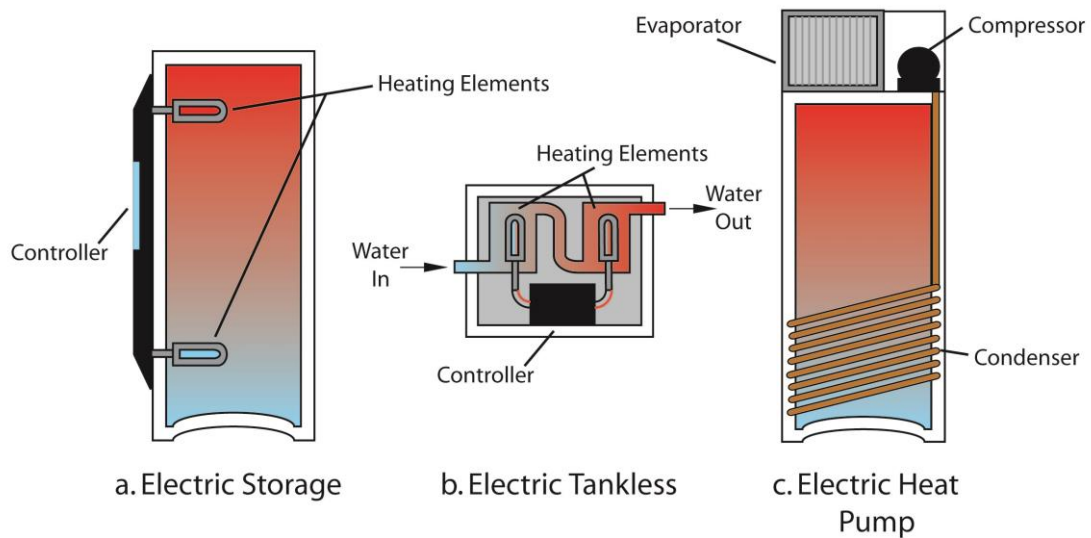


Figure 5.2: Schematic of electric water heaters

5.3.6 Electric Tankless

Electric tankless water heaters can be sized to meet the needs of a single location within a home (e.g., kitchen sink) or meet the needs of an entire home (Fig. 5.2b). As a result, capacities can range from a few kilowatts to tens of kilowatts. Heating rates of the systems surveyed here range from 18-38 kW. The high on-demand electrical need of these units requires dedicated high amperage breakers for many of these systems. Some residences may not be equipped to handle the electrical demand of the larger tankless units.

5.3.7 Electric Heat Pump

ENERGY STARTM qualifying *EF* values are one of several benefits of electric heat pump units. Energy Factor and *FHR* values of the units surveyed ranged from 2.35-3.0 and 216-289 liters, respectively. The corresponding Primary *EF* values ranged from 0.75-0.96. These units operate by pumping low grade heat from the surroundings to the desired water heating temperature, at which it is used to heat a water storage tank (Fig. 5.2c). Electric heat pump systems are designed to operate within ambient temperature ranges of 0-60°C. The working fluid of the electric heat pump depends on the unit, and manufacturers currently use R-410a and R-134a. In addition to the heat pump, the water heaters are equipped with an electric resistance back-up heater located in the top half of the tank. This heater can assist during periods of significant water draws or when the ambient temperature is outside the range of operation of the heat pump. Tomlinson and Murphy (2004) indicated that typical heat pump water heater operation did not require the use of this back up heater, which can be disabled in most systems.

Heat pump systems offer the benefits of better *EF* values, but with the penalty of increased system complexity, size and cost, making them more suitable primarily for large draw households where the payback period can be reduced. Other potential drawbacks are that the extraction of ambient heat by the heat pump may negatively impact conditioned space temperature, and the operational noise (compressor and fan) may disturb occupants.

5.4 Energy and Cost Analysis

The annual energy usage and operating cost of each technology is an important factor in the evaluation of water heater technologies. Typically, less expensive units use more energy and have higher operating costs, negating the benefit of the lower capital investment within a few years. On the other hand, technologies requiring increased capital and lower operating costs are not economically viable for low hot water usage situations. Therefore, water heaters are designed with specific residence capacities in mind.

Hot water usage, fuel cost and water heater efficiency are all important factors that contribute to the merits of a water heater. The average household in the U.S. uses 243 liters of hot water a day (DoE 2015c). This value is used in the base case evaluation of the technologies investigated here. Table 5.1 presents pricing information for fuels used by commercially available water heaters. The values presented are the average of residential price data for 2014 published by the Energy Information Agency (EIA 2015). The Energy Factor is the final input required for the estimation of annual energy consumption and is published by nationwide distributors and manufacturers as noted in the previous section. Figure 5.3 shows a plot of the Energy Factor ranges for these water

Table 5.1: Water heater fuel pricing (EIA 2015)

Fuel Type	Fuel Cost
Propane	0.76 \$ liter ⁻¹
Natural Gas	1.097 \$ therm ⁻¹
Electricity	0.125 \$ kWh ⁻¹
Heating Oil No. 2	0.99 \$ liter ⁻¹

heating technologies. It can be seen that many of the direct heated systems are approaching their theoretical limit of one, while heat pump systems have *EF* values greater than one. Accounting for inefficiencies in the generation and transmission of electricity (DoE 2015d) shows that a gas-fired heat pump would offer the highest Primary *EF*. It should be noted that an *EF* value of 3.14 or greater would be required for the electric heat pump to achieve Primary *EF* values of 1 or greater.

Equations 5.1 and 5.2 are used to estimate the annual energy usage and operating cost

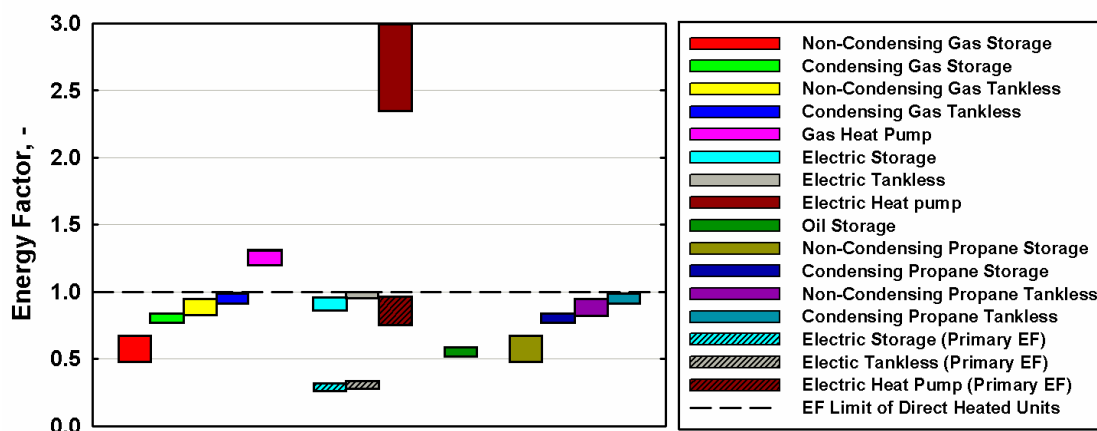


Figure 5.3: Energy Factors for systems under investigation

of a specific water heating system. The mass term is determined based on the assumed volume of water used in a day. The specific heat of water is calculated using the average temperature of water. The temperature difference is assumed to be 45 K based on the water being heated from a ground water temperature of 15°C to a stored temperature of 60°C. Fuel cost values presented in Table 5.1 are converted to appropriate units and used for applicable water designs.

$$Energy_{\text{annual}} = \frac{m \cdot cp_{\text{water,avg}} \cdot \Delta T_{\text{water}}}{EF_{\text{water-heater}}} \cdot 365 \text{ days} \quad (5.1)$$

$$Cost_{\text{annual}} = Energy_{\text{annual}} \cdot Cost_{\text{fuel}} \quad (5.2)$$

Representative water heating systems, of those surveyed above, were selected for each technology of interest (Table 5.2). Larger capacity units were selected for each technology, because this study focuses on comparison with advanced water heating technologies that are typically more suitable for larger residential water heating applications.

The (simple) payback period for each unit was calculated using Equation 5.3. The electric storage and non-condensing gas storage units are used as the baseline costs depending on the case under consideration. Payback periods are determined for the more efficient and expensive units to estimate the time required to recover the additional initial capital cost compared to the baseline units. This analysis provides an additional comparative metric and helps establish pricing targets for the emerging gas-fired heat pump water heater. Installation costs were approximated based on values reported from several sources (Lekov *et al.* 2011; Sachs *et al.* 2012; ACEEE 2015).

$$Payback = \frac{(Cost_{\text{water heater}} - Cost_{\text{baseline}})_{\text{Unit + Installation}}}{(Cost_{\text{baseline}} - Cost_{\text{water heater}})_{\text{Annual Operation}}} \quad (5.3)$$

5.5 Results and Discussion

Annual energy use and operating costs of selected water heating technologies are presented for the base case of 243 liters per day. The natural gas water heaters are then investigated for additional daily total draw volumes (303 and 379 liters) to allow for

Table 5.2: Water heating systems investigated

Fuel	Storage or Instantaneous	ENERGY STAR™	Heating Rate	Storage Volume	EF	Unit Cost
-	-	-	kW	L	-	\$
Gas	Storage	No	22.0	284	0.59	1,228
Gas	Storage (Condensing)	Yes	22.3	303	0.80	2,789
Gas	Instantaneous	Yes	58.6	-	0.82	1,023
Gas	Instantaneous (Condensing)	Yes	58.6	-	0.94	1,299
Gas	Storage (Heat Pump)	N/A	2.8	284	1.3	N/A
Propane	Storage	No	20.5	284	0.59	1,258
Propane	Storage (Condensing)	Yes	22.3	227	0.80	2,403
Propane	Instantaneous	Yes	58.6	-	0.82	1,154
Propane	Instantaneous (Condensing)	Yes	58.6	-	0.94	1,173
Electricity	Storage	No	11	303	0.92	591
Electricity	Instantaneous	No	36	-	0.98	848
Electricity	Storage (Heat Pump)	Yes	-	303	3.0	1,899
Oil No. 2	Storage	No	-	189	0.55	2,000

comparison of the more advanced gas-fired technologies.

5.5.1 Base Case of 243 Liters per Day

Figure 5.4 shows a graph of the estimated annual energy usage for each technology assuming a daily draw volume of 243 liters. The plot shows that energy usage is reduced with increased system complexity. The gas and electric heat pumps use the least energy of the systems investigated. This is expected, as the heat pumps use low grade heat from the ambient and pump it to a higher temperature. Heating oil based storage water heating uses the most energy annually due to its low *EF* value.

Figure 5.5 shows a graph of the estimated annual operating cost of each technology. All of the gas-fired systems, except for the non-condensing gas storage, have operating costs that are competitive with the electric heat pump. The gas-fired heat pump has the lowest operating cost of all units evaluated. The electric heat pump offers a significant operating cost reduction when compared to the other electric heating technologies. The high operating cost of the propane units is a function of fuel cost and fuel energy density.

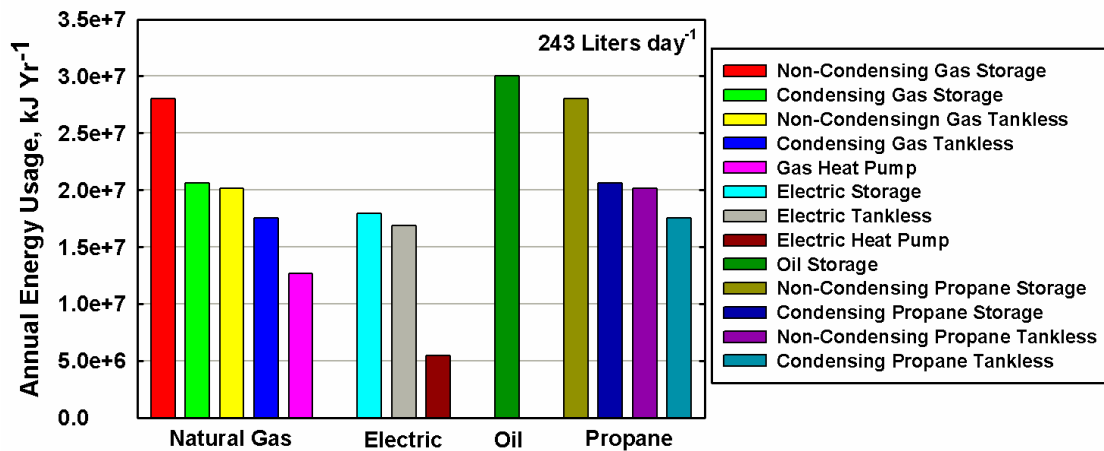


Figure 5.4: Annual energy usage of water heaters investigated

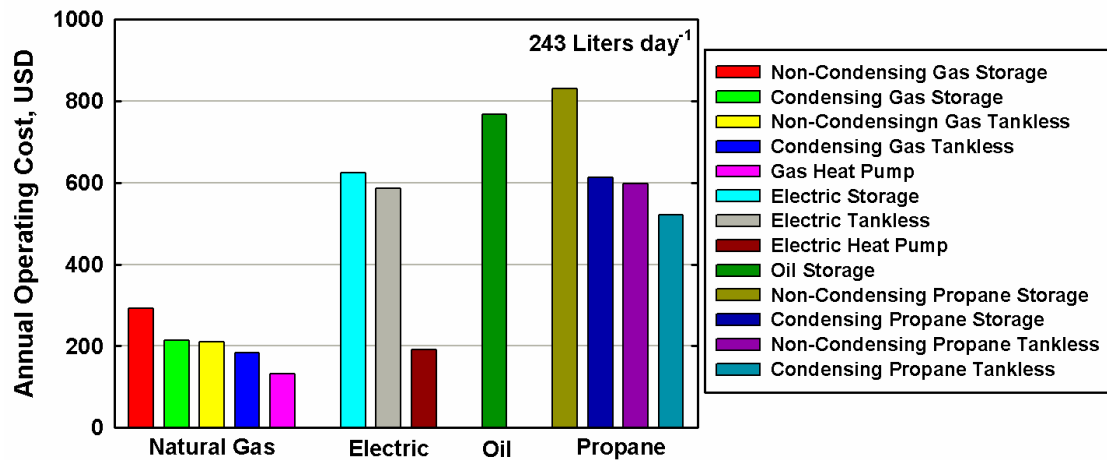


Figure 5.5: Annual operating cost of water heaters investigated

As noted previously, propane systems would primarily be used in locations where natural gas utilities are not available.

The payback period of water heating technologies, with respect to investment in an electric storage unit, were then investigated. The electric storage unit was chosen as the base case because of its low capital and installation cost. Unit costs were reported in Table 5.2 and installation costs were estimated based on available data (Lekov *et al.* 2011; Sachs *et al.* 2012; ACEEE 2015). The cost of the emerging gas-fired heat pump is unknown, and for the purpose of this study, a total cost (unit and installation) is assumed. If the gas heat pump has a cost equivalent to that of the electric heat pump system (\$2,400,) the payback period for the gas-fired heat pump is 3.1 years. The payback period for the electric heat pump is 3.6 years. These payback periods are below the 4 year threshold mentioned by Lekov *et al.* (2000). If the total gas-fired heat pump cost was reduced to \$2,000, a payback period of 2.3 years would be achieved. Figure 5.6 shows a graph of payback periods and includes the gas-fired heat pump case of \$2,000. If this

total cost is achieved, it will offer the lowest payback period (roughly two-thirds of the electric heat pump) of the water heating units considered.

Reducing unit cost and/or implementing these units in households with larger daily draw values will help meet this payback threshold. The graph also shows that the non-condensing gas storage and tankless units offer the second shortest payback periods. This is because of the low unit and operating costs. The significant capital costs and low *EF* values result in the long payback period for the condensing gas storage system.

Another important consideration for residential water heaters is that they are replaced every 10-15 years. Higher efficiency units will continue to save the user energy and money beyond the payback period. Figure 5.7 shows a plot of total unit cost over a 13 year period. For this graph, the initial cost of the gas-fired heat pump system is assumed to be \$2,000. The gas-fired heat pump unit has the lowest total cost after 13 years. The

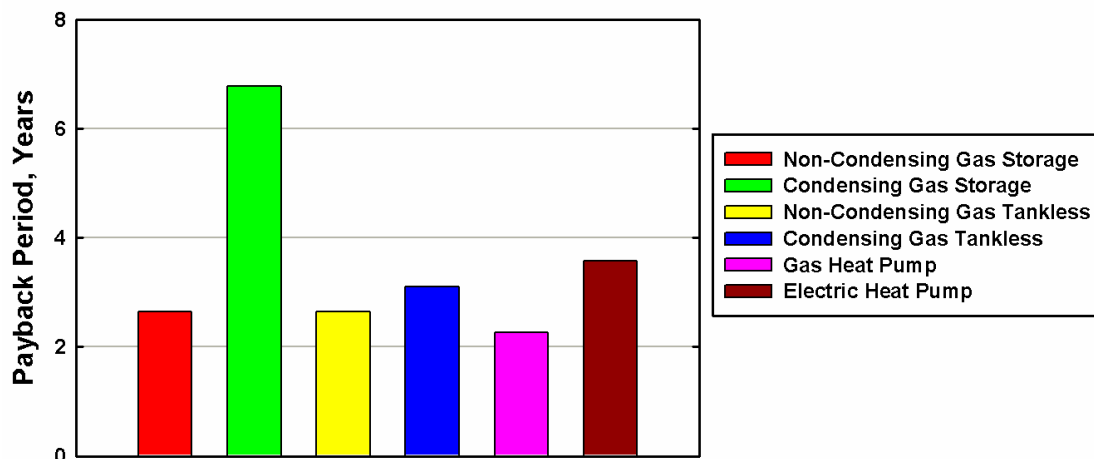


Figure 5.6: Estimated payback period for water heaters investigated

high EF values and comparatively low price of natural gas contribute to this result. The gas-fired heat pump has an estimated lifetime cost of \$3,800, while the electric heat pump has a lifetime cost of \$5,200. The electric and non-condensing gas storage units have lifetime costs of \$9,000 and \$5,600, respectively. The heat pump units offer substantial energy and cost saving when compared to their basic direct-heated counterparts.

5.5.2 Large Daily Total Draws

The total cost (unit and installation) of the gas-fired heat pump was estimated assuming a 4-year (simple) payback with the non-condensing gas storage unit as the base case. The total cost required was determined to be \$2,400. Increasing this gas-fired heat pump *EF* and minimizing total cost would help to reduce the payback period and make the unit more appealing to a consumer.

The study presented by Tomlinson and Murphy (2004) noted that daily total draw volumes can be as high as 417 liters per day, depending on the household. They reported that individual occupant usage ranged from 38 to 117 liters per day and averaged 73

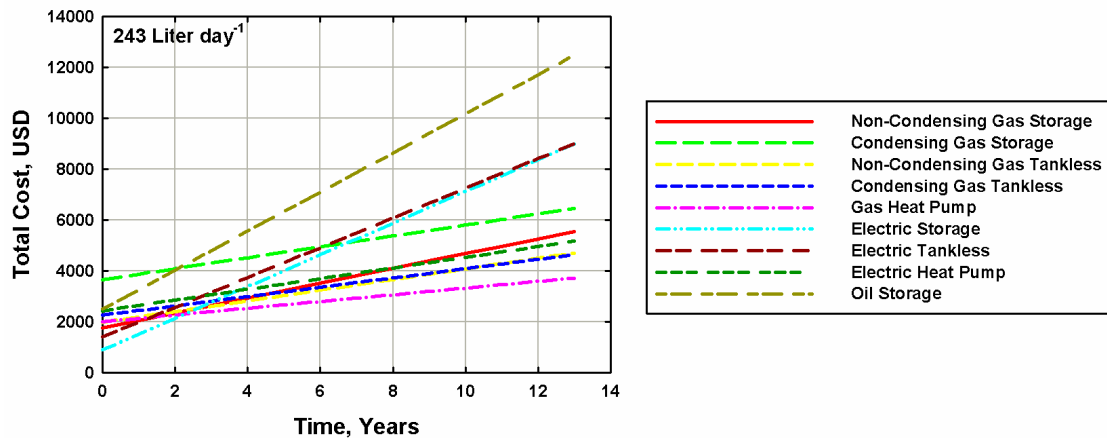


Figure 5.7: Total lifetime cost for water heaters investigated

liters. As a result, daily draw volumes of 303 and 379 liters were investigated, in addition to the 243 liter per day draw for gas water heaters and represented the addition of occupants. These larger daily draws are representative of households with more occupants. As previously noted, more advanced and more expensive units are targeted towards larger draw residences to minimize the payback period.

Figure 5.8 shows a graph of the estimated annual energy usage for the gas water heaters under consideration. For all cases, the gas-fired heat pump (with an *EF* of 1.3) uses approximately 45% of the energy required for the non-condensing gas storage system, a significant energy reduction.

The estimated annual operating cost for the gas water heaters was also investigated. For all cases considered, the gas heat pump operating cost is roughly 45% of the non-condensing gas storage operating cost. Assuming a total capital cost (unit and installation

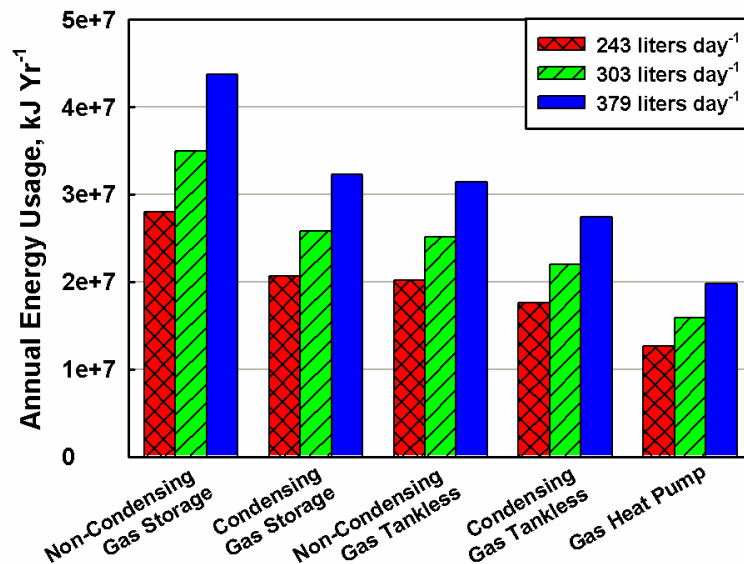


Figure 5.8: Annual energy usage for three daily draw amounts

costs) of \$2,400, the payback period for daily draws of 243, 303, and 379 liters are 4, 3.2 and 2.5 years, respectively, with the non-condensing gas water heater as the baseline system.

Targeting larger water draw households is a good way to minimize the payback period. However, large volume (≥ 212 liters) water heaters only account for roughly 4% of gas storage and 9% of electric storage water heater shipments (Lekov *et al.* 2011). As more advanced gas water heaters come to market, this small demographic will become more competitive and the ability to produce cost effective units will be important.

5.6 Conclusions

An assessment of commercially available water heating technologies was performed. Gas-fired, electric heated and oil-fired units were considered. The assessment found that low *EF* rated gas and electric units are available to meet most capacity and size requirements. Higher efficiency units are less populous and are targeted towards larger capacities to limit the payback of their more costly designs. Many direct heated systems are approaching their theoretical *EF* limit of one. Heat pump systems offer *EF* values greater than one, but only electrically driven heat pumps are available. A recently demonstrated gas-fired heat pump system was introduced as a high *EF* gas technology.

Annual energy and operating cost analysis showed that heat pump systems offer significant reductions when compared to conventional designs. Electric and gas-fired heat pump systems offered the lowest energy use and operating cost requirements compared to their respective baseline counterparts (gas or electric). The gas-fired heat pump had the lowest energy and operational costs among all technologies considered.

Meeting a 4 year or lower payback period highlighted the reason for the more complex systems being tailored to larger households. Assuming hot water use of 243 liters a day and a total initial cost of \$2,400, the electric heat pump required a 3.6 year payback period when compared to an electric storage unit. For daily draw volumes of 243, 303 and 379 liters and a total initial cost of \$2,400, the gas-fired heat pump required a 4, 3.2 and 2.5 year payback period when compared to a non-condensing gas storage unit, respectively.

The study showed the potential savings of these units over the lifetime of each product. The use of an electric heat pump, at a lifetime cost of \$5,200, would save \$3,800 over the life of the unit compared to an electric storage water heater (\$9,000). The gas heat pump, at a lifetime cost of \$3,800, would save \$1,800 over the life of the unit compared to a non-condensing gas storage water heater (\$5,600). It is clear that emerging heat pump technologies, especially gas-fired units, contribute significantly to the reduction of household energy consumption and provide considerable lifetime cost benefits despite somewhat higher initial costs.

CHAPTER 6. CONCLUSIONS AND RECOMMENDATIONS

6.1 Overview

A comprehensive study of a direct gas-fired ammonia-water absorption heat pump for multi-pass water heating using microchannel heat and mass exchangers was conducted. This study represents one of the first works to conceptualize, design, fabricate and successfully demonstrate such a system. The system has the ability to provide heating coefficients of performance greater than one, while typical direct gas-fired water heaters are limited to coefficients of performance less than one. The use of microchannel heat and mass exchangers enables implementation of this system in a compact package.

A detailed modeling study was performed to investigate system performance over a range of absorber, condenser and evaporator conditions. The system model was optimized at water inlet and ambient temperatures of 32°C and 20°C, respectively. The optimized baseline model was determined to have a heating duty and *COP* of 2.79 kW and 1.74, respectively. The model was then evaluated at absorber and condenser coupling fluid temperatures ranging from 14.5-60°C, and ambient temperatures ranging from 4.4-32°C. The model predicts significant pressure, concentration, and flow shifts over this range. However, these changes are gradual and are not expected to disrupt system performance. It is important to note that previous studies (modeling and experimental) of absorption systems have not considered operation over the extended range of conditions explored here. This is because absorption systems are typically designed to deliver heated

or chilled water at one specified delivery temperature. The system under investigation would heat water in multiple passes, which necessitates the investigation over the extended range of operating conditions.

The system model was then investigated in combination with a 227 liter storage tank model. Performance for three different heating scenarios was studied: a cold start, response to a 76-liter draw, and response to stand-by losses. The system was predicted to maintain high coefficients of performance for each case with *COP* values between 1.97 and 1.46. System performance was worst in the stand-by loss scenario; minimizing thermal losses will help in maximizing overall system performance. System run time ranged from 1.5 to over 4 hours depending on the scenario. The time required for the system to heat water is a major tradeoff of this higher efficiency device. However, the hot water storage tank is expected to mitigate concerns related to hot water shortages.

Discrete microchannel heat and mass exchangers were designed, fabricated and tested on a breadboard test facility. System and component performances were evaluated at the conditions for which the cycle model was optimized. At near-design conditions, the system had a heating duty and *COP* of 2.06 kW and 1.36, respectively. Experiments showed that the condenser, rectifier and desorber operated near design. The evaporator, refrigerant heat exchanger, and solution heat exchanger were determined to require size adjustments. The absorber was found to be the ‘bottle-neck’ of the system and an alternative design was pursued for the packaged unit. An improved understanding of the vapor-liquid interaction in the microchannel configuration absorber is needed before implementation in future systems.

A packaged prototype system, containing all main and auxiliary loop components, was developed with resized heat and mass exchangers (including an alternative absorber design). The diameter and height of the unit were 0.61 m and 0.51 m, respectively, which would fit well over a conventional residential hot water storage tank. The system achieved performance within 8% of model predictions at baseline conditions, delivering 2.58 kW of heat at a *COP* of 1.6. Performance of the system was investigated over a wide range of water inlet (10-60°C) and ambient conditions (10-32°C). The unit maintained stable operation over this large range of operating conditions and a high coefficient of performance for the majority of conditions. System performance was found to degrade more rapidly at higher water temperatures than was predicted by the design model.

A detailed model prediction-to-measured values comparison showed that several factors influenced system performance at off-design conditions. These factors included lower than design internal heat recovery, lower than design evaporator glide due to incomplete evaporation, and increased thermal loss at higher water temperatures. Adjustments were made to the cycle model, which resulted in improved model prediction-to-measured values agreement at all conditions. Addressing the highlighted factors in the actual system will improve performance and agreement between the optimized baseline model and experiment.

Additional experimental system limitations included low performance at high water and low ambient temperatures, condensation of water in the desorber flue tubes at low water temperatures, and the need for refrigerant and solution tanks with working fluid inventory to ensure stable operation. Review of individual heat and mass exchanger

temperature trends showed the variations in performance over the range of investigated water inlet and ambient air temperatures. The condenser, desorber, rectifier and absorber components performed well. The alternative absorber design was essential for achieving the system performance improvements over the breadboard experiments.

Energy and cost analysis showed that heat pump systems offer significant reductions in energy usage, operating costs and product life costs when compared to conventional direct heated designs. Assuming daily hot water use of 243 liters, an electric heat pump was determined to require a 5 year payback period when compared to a similar storage volume electric unit. For daily draw volumes of 243, 303 and 379 liters, the gas-fired heat pump required 4, 3.2 and 2.5 year pay back periods, respectively, when compared to a similar storage volume non-condensing gas storage unit.

Finally, new and modified engineering design tools resulted from the present study. In particular, performance equations for the heat pump water heater that are a function of water inlet and ambient temperatures were developed. These equations would allow for evaluation of an absorption heat pump for a specific application without the development of a complete cycle model. Adjustments based on experimental results from the breadboard and packaged unit tests were made to the heat exchanger design models to more accurately predict the required heat exchanger length for each component of interest.

6.2 Recommendations

The present study is a major advance in the field of small-capacity gas-fired absorption heat pumps and residential water heaters. However, due to the nature of a

study involving a first packaged prototype, there is room for further advancements. Also, during the course of this study, there were extensions of the presented work that could not be investigated fully. The following recommendations for future research will help to improve the fundamental, component, and system level understanding of small-capacity absorption systems using microchannel heat and mass exchangers.

Heat and mass exchanger component performance was evaluated to determine appropriate sizing during the transition from breadboard to packaged unit testing. During this evaluation, some components were found to limit system performance. These components had one or more fluids entering the unit as two-phase mixtures. During the design of the heat and mass exchangers, distribution into each channel is assumed to be equal, which is unlikely when the fluid enters as a two-phase mixture. A detailed study of two-phase flow distribution from header to channels would help to improve the fundamental understanding of flow maldistribution, and would allow for improved header and heat and mass exchanger design.

The microchannel absorber was determined to significantly limit system operation during breadboard testing. As a result, an alternative absorber design was pursued for the packaged prototype system. Improving the understanding of the absorption process in microchannels, and vapor-liquid interaction is essential to the successful design and development of a convective flow microchannel absorber. Detailed visualization, computational and experimental studies, specifically focused on this component, are needed.

Heat exchangers used in this study were fabricated in a multi-step process where vacuum brazing resulted in hermetically sealed components. The use of braze material in this bonding process helps to ensure this seal but opens the potential for reduction of channel area and channel blockage as the braze material is in a liquid state during the bonding process. Continued efforts are needed to hone this microchannel heat exchanger fabrication technique. Improved fabrication techniques should also help to reduce material requirements for these components. Half inch thick cover plates were used for the monolithic heat exchanger, and are heavy and costly. Refinements of these features will improve effective heat exchange area, and reduce component size, weight, and cost.

The breadboard and packaged prototype systems were manually controlled. This included control of pump speeds and expansion valve positioning. Targeting and maintaining a refrigeration temperature glide with manual control of the refrigerant expansion valve is challenging and would benefit from automation. Automated control of the refrigerant expansion valve will allow for more continuous and optimized control of the glide. In addition, development of control systems for the entire system would be helpful in transitioning from a first packaged prototype to a stand-alone field test unit. System start-up and shut-down of the prototype system were performed manually. These instances of transient operation require controls development and are critical to the implementation of a stand-alone unit.

The successful demonstration of the residential capacity absorption heat pump water heater highlights the potential energy and monetary savings of these systems. Success of this compact system is due in part to the use of microchannel heat and mass exchangers.

These components allowed for the implementation of an advanced system while maintaining the footprint of a typical water heater. Because of this, the investigation of other small-capacity heating and cooling applications where absorption systems were previously overlooked is warranted. These systems could help to reduce energy consumption in residential, commercial and industrial applications. Smaller capacity systems could be used in a modular fashion where increasing or decreasing the number of systems in operation would allow a user to increase or decrease cooling or heating delivered. This would be similar to operating a large capacity system at a reduced load, but could maintain a higher overall efficiency at the lower loads.

The monolith used in the present study helped to simplify heat exchanger fabrication and plumbing. The ability to integrate components of a more complex cycle into a monolithic unit could help to reduce fabrication and plumbing costs. More complex absorption systems, such as the GAX or double effect, require additional heat exchangers and are often regarded as too complex and costly. The use of integrated heat and mass exchangers containing multiple components would potentially make these systems more practical and cost-effective. The benefits of using integrated heat and mass exchangers for these more complex systems should be explored.

APPENDIX A: BREADBOARD EXPERIMENTAL DETAILS

A.1. Breadboard Heat and Mass Exchanger Details

Additional details for the discrete heat and mass exchangers discussed in Chapter 3 are presented here. A table with details is provided for each component of interest. Dimensions, design specifics, and whether the component is off-the-shelf or was custom fabricated are provided.

Table A.1.1: Absorber Details

Characteristic	Value
Off-the-Shelf or Custom Fabrication	Custom Fabrication
Heat Exchanger Type	Microchannel
Flow Configuration	Counter Flow
Fluid in Flow Passage 1	Ammonia-Water Solution
Fluid in Flow Passage 2	Distilled Water
Material	304L Stainless Steel
Shim Design Numbers	EX1180, EX1181
Shim Thickness	0.762 mm
Total number of Shims	30
Channels per shim	55
Channel Hydraulic Diameter	0.402 mm
Channel Length	0.156 m
Overall Heat Exchanger Dimensions	0.283 × 0.081 × 0.029 m

Table A.1.2: Condenser Details

Characteristic	Value
Off-the-Shelf or Custom Fabrication	Custom Fabrication
Heat Exchanger Type	Microchannel
Flow Configuration	Counter Flow
Fluid in Flow Passage 1	Refrigerant
Fluid in Flow Passage 2	Distilled Water
Material	304L Stainless Steel
Shim Design Numbers	EX1015, EX1016
Shim Thickness	0.762 mm
Total number of Shims	30
Channels per shim	55
Channel Hydraulic Diameter	0.402 mm
Channels Length	0.152 m
Overall Heat Exchanger Dimensions	0.229 × 0.081 × 0.029 m

Table A.1.3: Desorber Details

Characteristic	Value
Off-the-Shelf or Custom Fabrication	Custom Fabrication
Heat Exchanger Type	Shell and Tube
Flow Configuration	Counter Flow
Shell Side Fluid	Ammonia-Water Solution
Tube Side Fluid	Combusted Gas
Material	Stainless Steel
Manufacturer	Stone Mountain Technologies Inc.
Shell Outside Diameter	0.051 m
Total Shell Height	0.432m
Notes: Component includes chamber at bottom where the natural gas-air mixture is combusted. Generation 01 component	

Table A.1.4: Evaporator Details

Characteristic	Value
Off-the-Shelf or Custom Fabrication	Custom Fabrication
Heat Exchanger Type	Microchannel
Flow Configuration	Counter Flow
Fluid in Flow Passage 1	Refrigerant
Fluid in Flow Passage 2	Glycol-Water Mixture
Material	304L Stainless Steel
Shim Design Numbers	EX1011, EX1012
Shim Thickness	0.762 mm
Total number of Shims	30
Channels per shim	55
Channel Hydraulic Diameter	0.402 mm
Channel Length	0.102 m
Overall Heat Exchanger Dimensions	0.178 × 0.081 × 0.029 m

Table A.1.5: Rectifier Details

Characteristic	Value
Off-the-Shelf or Custom Fabrication	Custom Fabrication
Heat Exchanger Type	Shell and Tube
Flow Configuration	Counter Flow
Shell Side Fluid	Refrigerant Vapor
Tube Side Fluid	Concentrated Solution
Material	Stainless Steel
Manufacturer	Stone Mountain Technologies Inc.
Shell Outside Diameter	0.051 m
Total Shell Length	0.102 m

Table A.1.6: Refrigerant Heat Exchanger Details

Characteristic	Value
Off-the-Shelf or Custom Fabrication	Custom Fabrication
Heat Exchanger Type	Microchannel
Flow Configuration	Counter Flow
Fluid in Flow Passage 1	High Pressure Refrigerant
Fluid in Flow Passage 2	Low Pressure Refrigerant
Material	304L Stainless Steel
Shim Design Numbers	EX1187, EX1188
Shim Thickness	0.762 mm
Total number of Shims	30
Channels per shim	25
Channel Hydraulic Diameter	0.402 mm
Channel Length	0.089 m
Overall Heat Exchanger Dimensions	0.130 × 0.044 × 0.029 m

Table A.1.7: Solution Heat Exchanger Details

Characteristic	Value
Off-the-Shelf or Custom Fabrication	Custom Fabrication
Heat Exchanger Type	Microchannel
Flow Configuration	Counter Flow
Fluid in Flow Passage 1	Dilute Solution
Fluid in Flow Passage 2	Concentrated Solution
Material	304L Stainless Steel
Shim Design Numbers	EX1011, EX1012
Shim Thickness	0.762 mm
Total number of Shims	20
Channels per shim	55
Channel Hydraulic Diameter	0.402 mm
Channel Length	0.102 m
Overall Heat Exchanger Dimensions	0.178 × 0.081 × 0.023 m

A.2. Breadboard Instrumentation Details

Additional details for the instrumentation used during the breadboard experiments discussed in Chapter 3 are presented here.

Table A.2.1: Summary of instrumentation on the breadboard test facility

Parameter/ Instrument	Model	Manufacturer	Quantity	Range	Accuracy	Operating Limits
Flow meters and transmitter specifications						
Conc./ Dil. Solution	RHM030	Rheonik, GE Sensing	2	0-0.083 kg s ⁻¹	±0.1%	T: -20 to 120°C P: 20 MPa
Conc./ Dil. Solution Transmitter	RHM030	Rheonik, GE Sensing	2			T: -40 to 65°C
Refrigerant	RHM015	Rheonik, GE Sensing	1	0-0.010 kg s ⁻¹	±0.1%	T: -20 to 120°C P: 20 MPa
Refrigerant Transmitter	RHM015	Rheonik, GE Sensing	1			T: -40 to 65°C
Absorber Coupling Fluid	8711	Rosemount	1	0-1.262 ×10 ⁻³ m ³ s ⁻¹	±0.5%	T: -29 to 149°C P: 5.1 MPa
Absorber Coupling Fluid Transmitter	8712C	Rosemount	1			T: -29 to 60°C (Ambient)
Condenser/ Evaporator Coupling Fluid	CMF025 Elite	MicroMotion Inc.	2	0-0.6048 kg s ⁻¹ 0-6.309 ×10 ⁻⁴ m ³ s ⁻¹	±0.1% (Flow) ±0.5 kg m ⁻³ (Density)	T: -240 to 350°C P: 10 MPa
Condenser/ Evaporator Coupling Fluid Transmitter	1700 – Field Mounting	MicroMotion Inc.	2	0-5000 kg m ⁻³ -240 to 450°C		T: -40 to 60°C (Ambient)
Natural Gas	DTM – 200A	Elster American Meter	1	0-200 ft ³ hr ⁻¹	±0.01 ft ³	T: -40 to 70°C P: 0-34 kPa

Table A.2.1: Continued

Parameter/ Instrument	Model	Manufacturer	Quantity	Range	Accuracy	Operating Limits
Pressure transducer and dial gauge specifications						
Absolute	MMA 500	Omega Engineering	2	0-3.45 MPa	±0.035% of Span	T: -45 to 121°C
Absolute	2088	Rosemount	1	0-1.034 MPa	±0.25% of Calibrated Span	T: -40 to 121°C
Dial Gauge	1008SL- 02-600	Ashcroft	2	0-4.14 MPa	±3% of Span	T: -6 to 82°C
Dial Gauge	1008SL- 02-400	Ashcroft	2	0-2.76 MPa	±3% of Span	T: -6 to 82°C
Dial Gauge	1005P	Ashcroft	3	0-689.5 kPa	±3% of Span	T: -40 to 65°C
Thermocouple Specifications						
Thermo couple	T-type	Omega Engineering Inc.	44	-270 to 240°C	±0.25°C	

A.3. Breadboard Experimental Data Analysis

Sample data analysis calculations are presented here for the breadboard experiments reported in Chapter 3. Calculation of the solution and refrigerant stream concentrations is reviewed. The concentration values are used as the third property to fix the state of the ammonia-water flow at the inlet and outlet of most components. An example enthalpy calculation is presented, as enthalpies are needed for component heat duty calculations. Example heat duty, LMTD and overall conductance UA calculations are presented. The total heating duty and absorption system COP calculation are also presented.

Table A.3.1: Example Breadboard System Data Analysis and Uncertainty Calculation

Inputs	Equations	Results
Solution and Refrigerant Concentrations		
Dilute Solution		
$T_{\text{Des,DS,out}} = 104.5^{\circ}\text{C} \pm 0.25^{\circ}\text{C}$ $P_{\text{high-side}} = 1505 \text{ kPa} \pm 8.6 \text{ kPa}$ $q_{\text{Des,DS,out}} = 0$	$x_{\text{DS}} = x_{\text{NH}_3\text{-H}_2\text{O}}(T_{\text{Des,DS,out}}, P_{\text{high-side}}, q_{\text{Des,DS,out}})$	$x_{\text{DS}} = 0.3697 \pm 0.0017$
Refrigerant		
$T_{\text{Rect,ref,out}} = 56.63^{\circ}\text{C} \pm 0.25^{\circ}\text{C}$ $P_{\text{high-side}} = 1505 \text{ kPa} \pm 8.6 \text{ kPa}$ $q_{\text{Rect,ref,out}} = 1$	$x_{\text{Ref}} = x_{\text{NH}_3\text{-H}_2\text{O}}(T_{\text{Rect,ref,out}}, P_{\text{high-side}}, q_{\text{Rect,ref,out}})$	$x_{\text{Ref}} = 0.9979 \pm 0.0001$
Concentrated Solution		
$\dot{m}_{\text{CS}} = 2.1 \times 10^{-3} \text{ kg s}^{-1} \pm 1.7 \times 10^{-6} \text{ kg s}^{-1}$ $\dot{m}_{\text{DS}} = 1.6 \times 10^{-3} \text{ kg s}^{-1} \pm 1.6 \times 10^{-6} \text{ kg s}^{-1}$ $\dot{m}_{\text{Ref}} = 0.49 \times 10^{-3} \text{ kg s}^{-1} \pm 4.9 \times 10^{-7} \text{ kg s}^{-1}$ $x_{\text{DS}} = 0.3697 \pm 0.0017$ $x_{\text{Ref}} = 0.9979 \pm 0.0001$	$\dot{m}_{\text{CS}} \cdot x_{\text{CS}} = \dot{m}_{\text{DS}} \cdot x_{\text{DS}} + \dot{m}_{\text{Ref}} \cdot x_{\text{Ref}}$	$x_{\text{CS}} = 0.5113 \pm 0.0013$

Table A.3.1: Continued

Inputs	Equations	Results
Properties at Ammonia-Water State-points		
Example: Condenser Refrigerant Outlet		
$T_{\text{Cond,Ref,out}} = 37.63^{\circ}\text{C} \pm 0.25^{\circ}\text{C}$ $P_{\text{high-side}} = 1505 \text{ kPa} \pm 8.6 \text{ kPa}$ $x_{\text{Ref}} = 0.9979 \pm 0.0001$	$h_{\text{Cond,Ref,out}} = h_{\text{NH}_3\text{-H}_2\text{O}}(T_{\text{Cond,Ref,out}}, P_{\text{high-side}}, x_{\text{Ref}})$ $v_{\text{Cond,Ref,out}} = v_{\text{NH}_3\text{-H}_2\text{O}}(T_{\text{Cond,Ref,out}}, P_{\text{high-side}}, x_{\text{Ref}})$ $q_{\text{Cond,Ref,out}} = q_{\text{NH}_3\text{-H}_2\text{O}}(T_{\text{Cond,Ref,out}}, P_{\text{high-side}}, x_{\text{Ref}})$	$h_{\text{Cond,Ref,out}} = 177.7 \text{ kJ kg}^{-1} \pm 1.2 \text{ kJ kg}^{-1}$ $v_{\text{Cond,Ref,out}} = 1.72 \times 10^{-3} \text{ m}^3 \text{ kg}^{-1} \pm 1.25 \times 10^{-6} \text{ m}^3 \text{ kg}^{-1}$ $q_{\text{Cond,Ref,out}} \rightarrow \text{subcooled}$
Component Heat Duty, LMTD and UA Calculations		
Example: Condenser		
$\dot{m}_{\text{Ref}} = 0.49 \times 10^{-3} \text{ kg s}^{-1} \pm 4.9 \times 10^{-7} \text{ kg s}^{-1}$ $h_{\text{Cond,Ref,in}} = \text{kJ kg}^{-1} \pm \text{kJ kg}^{-1}$ $h_{\text{Cond,Ref,out}} = 177.7 \text{ kJ kg}^{-1} \pm 1.2 \text{ kJ kg}^{-1}$ $\dot{m}_{\text{Cond,CF}} = 0.02.21 \text{ kg s}^{-1} \pm 2.22 \times 10^{-5} \text{ kg s}^{-1}$ $c_{p\text{Cond,CF}} = 4,180 \text{ J kg}^{-1} \text{ K}^{-1} \pm 1.0 \times 10^{-2} \text{ J kg}^{-1} \text{ K}^{-1}$ $T_{\text{Cond,CF,in}} = 31.04^{\circ}\text{C} \pm 0.25^{\circ}\text{C}$ $T_{\text{Cond,CF,out}} = 37.73^{\circ}\text{C} \pm 0.25^{\circ}\text{C}$	$Q_{\text{Cond,Ref}} = \dot{m}_{\text{Ref}} \cdot (h_{\text{Cond,Ref,in}} - h_{\text{Cond,Ref,out}})$ $Q_{\text{Cond,CF}} = \dot{m}_{\text{Cond,CF}} \cdot c_{p\text{Cond,CF}} \cdot (T_{\text{Cond,CF,out}} - T_{\text{Cond,CF,in}})$	$Q_{\text{Cond,Ref}} = 568.6 \text{ W} \pm 1.1 \text{ W}$ $Q_{\text{Cond,CF}} = 618.5 \text{ W} \pm 32.7 \text{ W}$

Table A.3.1: Continued

Inputs	Equations	Results
Component Heat Duty, LMTD and UA Calculations		
Example: Condenser		
$T_{\text{Cond,Ref,sat}} = 38.87^{\circ}\text{C} \pm 0.21^{\circ}\text{C}$ $T_{\text{Cond,CF,in}} = 31.04^{\circ}\text{C} \pm 0.25^{\circ}\text{C}$ $T_{\text{Cond,CF,out}} = 37.73^{\circ}\text{C} \pm 0.25^{\circ}\text{C}$	$\text{LMTD}_{\text{Cond}} = \frac{((T_{\text{Cond,Ref,Sat}} - T_{\text{Cond,CF,out}}) - (T_{\text{Cond,Ref,Sat}} - T_{\text{Cond,CF,in}}))}{\ln((T_{\text{Cond,Ref,Sat}} - T_{\text{Cond,CF,out}}) \div (T_{\text{Cond,Ref,Sat}} - T_{\text{Cond,CF,in}}))}$	$\text{LMTD}_{\text{Cond}} = 3.47 \text{ K} \pm 0.39 \text{ K}$
$Q_{\text{Cond}} = 594 \text{ W} \pm 16 \text{ W}$ $\text{LMTD}_{\text{Cond}} = 3.47 \text{ K} \pm 0.39 \text{ K}$	$UA_{\text{Cond}} = Q_{\text{Cond}} \cdot \text{LMTD}_{\text{Cond}}^{-1}$	$UA_{\text{Cond}} = 171 \text{ W K}^{-1}$ $\pm 21 \text{ W K}^{-1}$
System Heating Duty and COP		
$Q_{\text{Condenser}} = 594 \text{ W} \pm 16 \text{ W}$ $Q_{\text{Absorber}} = 1,017 \text{ W} \pm 37 \text{ W}$	$Q_{\text{Heating}} = Q_{\text{Condenser}} + Q_{\text{Absorber}}$	$Q_{\text{heating}} = 1,611 \text{ W} \pm 41 \text{ W}$
$Q_{\text{Heating}} = 1,611 \text{ W} \pm 41 \text{ W}$ $Q_{\text{Desorber}} = 1,438 \text{ W} \pm 33 \text{ W}$	$\text{COP}_{\text{Heating}} = Q_{\text{Heating}} \cdot Q_{\text{Desorber}}^{-1}$	$\text{COP}_{\text{Heating}} = 1.12 \pm 0.04$

APPENDIX B: PACKAGED UNIT EXPERIMENTAL DETAILS

B.1 Packaged System Component Details

Additional details for the components integrated into the packaged prototype unit discussed in Chapter 4 are presented here. A table with details is provided for each component of interest. Dimensions, design specifics, and whether the component is off-the-shelf or was custom fabricated are provided.

Table B.1.1: Absorber Details

Characteristic	Value
Off-the-Shelf or Custom Fabrication	Custom Fabrication
Heat Exchanger Type	Shell and Tube
Flow Configuration	Counter Flow
Shell Side Fluid	Ammonia-Water Solution
Tube Side Fluid	Distilled Water
Material	Carbon Steel
Manufacturer	Stone Mountain Technologies Inc.
Shell Outside Diameter	0.051 m
Total Shell Height	0.47 m

Table B.1.2: Desorber Details

Characteristic	Value
Off-the-Shelf or Custom Fabrication	Custom Fabrication
Heat Exchanger Type	Shell and Tube
Flow Configuration	Counter Flow
Shell Side Fluid	Ammonia-Water Solution
Tube Side Fluid	Combusted Gas
Material	Stainless Steel
Manufacturer	Stone Mountain Technologies Inc.
Shell Outside Diameter	0.0635 m
Total Shell Height	0.432 m
Notes: Component includes chamber at bottom where the natural gas-air mixture is combusted. Generation 02 component	

Table B.1.3: Rectifier Details

Characteristic	Value
Off-the-Shelf or Custom Fabrication	Custom Fabrication
Heat Exchanger Type	Shell and Tube
Flow Configuration	Counter Flow
Shell Side Fluid	Refrigerant Vapor
Tube Side Fluid	Concentrated Solution
Material	Stainless Steel
Manufacturer	Stone Mountain Technologies Inc.
Shell Outside Diameter	0.051 m
Total Shell Length	0.102 m

Table B.1.4: Monolith Heat Exchanger Details

Characteristic	Value
Off-the-Shelf or Custom Fabrication	Custom Fabrication
Heat Exchanger Type	Microchannel
Flow Configuration	Counter Flow
Material	304L Stainless Steel
Component Model #	HPWH1300
Shim Design #	HPHX1301, HPHX1302
Shim Thickness	0.762 mm
Total Number of Shims	40
Number of Heat Exchange Areas	4
Channels per Shim per Heat Exchange Area	55
Channel Hydraulic Diameter	0.402 mm
Overall Heat Exchanger Dimensions	0.39 × 0.22 × 0.054 m
Condenser and Evaporator Heat Exchangers	
Channel Length	0.152 m
Open Header Fluid	Refrigerant
Angled Header Fluid	Coupling Fluid
Refrigerant and Solution Heat Exchangers	
Channel Length	0.102 m
RHX Open Header Fluid	Low Pressure Refrigerant
RHX Angled Header Fluid	High Pressure Refrigerant
SHX Open Header Fluid	Dilute Solution
SHX Angled Header Fluid	Concentrated Solution

Table B.1.5: Solution Pump and Motor

Characteristic	Value
Pump	
Off-the-Shelf or Custom Fabrication	Custom Fabrication
Pump Type	Piston-Diaphragm
Material	Carbon Steel
Manufacturer	Stone Mountain Technologies Inc.
Overall Component Dimensions	0.051 × 0.051 × 0.140 m
Notes: Pump designed to meet requirements of high pressure difference, low flow rate and low viscosity-near saturation fluid	
Motor	
Off-the-Shelf or Custom Fabrication	Off-the-Shelf
Motor Type	1/6 HP DC Motor
Manufacturer	Leeson
Model #	CM31D17NZ8Dm
Motor Voltage	90 VDC
Maximum Speed	1750 RPM

Table B.1.6: Coupling Fluid Pump Details (Absorber-Condenser and Evaporator Loops)

Characteristic	Value
Off-the-Shelf or Custom Fabrication	Off-the-Shelf
Pump Type	Centrifugal
Material	Polypropylene
Manufacturer	IWAKI Industries
Model #	MD-30RT-115NL
Motor Type	1/16 HP AC Motor
Motor Voltage	115 Volts AC
Maximum Speed	3150 RPM

Table B.1.7: Ambient Heat Exchanger

Characteristic	Value
Off-the-Shelf or Custom Fabrication	Off-the-Shelf
Heat Exchanger Type	Air-to-Liquid
Flow Configuration	Cross Flow
Tube Side Fluid	Glycol-Water
Material	Aluminum
Manufacturer	Lytron
Model #	ES0714G23
Overall Heat Exchanger Dimensions	0.214 × 0.457 × 0.079 m
Quantity	2
Notes: In the packaged unit, two heat exchangers are stacked vertically to provide total combined heat exchanger dimensions of 0.428 × 0.457 × 0.079 m.	

Table B.1.8: Ambient Heat Exchange Fan

Characteristic	Value
Off-the-Shelf or Custom Fabrication	Off-the-Shelf
Fan Type	Inline - Single Speed
Material	Galvanized Steel
Diameter	0.33 m
Model #	1850K27
Motor Type	120 VAC
Maximum Airflow	1,350 cfm at 0 in sp.
Maximum Speed	1,500

B.2 Packaged Unit Instrumentation Details

Additional details for the instrumentation used during the packaged prototype experiments discussed in Chapter 4 are presented here.

Table B.2.1: Summary of instrumentation on the packaged unit test facility

Parameter/ Instrument	Model	Manufacturer	Quantity	Range	Accuracy	Operating Limits
Flow meters and transmitter specifications						
Absorber- Condenser Coupling Fluid	CMF025 Elite	MicroMotion Inc.	1	0-0.6048 kg s ⁻¹ 0-6.309 ×10 ⁻⁴ m ³ s ⁻¹	±0.1% (Flow) ±0.5 kg m ⁻³ (Density)	T: -240 to 350°C P: 10 MPa
Absorber- Condenser Coupling Fluid Transmitter	1700 – Field Mounting	MicroMotion Inc.	1	0-5000 kg m ⁻³ -240 to 450°C		T: -40 to 60°C (Ambient)
Natural Gas	DTM – 200A	Elster American Meter	1	0-200 ft ³ hr ⁻¹	±0.01 ft ³	T: -40 to 70°C P: 0-34 kPa
Pressure transducer and dial gauge specifications						
Absolute	MMA 500	Omega Engineering	3	0-3.45 MPa	±0.035% of Span	T: -45 to 121°C
Dial Gauge	1008SL- 02-600	Ashcroft	1	0-4.14 MPa	±3% of Span	T: -6 to 82°C
Dial Gauge	1008SL- 02-400	Ashcroft	2	0-2.76 MPa	±3% of Span	T: -6 to 82°C
Dial Gauge	1005P	Ashcroft	2	0-689.5 kPa	±3% of Span	T: -40 to 65°C
Thermocouple Specifications						
Thermo couple	T-type	Omega Engineering Inc.	40	-270 to 240°C	±0.25°C	

B.3 Packaged Unit Experimental Data Analysis

Sample data analysis calculations are presented here for the packaged unit experiments reported in Chapter 4. Calculation of the solution and refrigerant stream concentrations is reviewed. The concentration values are used as the third property to fix the state of the ammonia-water flow at the inlet and outlet of most components. Individual component heat duty, LMTD and overall conductance UA calculations are not presented. High uncertainties are associated with these calculations, because fluid flow rates for each component were not measured. The total heating duty and absorption system COP calculation are also presented.

Table B.3.1: Example Packaged Unit Data Analysis and Uncertainty Calculation

Inputs	Equations	Results
Solution and Refrigerant Concentrations		
Dilute Solution		
$T_{\text{Des,DS,out}} = 126.9^{\circ}\text{C} \pm 0.25^{\circ}\text{C}$ $P_{\text{high-side}} = 1361 \text{ kPa} \pm 8.6 \text{ kPa}$ $q_{\text{Des,DS,out}} = 0$	$x_{\text{DS}} = x_{\text{NH}_3\text{-H}_2\text{O}}(T_{\text{Des,DS,out}}, P_{\text{high-side}}, q_{\text{Des,DS,out}})$	$x_{\text{DS}} = 0.2586 \pm 0.0016$
Refrigerant		
$T_{\text{Rect,ref,out}} = 58.68^{\circ}\text{C} \pm 0.25^{\circ}\text{C}$ $P_{\text{high-side}} = 1361 \text{ kPa} \pm 8.6 \text{ kPa}$ $q_{\text{Rect,ref,out}} = 1$	$x_{\text{Ref}} = x_{\text{NH}_3\text{-H}_2\text{O}}(T_{\text{Rect,ref,out}}, P_{\text{high-side}}, q_{\text{Rect,ref,out}})$	$x_{\text{Ref}} = 0.9968 \pm 0.0001$
Concentrated Solution		
$T_{\text{Abs,CS,out}} = 34.81^{\circ}\text{C} \pm 0.25^{\circ}\text{C}$ $P_{\text{low-side}} = 581.2 \text{ kPa} \pm 8.6 \text{ kPa}$ $q_{\text{Abs,CS,out}} = 0$	$x_{\text{CS}} = x_{\text{NH}_3\text{-H}_2\text{O}}(T_{\text{Abs,CS,out}}, P_{\text{low-side}}, q_{\text{Abs,CS,out}})$	$x_{\text{CS}} = 0.5683 \pm 0.0041$

Table B.3.1: Continued

Inputs	Equations	Results
Properties at Ammonia-Water State-points		
Example: Condenser Refrigerant Outlet		
$T_{\text{Cond,Ref,out}} = 35.38^{\circ}\text{C} \pm 0.25^{\circ}\text{C}$ $P_{\text{high-side}} = 1361 \text{ kPa} \pm 8.6 \text{ kPa}$ $x_{\text{Ref}} = 0.9968 \pm 0.0001$	$h_{\text{Cond,Ref,out}} = h_{\text{NH}_3\text{-H}_2\text{O}}(T_{\text{Cond,Ref,out}}, P_{\text{high-side}}, x_{\text{Ref}})$ $v_{\text{Cond,Ref,out}} = v_{\text{NH}_3\text{-H}_2\text{O}}(T_{\text{Cond,Ref,out}}, P_{\text{high-side}}, x_{\text{Ref}})$ $q_{\text{Cond,Ref,out}} = q_{\text{NH}_3\text{-H}_2\text{O}}(T_{\text{Cond,Ref,out}}, P_{\text{high-side}}, x_{\text{Ref}})$	$h_{\text{Cond,Ref,out}} = 165.8 \text{ kJ kg}^{-1}$ $\pm 1.1 \text{ kJ kg}^{-1}$ $v_{\text{Cond,Ref,out}} = 1.71 \times 10^{-3} \text{ m}^3 \text{ kg}^{-1}$ $\pm 1.13 \times 10^{-6} \text{ m}^3 \text{ kg}^{-1}$ $q_{\text{Cond,Ref,out}} \rightarrow \text{subcooled}$
Heat Duty and COP		
$\dot{m}_{\text{Abs-Cond,CF}} = 0.1184 \text{ kg s}^{-1}$ $\pm 0.00012 \text{ kg s}^{-1}$ $T_{\text{Abs-Cond,Aux,in}} = 37.71^{\circ}\text{C} \pm 0.25^{\circ}\text{C}$ $T_{\text{Abs-Cond,Aux,out}} = 32.49^{\circ}\text{C} \pm 0.25^{\circ}\text{C}$ $c_{p\text{Abs-Cond,CF}} = 4.179 \text{ kJ kg}^{-1} \text{ K}^{-1}$ $\pm 3.6 \cdot 10^{-6} \text{ kJ kg}^{-1} \text{ K}^{-1}$	$Q_{\text{Heating}} = \dot{m}_{\text{Abs-Cond,CF}} \cdot c_{p\text{Abs-Cond,CF}} \cdot (T_{\text{Abs-Cond,Aux,in}} - T_{\text{Abs-Cond,Aux,out}})$	$Q_{\text{Heating}} = 2.55 \text{ kW} \pm 0.14 \text{ kW}$
$Q_{\text{gas}} = 1.86 \text{ kW} \pm 0.044 \text{ kW}$ $\text{CE} = 0.861 \pm 0.04$	$Q_{\text{desorber}} = Q_{\text{gas}} \cdot \text{CE}$	$Q_{\text{desorber}} = 1.603 \text{ kW} \pm 0.084 \text{ kW}$

Table B.3.1: Continued

Inputs	Equations	Results
Heat Duty and COP		
Q _{Heating} = 2.55 kW ±0.14 kW Q _{desorber} = 1.603 kW ±0.084 kW	COP _{Heating} = Q _{Heating} · Q _{Desorber} ⁻¹	COP _{Heating} = 1.59 ±0.12

APPENDIX C: HEAT EXCHANGER FABRICATION DETAILS

The fabrication techniques used to make the microchannel heat exchangers (discrete or monolithic) are discussed briefly in the thesis text. This Appendix provides a more detailed description of these fabrication processes. These fabrication techniques are also described by Determan (2008) and Nagavarapu (2012).

The heat exchangers were fabricated in a multi-step process. Thin sheets of stainless steel (shims) with micro-scale features serving as flow passages were produced by photochemical etching. This machining process produced the shims that make up the heat exchange layers of each component. Each shim was electrochemically plated with a Nickel-based alloy. Shims were then stacked in an alternating fluid passage order to assemble the individual pre-bonded component. The components were brazed in a vacuum furnace, resulting in a hermetically sealed heat exchanger.

C.1 Photo-chemical Etching Process

A photochemical etching process was used to fabricate the individual shims that form the layers of the microchannel heat exchangers. For the present study, this etching was conducted by Company, City, State. The major steps of the etching process are outlined in Figure C.1. The substrate, stainless steel in the case of the heat exchangers, was cleaned to allow for the application of an uncured photoresist. This cleaning process is very important because any contaminants or scaling on the surface prevents the machining process from producing the desired design and meeting the specified tolerances. After the cleaning process, a photo resist was applied to both sides of the substrate sheet. Masks containing transparent and opaque sections, based on the desired

etch patterns, were applied to both sides of the resist-substrate-resist sheet. Alignment of the front and back masks is critical to ensure features are etched properly. The sheet was then exposed to UV light which cures the photo resist that is not shaded by opaque masking. The masking and uncured photo resist were removed. The resist-substrate-resist sheet now contained the pattern required to etch the designated features. The resist-

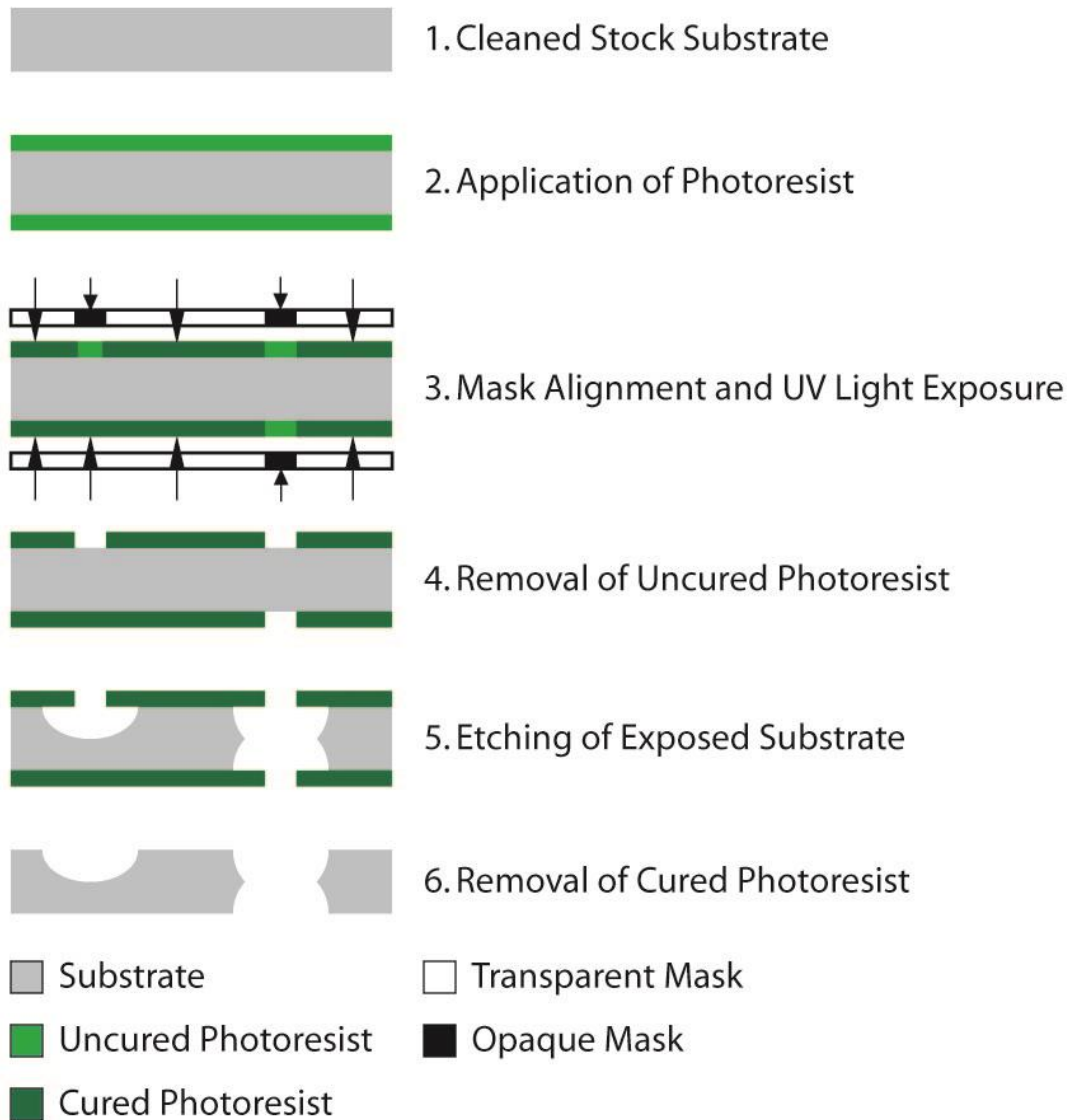


Figure C.1: Photo-chemical etching process

substrate-resist sheet was placed in a chemical bath where the exposed substrate was removed by the chemical etching process. The sheet was removed from the chemical bath once the desired features were machined onto the substrate. The cured photoresist was then removed and the machined substrate that results was cleaned and inspected. If the machined features met the desired tolerances, the individual shims were ready for the next step of the manufacturing process. It should be noted that the photoresist application and etching process were conducted in a clean room to mitigate the risk of contamination throughout the entire process.

C.2 Vacuum Brazing

The vacuum brazing process was used to fabricate the hermetically sealed discrete and monolithic heat exchange components. For the present study, brazing was conducted by Company, City, State. The process starts with inspection and cleaning of the shims produced in the chemical etching process. Burrs and contaminants can inhibit hermetic sealing of a component by preventing adjacent shims from sitting flush during the bonding process. The shims were then electrochemically plated with a nickel braze alloy. The endplates and shims were stacked in an alternating fluid passage order to produce the pre-bonded component assembly. The component was then installed in one of two fixtures (Figure C.2). In both fixtures, the heat exchanger was sandwiched between graphite sheets. The fixtures differ in the manner in which pressure is applied and alignment is maintained. Fixture 1 applies pressure to the assembly with the tightening of bolts that connect outer plates. This clamping pressure aided in the bonding process and was sufficient to prevent the movement of shims when the braze material is liquid. Fixture 2 applied pressure to the assembly with the addition of weights to the surface of

the top graphite sheet. Alignment pins were used to keep the shims aligned vertically. The component and fixturing assembly was placed in the furnace after the component was secured in the selected fixturing. The furnace was then evacuated and the temperature elevated (~1000°C) for a designated period of time. While the component was at this elevated temperature, the braze material melted, flowed along the joints and diffused at the interfaces. The bonding that occurred at the shim interfaces produced a hermetically sealed component. The component was removed from the furnace and fixturing upon completion of the vacuum brazing process. Inspection to verify airtight seal was performed before deeming the heat exchanger safe for use.

Fabricated heat and mass exchange components were tested to ensure hermetic sealing of the fluid passages. Leak testing was performed by pressurizing the components with compressed nitrogen to 689.5 kPa. If no leaks were detected, the components were pressurized with water up to 2758 kPa to ensure that they would not fail at pressures expected during operation. Laminar flow pressure drop testing was performed on all

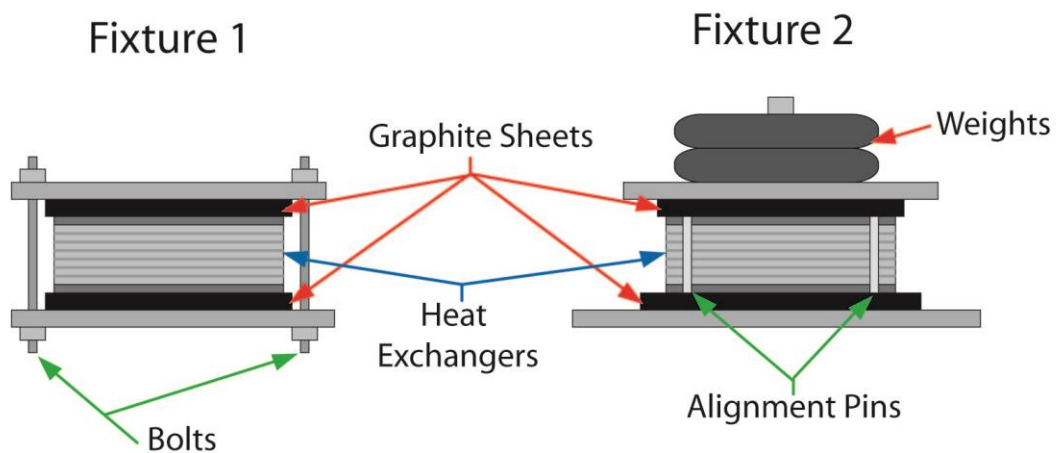


Figure C.2: Fixtures used in vacuum brazing process

vacuum brazed components to investigate any potential blockage due to the flow of braze material into the microscale flow passages during the bonding process. Water was pumped through each fluid passage of the component while the pressure loss and flow rates were measured. Results from the laminar flow tests were compared with theoretical pressure drop predictions to evaluate number of active channels within a heat exchanger. After this series of tests was completed, the heat exchangers were installed on the breadboard test facility.

REFERENCES

- ACEEE (2012). Water Heating. www.aceee.org. **2014**.
- ACEEE (2015). Replacing your Water Heater. smarterhouse.org. **2015**.
- AHRI (2014). Residential Storage Water Heaters Historical Data. <http://www.ahrinet.org>. **2014**.
- Beutler, A., Hoffmann, L., Ziegler, F., Alefeld, G., Gommed, K., Grossman, G. and Shavit, A. (1996), "Experimental Investigation of Heat and Mass Transfer on Horizontal and Vertical Tubes," *Proceedings of the International Ab-Sorption Heat Pump Conference*, Montreal, Canada, pp. 409-419.
- Cassard, H., Denholm, P. and Ong, S. (2011), "Technical and economic performance of residential solar water heating in the United States," *Renewable and Sustainable Energy Reviews*, **15** (8): 3789-3800.
- Cheung, K., Hwang, Y., Judge, J. F., Kolos, K., Singh, A. and Radermacher, R. (1996), "Performance assessment of multistage absorption cycles," *International Journal of Refrigeration*, **19** (7): 473-481.
- Chua, K. J., Chou, S. K. and Yang, W. M. (2010), "Advances in heat pump systems: A review," *Applied Energy*, **87** (12): 3611-3624.
- Determan, M. D. (2008). "Thermally Activated Miniaturized Cooling System," Mechanical Engineering, Georgia Institute of Technology, Atlanta.
- Determan, M. D. and Garimella, S. (2011), "Ammonia–water desorption heat and mass transfer in microchannel devices," *International Journal of Refrigeration*, **34** (5): 1197-1208.
- Determan, M. D. and Garimella, S. (2012), "Design, fabrication, and experimental demonstration of a microscale monolithic modular absorption heat pump," *Applied Thermal Engineering*, **47** (0): 119-125.
- DoE (2013), Technical Reference - Source Energy, U.S. Department of Energy, energystar.gov, Energy Star Portfolio Manager: pp. 1-17.
- DOE (2014). Everything You Need to Know About Water Heaters. www.energy.gov. **2014**.
- DoE (2015a), 10 CFR, Part 430, Subpart B, Appendix E - Uniform Test Method For Measuring the Energy Consumption of Water Heaters, U.S. Department of Energy, ecfr.gov, U.S. Government Publishing Office.
- DOE (2015b). Clothes Washers for Consumers. U.S. Department of Energy, energystar.gov/products/certified-products/detail/clothes-washers. **2015**.
- DoE (2015c). Everything You Need to Know About Water Heaters. U.S. Department of Energy, energy.gov. **2015**.
- DoE (2015d). Residential Water Heaters Key Product Criteria: ENERGY STAR. U.S. Department of Energy, energystar.gov. **2015**.
- EIA (2015). eia.gov. **2015**.
- Engler, M., Grossman, G. and Hellmann, H. M. (1997), "Comparative simulation and investigation of ammonia-water: absorption cycles for heat pump applications," *International Journal of Refrigeration*, **20** (7): 504-516.

- Garimella, S. (1999), "Miniaturized Heat and Mass Transfer Technology for Absorption Heat Pumps," *Proceedings of the International Sorption Heat Pump Conference*, Munich, Germany, pp. 661-670.
- Garimella, S., Christensen, R. N. and Lacy, D. (1996), "Performance evaluation of a generator-absorber heat-exchange heat pump," *Applied Thermal Engineering*, **16** (7): 591-604.
- Garimella, S., Determan, M. D., Meacham, J. M., Lee, S. and Ernst, T. C. (2011), "Microchannel component technology for system-wide application in ammonia/water absorption heat pumps," *International Journal of Refrigeration*, **34** (5): 1184-1196.
- Garimella, S., Keinath, C. M., Delahanty, J. C., Hoysall, D. C., Staedter, M. A., Goyal, A. and Garrabrant, M. A. (2015), "Development and demonstration of a compact ammonia-water absorption heat pump prototype with microscale features for space-conditioning applications," *Applied Thermal Engineering*, **Under Review**.
- Garrabrant, M. A., Stout, R., Glannville, P. and Fitzgerald, J. (2014). Residential Gas Absorption Heat Pump Water Heater Prototype Performance Test Results. International Sorption Heat Pump Conference. College Park, MD.
- Garrabrant, M. A., Stout, R., Glannville, P., Fitzgerald, J., Keinath, C. and Garimella, S. (2013a), Development and Validation of a Gas-Fired Residential Heat Pump Water Heater - Final Report, DOE Contract EE0003985.
- Garrabrant, M. A., Stout, R., Glannville, P., Keinath, C. and Garimella, S. (2013b). Development of Ammonia-Water Absorption Heat Pump Water Heater for Residential and Commercial Applications. ASME International Conference on Energy Sustainability. Minneapolis, MN.
- Goodman, C., Fronk, B. M. and Garimella, S. (2011a), "Transcritical carbon dioxide microchannel heat pump water heaters: Part I – validated component simulation modules," *International Journal of Refrigeration*, **34** (4): 859-869.
- Goodman, C., Fronk, B. M. and Garimella, S. (2011b), "Transcritical carbon dioxide microchannel heat pump water heaters: Part II – System simulation and optimization," *International Journal of Refrigeration*, **34** (4): 870-880.
- Hepbasli, A. and Kalinci, Y. (2009), "A review of heat pump water heating systems," *Renewable and Sustainable Energy Reviews*, **13** (6–7): 1211-1229.
- HomeDepot (2015). homedepot.com. **2015**.
- Hoysall, D. C., Keniar, K. and Garimella, S. (2015). Visualization of two-phase flow through microchannel heat exchangers. ASME International Conference on Nanochannels, Microchannels and Minichannels. San Francisco, CA.
- Hu, J. S. and Chao, C. Y. H. (2008), "Study of a micro absorption heat pump system," *International Journal of Refrigeration*, **31** (7): 1198-1206.
- Keinath, C. M., Garimella, S. and Garrabrant, M. A. (2015), "Modeling of an ammonia-water absorption heat pump water heater for residential applications," *Applied Thermal Engineering*, **Under Review**.
- Klein, S. A. (2014). Engineering Equation Solver. V9.452, F-Chart Software.
- Lee, S., Bohra, L. K., Garimella, S. and Nagavarapu, A. K. (2012), "Measurement of absorption rates in horizontal-tube falling-film ammonia-water absorbers," *International Journal of Refrigeration*, **35** (3): 613-632.

- Lekov, A., Franco, V., Meyers, S., Thompson, L. and Letschert, V. (2011), "Energy Efficiency Design Options for Residential Water Heaters: Economic Impacts on Consumers," *ASHRAE Transactions*, **117** (1): 103-110.
- Lekov, A. B., Lutz, J. D., Camilla Dunham, W. and McMahon, J. E. (2000), "Cost of increased energy efficiency for residential water heaters / Discussion," *ASHRAE Transactions*, **106**: 875.
- Meacham, J. M. and Garimella, S. (2003), "Modeling of local measured heat and mass transfer variations in a microchannel ammonia-water absorber," *ASHRAE Transactions*, **109** (1): 412-422.
- Meacham, J. M. and Garimella, S. (2004), "Ammonia-water absorption heat and mass transfer in microchannel absorbers with visual confirmation," *ASHRAE Transactions*, **110** (1): 525-532.
- Nagavarapu, A. K. (2012). "Binary Fluid Heat and Mass Exchange at the Microscales in Internal and External Ammonia-Water Absorption," George W. Woodruff School of Mechanical Engineering, Georgia Institute of Technology
- Nagavarapu, A. K. and Garimella, S. (2011), "Design of Microscale Heat and Mass Exchangers for Absorption Space Conditioning Applications," *Journal of Thermal Science and Engineering Applications*, **3** (2).
- NREL (2010). System Advisor Model. <https://sam.nrel.gov/>, National Renewable Energy Laboratory.
- Pence, D. (2010), "The simplicity of fractal-like flow networks for effective heat and mass transport," *Experimental Thermal and Fluid Science*, **34** (4): 474-486.
- Ryan, D., Long, R., Lauf, D., Ledbetter, M. and Reeves, A. (2010), Energy Star Water Heater Market Profile; Efficiency Sells, U. S. D. o. Energy.
- Ryan, D., Long, R., Lauf, D., Ledbetter, M., Reeves, A. (2010), Energy Star Water Heater Market Profile; Efficiency Sells, U.S. Department of Energy.
- Sachs, H., Talbot, J. and Kaufman, N. (2012). Emerging Hot Water Technologies and Practices for Energy Efficiency as of 2011. ACEEE.org.
- Schoenbauer, B., Hewett, M. and Bohac, D. (2011), "Actual Savings and Performance of Natural Gas Instantaneous Water Heaters," *ASHRAE Transactions*, **117** (1): 657-672.
- Srikhirin, P., Aphornratana, S. and Chungpaibulpatana, S. (2001), "A review of absorption refrigeration technologies," *Renewable and Sustainable Energy Reviews*, **5** (4): 343-372.
- Tomlinson, J. J. and Murphy, R. W. (2004), "Measured Performance and Impacts of "Drop-In" Residential Heat Pump Water Heaters," *ASHRAE Transactions*, **110** (2): 664-670.
- Wu, W., Wang, B., Shi, W. and Li, X. (2014), "Absorption heating technologies: A review and perspective," *Applied Energy*, **130** (0): 51-71.
- Zogg, R., Dieckmann, J., Roth, K. and Brodrick, J. (2005), "Heat Pump Water Heaters," *ASHRAE Journal*, **47** (3): 98-99.
- Zogg, R., Roth, K., Radermacher, R. and Brodrick, J. (2007), "CO₂ Heat Pump Water Heaters," *ASHRAE Journal*, **49** (11): 52-54.